博士論文

High Speed Robotic Manipulation for Rotation Control using Visual Encoder

（ビジュアルエンコーダを用いた回転制御のための

高速ロボットマニピュレーション）

金　賢梧 / Hyuno Kim

Acknowledgements

This dissertation could not have been completed without the great supports from many people. I would like to express my deepest gratitude to all of those who helped me throughout my academic journey as well as the process of writing this thesis.

First of all, I would like to express my sincere gratitude to Prof. Masatoshi Ishikawa, who is the supervisor of my doctoral research. I have received a lot of guidance and assistance from him on the research, and he encouraged me many times despite the slow progress of the research. Also, thanks to him I had the opportunity to use various excellent equipments for the experiments. I would like to appreciate him again for opening the way for me to pursue academic career. I would also like to thank Prof. Yoshihiro Watanabe in the same laboratory. I have received a lot of help throughout my laboratory life and have received a lot of advice on the research.

I would like to thank all the members in the Sensor Fusion group. First, the co-leaders, Prof. Taku Senoo and Prof. Yuji Yamakawa, gave me plenty of advice over the doctoral course, and Prof. Niklas Bergstrom helped in reviewing papers and shared an excellent program library. Also, Mr. Kenichi Murakami who was a tutor at the beginning of my laboratory life gave me a lot of help in experimental matters. I would also like to thank Dr. Shouren Huang, Prof. Christopher Raabe and the other members whose names are not written here. And I especially thank Dr. Carson Reynolds who gave me a lot of information related to the research and plenty of guidance on the attitude and the passion toward the research. Although he passed away and we could not finish this study together, I am highly indebted to him and will always remember his passion.

In addition, I would like to appreciate Prof. Koji Ikuta, Prof. Hiroyuki Shinoda and Prof. Masahiko Inami who are the degree committee members for providing me with many valuable advice at the oral examination. I was able to improve the quality of my thesis thanks to the advice from the insights of those top experts. I would also like to thank Prof. Yasuyoshi Yokokohji in Kobe University who opened the way for me to be a researcher and gave me the opportunity to start my doctoral study in Japan.

Finally, I want to express my gratitude to my family who have encouraged me for a long time. I would especially like to express my best gratitude to my beloved wife Seohyun Lee who has supported me with her smile even in difficult circumstances. I was able to finish the doctoral course without giving up, thanks to her support and encouragement. This thesis is dedicated to Seohyun Lee with my love.

Abstract

A rotor takes a key responsibility in various mechanical systems, for power generation, power transmission as well as transportation, via the rotation in the system. In particular, a rotary system which includes a flexible object, such as thread, shows beneficial features in that the flexibility enhances the tolerance related to the connection between the rotor and the other parts owing to the morphologic characteristics. Accordingly, the precise control for the rotation of the rotor has been considered as a significant function for robotic systems. However, since the model for a flexible thread is complicated to construct and the nonlinear dynamics of the flexible thread is intricate to handle, the high-speed rotation control via thread by a robotic manipulator has been regarded as a difficult task. In order to simplify this problem, a high-speed vision-robot system with a simple PD controller can be suggested as a promising method, because this system can handle an event for a very short time interval and can be less influenced by the nonlinearity as well as by the modeling error. Also, since the conventional measurement methods were not suitable in terms of accuracy and robustness for the rotation control via thread, a new robust measurement method that can replace the existing methods is required, to exploit the high-speed vision-robot system for the rotation control.

This dissertation firstly introduces a new method to measure the rotation angle of a rotor, which is named as a visual encoder method, and then presents its applications into the field of robotic manipulation for the rotation control. The visual encoder method is developed in order to provide with a robust and precise measurement result for a rotor that rotates at high speed, even under the condition that the rotation axis is movable and experiences a fluctuation in the space. To achieve such features, the principles of vision-based method and the optical encoder are exploited with high-speed vision system. With the ability of the visual encoder in its operation at high-speed up to 6,000 rpm, a new kind of robotic manipulation regarding ‘high-speed rotation’ via thread is now accomplishable. The method to sense and control the high-speed rotation of the rotor by a robotic manipulator system, which involves dynamic motion, is described with the consideration of the academic and the industrial contribution.

The rotation control for the objects with flexible part is conducted in two applications: the robotic ‘button spinner’ and the robotic ‘yo-yo’ are selected in order to prove the visual encoder method for the rotation control via twisting and bending of the thread, respectively. In the applications, the transformation of thread is modeled with the complicated dynamics, and the nonlinearity as well as the modeling error are evaluated to define the limitation of the conventional approach for the tasks. As a result, in case of the robotic button spinner, the position and the rotation of the rotor are controlled within 1 mm and in sub-turn order, respectively, using high-speed visual feedback with the visual encoder method. Also, a stable performance of the robotic yo-yo is achieved in two example tasks, ‘releasing and catching’ and ‘continuous playing’, using the rotation-based feedback control. Consequently, the performance of the high-speed vision-robot system with visual encoder method was successfully verified in both applications. Additionally, in order to compensate the occlusion problem of the visual encoder, a high-speed distributed camera network is suggested and confirmed in the capability of synchronization among the camera nodes, based on MPI and RTC.

ビジュアルエンコーダを用いた回転制御のための高速ロボットマニピュレーション

概要

ローターの回転制御はオートメーションやロボットマニピュレーション分野において重要な役割を果たしており、多く研究されてきた。しかし、糸の変形特性を利用したローターの回転運動は、回転系における高速性や非線形性などが問題となり、モデル化を始め制御が難しいと考えられる。この問題を解決する手法として、高速ビジュアルフィードバックシステムを利用したモデル無し制御法が期待されている。この手法により、ある物理的なイベントが極短い時間内で処理できるので、モデル化誤差のみならず、非線形性などによる影響も抑制できる。高速な回転を高い精度でロバストに測定するためには、従来の手法を代替する新しい計測手法が必要となる。

本論文では、ビジュアルエンコーダと名付けた、新しい計測手法を導入し、「回転制御のためのロボットマニピュレーション」といった分野への応用例を示す。ビジュアルエンコーダは回転軸が移動したり、空中で揺動したりする条件下でも、数千 rpm といった高速で回転するローターの回転角を高精度且つロバストに計測できる。その優れた性能は既存の光学エンコーダと高速なビジョンシステムを用いた画像処理手法の動作原理を融合・応用することにより得られる。動的運動を含むローターの高速回転を、ビジョン・ロボットシステムを用いて計測・制御する手法について、その学術的及び工学的側面から考察しながら述べる。

柔軟な要素を有する回転系の制御に関連する二つのアプリケーションとして、ロボットによる「ボタンスピナー」と「ヨーヨー」の実現を取り上げ、ビジュアルエンコーダが糸のねじりと曲げによる回転制御において有効であることを証明する。ロボットボタンスピナーでは、ビジュアルエンコーダを用いた高速視覚フィードバック制御を行い、回転においてはサプターン、重心位置においては１ミリ以下の制御が実現される。また、ヨーヨーでは「リリーシングとキャッチング」と「連続プレイ」といったスキルにおいて安定な操作が達成される。結果として、ビジュアルエンコーダを取り入れた高速ビジュアルフィードバックシステムの有効性がこの応用例で成功的に確認できる。さらに、ビジュアルエンコーダ使用時に起こり得るオクルージョン問題を補完するため、MPI や RTC を利用した分散型高速カメラネットワークが提案され、カメラノード間における十分な同期性能が確認される。

Table of contents

List of figures

List of tables

Chapter 1

Introduction

This dissertation introduces a new method to measure the rotation angle of a rotor, which is named as the visual encoder methods, and presents its applications into the field of robotic manipulation for rotation control. Visual encoder method provides robust and precise measurement result for a rotor that rotates at high speed, even under the condition that the rotation axis is movable and fluctuating in the space. These features are advantageous to a new kind of robotic manipulation regarding 'high-speed rotation' via thread. The method to sense and control high-speed rotation of the rotor by a robotic manipulator, which involves dynamic motion, will be described with the consideration of its academic and industrial contribution.

1.1 Background and Motivation

1.1.1 Rotor and Rotation Control

The wheel is one of the most revolutionary inventions throughout human history which has brought a breakthrough in various technologies. In fact, the simple structure of the wheel, consisting of one rotation axle and an axially symmetrical body, has been developed into many shapes of rotors. A rotor can be referred as the rotating part of mechanical system, which is also called as rotary system, such as electric motor, generator, power turbine, crank, rotary engine, and other practical forms, as shown in Fig. 1.1. Since these systems have played important roles not only in everyday life but also in the field of many related industries, it is hard to imagine our life these days without them. Because the main role of the rotors is to produce a rotation motion in mechanical systems for power generation, power transmission and transportation, it is indispensable in technologies that support modern so-

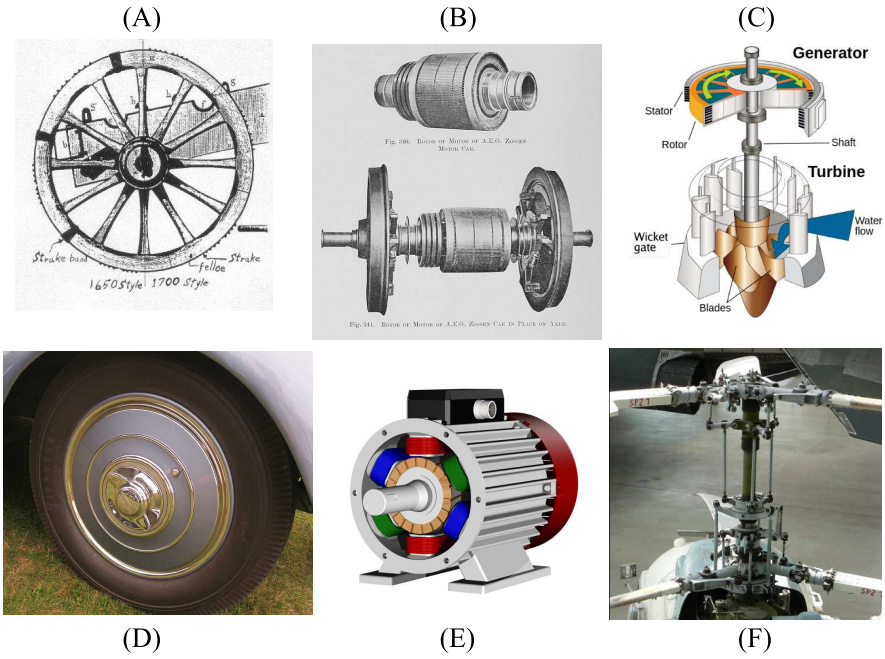

Fig. 1.1 Various rotors in everyday life. (A) Parts of the Strake Wheel [1]. (B) Rotor of motor [2]. (C) Water turbine [3]. (D) Wire wheel covered of DVLA [4]. (E) Electric Motor [5]. (F) Main rotor head of helicopter Kamov Ka-26 [6].

ciety. Therefore, appropriate rotation control of the rotor for the intended function, should be performed precisely as well as accurately.

Rotation control is to regulate the rotation angle, speed, and torque of a rotor separately, or concurrently. In many cases, the rotor is connected to the other mechanical parts, such as loads, supporters, and end-effector, which makes the control more complicated due to the disturbance from the interactions with those parts. As aforementioned, since the rotation control is essential particularly in the industrial field, many researches have been conducted regarding the stabilization of the rotation control. For example, suppressing mechanical vibration, positioning at high angular resolution, and decreasing the torque ripple are the main subjects of those researches. The stabilization is now considered to be a well-formulated problem in that there had been many efforts to increase the performance of the rotary system, as far as we limit the control problem to the conventional rotary system whose rotation axis is fixed.

Recently, through the technological innovation regarding sensor network, now the control of rotation is not only limited as a conventional rotary system but started to be applied to more dynamic systems. The noticeable difference that distinguishes between these two

is the location of sensor to measure the rotation angle of the rotor. The former, conventional rotary system aways includes the sensor within the volume of the system itself. In contrast, the latter, the newly designed rotary system, does not have to contain the sensor inside the system. Rather, the sensor can be placed outside in this case. This flexibility due to the separation of the sensor from the rotor provides a new possibility into the robotic manipulation for the control of the rotation.

1.1.2 Robotic Manipulation for Rotation Control

Robotic technology has been developed as reflecting various needs from society and been effected by the relevant technologies, for past several decades. The initial demands for robotic technology were mostly related to the automation of mass production in factories. With the mechanics, the most affiliated technology, the robotic technology has contributed to the industrial innovation which brought material wealth to human society. The next demand had moved on to improve the convenience in the daily life by replacing the unskilled labor that has been performed by human and by assisting the human action in elementary step. Representatively, the invention of electric washing machine and the automatic door are two examples of how robotic technology has met those needs. The development in robotics for such demand has been indebted to the evolution of electric science and electronics which are able to provide simpler sensing and controlling methods. Recently, thanks to the innovation in the information technology and nano technology, the desire and expectation to more enhanced robotic technology that is able to support human life with more active as well as flexible shape are growing up. This trend can be observed from many robot contests [7], such as DARPA Robotics Challenges [8], where robots are required to perform complicated actions that so far only humans were able to fulfill.

To achieve the complicated human's motion by robot, more advanced and flexible robotic manipulations are required. Robotic manipulation is a kind of interaction between a robotic end-effector and the target object to lead a certain intended variety in several aspects of the target object, such as the geometrical form, position, orientation and contact status. There have been conducted many researches respecting the robotic manipulations that are related to basic actions of human, such as grasping, throwing and catching of an object. Furthermore, recent studies are making an effort to expand the robotic skills for more various targets, such as form-changeable flexible objects. Robotic manipulation for rotation control shares coherency with this trend of study, as an endeavor to enlarge the capability of the robots. Then, how the robotic manipulation of the rotation control can be specified here? In

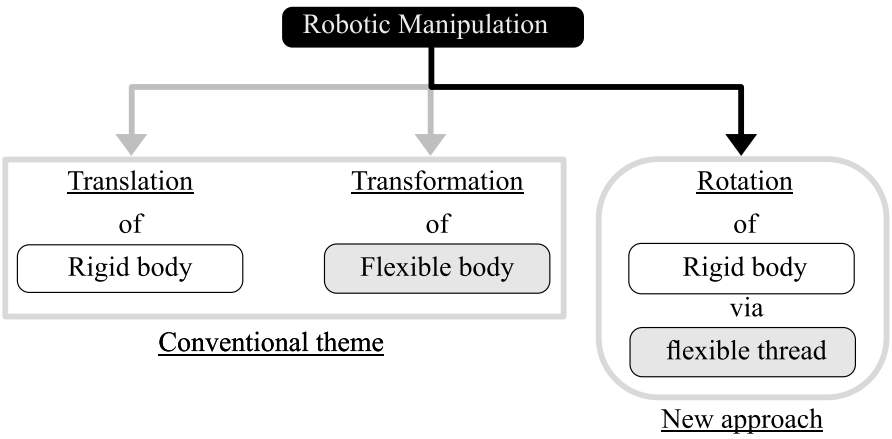

Fig. 1.2 Positioning of this research

this research, it is defined as 'managing the robotic system to regulate the rotation of certain target object', by merging the aforementioned definition. From the practical perspective, the target object is considered to be an axial-symmetric rotor, but not always restricted to.

The rotation control by a robotic manipulator can be applied to many practical applications. For example, rotating a hand wheel is a typical task performed in various situations, such as driving a car and controlling on-and-off state of a water pipe. These tasks require quasi-static re-grasping and have been main topics of many researches. On the other hand, very few researches are conducted concerning the manipulation of dynamic rotation, where the speed of a rotor is relatively high as much as reaching tens of thousand revolutions per minute (RPM), rotation axis is movable, and the transmitter to transfer the torque is required. This dynamic rotation can be observed in pump-drill and windlass in which the spinning of a rotor occurs through a flexible rope. Accordingly, the rotation of a rotor via flexible thread is selected as a primary task and a new robotic manipulation method for the task is studied in this research.

To avoid the confusion in understanding the term 'high-speed robotic manipulation' in the title, it is required to specify the definition of a robot in this research. Generally, the robot indicates a robotic hand system, and a rotor is considered as a target object when dealing with the robotic manipulation for the rotation control. Therefore, the control of a high-speed rotation of the rotor does not always mean the 'high-speed robotic manipulation'. However, in the case that the rotor is regarded as an end effector of the robotic hand system, it is possible to consider the rotor as a part of the robot, and the phrase can be interpreted

in the literal sense. In addition, the term ‘high-speed’ can indicate both the swiftness in the speed of response and the rapidity of the motion.

1.2 Rotation Control via Flexible Thread

The greatest benefit in using of thread-like object such as a rope in rotary system, comes from the flexibility of the thread. Generally, the flexibility increases the tolerance associated to the physical connection between the rotor and the other parts. In this case, the flexibility works to reduce the negative effect caused by undesirable mechanical vibration, and it also enables easy change in the direction of applied force. Moreover, easy transformation in the shape of thread makes it possible for the thread to be wound along the circumferential direction of the rotor, which plays a role as a preparation before producing the rotation. By the virtue of aforementioned features, a rotary system with thread has the advantage to produce high-speed rotation of a rotor through simple pulling motion at the end of the thread. Although it is now considered to be old-fashioned, human-powered technique to start an engine by pulling a string that is wound around a pulley can help to imagine the above example.

However, the flexibility can also bring several problems into sensing and controlling of the dynamic rotary system. First of all, in the case of sensing, the rotor as a control target can be moved easily in the space, because the rotor is supported by the thread which can change its shape freely. Therefore, how to track the rotor and how to measure its rotation during such movement become the problems to solve, before considering the manipulation method. Secondly, in the case of manipulation, the applied force via thread is unidirectional, which means that the thread cannot transfer force unless it is fully stretched and thus hampers the continuity in manipulation. This kind of defection in the continuity should be carefully considered when developing the control strategy. Finally, as a flexible thread can be bent and twisted at anytime, target system cannot always be explained by unique system parameters. Hence, the appropriate system model should be built so that it can handle the physical transformation as well as a sort of uncertainty.

These problems can be reorganized for the simplification and convenience as followings: (1) the principle to measure the rotation angle of a floating rotor, (2) system modeling and designing of control strategy for rotation control via twisting thread, and (3) rotation control via bending thread. Because of the respective background and the different features in the physical model, the twisting and the bending will be dealt with separately. Aforementioned

three problems are discussed as introducing the related works and clarifying what to be solved here in detail.

1.2.1 Measurement of Rotation Angle

As mentioned previously, the rotor has played an essential role in various mechanical systems. Also, how to control the rotation of the rotor accurately and stably has been one of the prime themes, and it has been dealt with in many related researches. In those researches, the feedback control has been exploited to regulate the rotation angle, speed or torque as the parameters of system output, according to the aimed rotary system. Since the rotation angle is considered as the most basic parameter, despite the mutual influence with the rest of parameters, the measurement quality of the rotation angle is generally considered to be a crucial factor for the feedback control. This is the reason why various types of methods to measure the rotation angle have been developed for past several decades.

Conventional Rotary Encoder

Dimmler et al. gave a good summary to survey various types of rotary encoders with their different features [9], where several types of rotary encoder were introduced. Among the conventional encoders, the optical type of rotary encoder has been applied the most broadly due to its advantages in easy signal processing and high resolution. Actually, the optical encoder is preferred for the primary sensor in many actuators, especially in electric servo motors.

The optical encoder consists of two main parts: a pattern disc, and an optical sensor set with a transceiver and a receiver of the light signal. The base of the pattern disc is generally made of thin glass or plastic-based material which is transparent, and the repeating opaque patterns are located on the base. While various patterns are used depending on the purposes, the stripe is exploited as a basic shape of the pattern. The optical transceiver and the receiver, such as LED and photodiode are located close to the both sides of surface of the disc, respectively. In this case, the light ray which is emitted from the transceiver passes through the disc is detected on the receiver. According to whether the current position of the disc, at which the light ray intersects with the disc plane, is transparent or opaque, the signal translated by receiver can take a digitized value, either one or zero. Since the light ray travels fast enough to detect the delay time in its path, from the transceiver to receiver, the digitized signals can be clearly distinguished. For example, if the distance between the transceiver and the receiver is about 1 cm, the travel time of the ray for this distance is

less than 30 picosecond. Therefore, the high-resolution sensing can be secured, because the digitization of the received signal is guaranteed. By counting up the number of turns that the signal value changes, the number of pattern passed the light ray can be recognized, and the amount of rotation of the disc is calculated.

Despite several benefits of the optical encoder such as the facility in protecting the sensor from external dusts and in keeping the measurement environment uniform, this 'envelopment' limits its functionality to the dedicated use only. When considering a rotary system in which the rotor is not only exposed outside but also movable freely in space, most conventional rotary encoders cannot be used due to the limitation.

Vision-based Method

Recently, the computer vision has been exploited for object tracking, where the pose - the position and the orientation - of an object in three dimensional space, can be easily acquired by selecting appropriate vision-based method. The representative method is model-based tracking methods [10, 11], which gives a real-time estimation of the pose of objects with a CAD model. This method uses graphical rendering technology in which a wire-frame of CAD model is projected onto the real camera image. In this method, from the differential between the wire-frame and the contour of the target object, the pose is calculated by solving an optimization problem for geometric motion estimation, with various iterative solutions to minimize the differential. On the other hand, model-free method is applied when the prior knowledge of the object, such as CAD data, is unavailable [12, 13]. In this case, generally, the feature points are obtained by the techniques such as SIFT[14], SURF[15], Fast corner detection[16], and other alternatives. Then, the acquired points are used for mapping of the geometrical relation between the camera and the object, and also for tracking of the change in the relation, i.e. pose. Between two methods described above, the latter is considered as more appropriate method to detect the rotation angle of a rotor, because many rotors have no changes in their silhouette owing to the axial symmetry in geometric shape.

Several vision-based methods that are focusing on the rotation measurement of a rotor have been reported. Most of the following methods used a kind of marker that helps to extract feature points, as illustrated in Fig. 1.3, because a rotor has few feature points due to its symmetry and the monotony in the geometric shape. The calibration pattern with spot array [17, 18], simply distributed dots [19, 20], and color gradient [21] are used as the marker for the respective method. Generally, the number and the arrangement of the feature points affects the accuracy and the resolution of the measurement. Actually, a large number of feature points increase aforementioned measurement quality, but raise the image

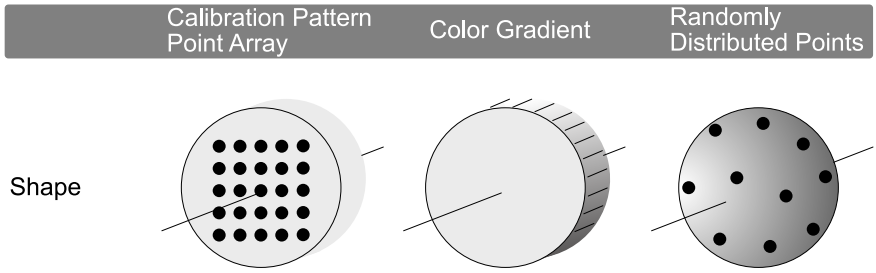

Resolution	Very High	High	Middle
Available Target Size	Big	Small to Big	Middle to Big
Processing Cost	Very High	Low	High

Fig. 1.3 Marker types for vision-based rotation measurement

processing cost, too. In addition, it can be a problem to place the whole feature points in the limited volume of the target object. Practically, the existing vision-based methods are too slow to apply to a real-time feedback control in the dynamic mechanical system.

Combination of Two Methods

A combination of the two methods, the conventional optical encoder and the vision-based method, can be an alternative solution to measure the rotation of a rotor more robustly and accurately at high speed. However, a proper integrating of these two mechanisms without a loss of respective beneficial feature is an important issue. Therefore, the integrated method should be thoroughly evaluated with the experiment results.

1.2.2 Rotation Control via Twisting

Twisted Thread and Applications

Historically, one of the oldest devices which take advantages of a twisted thread to rotate a rotor for a practical use, is a pump-drill. A pump-drill is a primitive device which had been used for making fire from the friction energy by drilling holes in hard materials. Basically, the pump-drill effectively converts the hand motion of moving up and down to the high-speed rotation of a drill-like shaft that plays a role as a rotor. When its use is limited to the original purpose, the rotation angle or the speed of the pump-drill is not crucial factor for

the operation itself. However, it is important for most modern equipments that employ the operation mechanism.

Currently, a twisted thread actuator, or a twisted string actuator, has been attracting many researchers' attentions as an application that adopted the basic mechanism of pump-drill. The principle of this application is the inverted form of pump-drill's, in which the rotation of the rotor is converted to the linear displacement of the thread end, via twisting the thread. According to the degree of the twisting of the thread, the natural length of the thread is changed, and the stretched length causes the force to be applied to the thread end. Many system structures [22, 23] and control schemes [24–26] that are related to the twisted thread actuator have been suggested, leading the development of practical actuators that are actually used for the light-weight robotic fingers and adapted in several robotic hand and arm systems [27–29]. Since twisted thread replaces the mechanical parts which are used to connect the power source and the end-effector, it helps to build a kind of flexible power transmitter as well as contributes to the weight reduction of the mechanical parts. However, because the twisted thread actuator itself only deals with the 'twisting' unidirectionally, rotation to linear motion, it is worth considering about the other aspect of the twisting in the reverse direction, linear motion to rotation.

Notwithstanding its unique feature and the potential for the development of new applications, the original type of application which exploits the principle of operation used in pump-drill, has been rarely reported. The biggest reason of such scarcity is that flexibility is not an essential factor than the solidity acquired from mechanical parts such as gearbox or propeller shaft, in case of many conventional systems with fixed rotation axis. In general, the rigid body makes the control problem easier, due to its simple modeling without non-linearity, while the flexible body has the opposite feature. However, the rotation of a rotor via twisted thread features following benefits: Firstly, since there is no requirement to equip any complicated parts for power transfer except thread, it contributes to the reduction of energy loss caused by friction and the improvement of freedom in structure design. Secondly, it is suitable for producing high-speed rotation of rotor with less effort. Consider that even the prehistoric pump-drill constructed with only primitive materials in simple structure, was able to effectively produce high-speed rotation of the drill by relatively slow hand motion. Actually, only one or two Hz of linear motion is required to produce a rotation of thousands RPM. Lastly, it does not require additional supporter for the rotor, such as a bearing, because the thread itself can play a role as a supporter. Additionally, The rotor hung in the three dimensional space by the thread, can be free from the mechanical vibration. Furthermore, the thread can play a role as a shock absorber between the rotor and the external manipulator,

which increases the robustness of the system against the external force. These advantageous features explained above can be observed in following application: the button spinner.

Robotic Button Spinner

A button spinner, consisting of a button as the rotor and two pairs of twisted thread as the power transmitter, has been played for a long time since the old days, even though it is not as much as popular when compared to the similar hand-toy, yo-yo [30]. The principle of operation for a button spinner is mostly the same with that of pump-drill, but shows the difference in that a button spinner includes two symmetric pairs of thread instead of one, and it makes the rotor hung in the air. This symmetric structure and the hanging rotor grant a button spinner several beneficial features to study the rotation via twisted thread. Firstly, unlike the pump-drill, a button spinner is able to work as a stand-alone application for the rotation control, since it does not require any external supporting point for the rotor. Accordingly, it makes easy to observe the relation between the hand motion and the rotation of the rotor. Secondly, the rotation of the rotor is less influenced by any external force, because the rotor is floating in the air and thus has no contact except with the thread. Finally, the two pairs of twisted thread can increase the rotation torque by the factor of two, which takes a benefit when producing a rotation of higher speed.

Despite these advantageous features shown above, playing a button spinner by robotic manipulator is not tried yet in any researches, while other similar applications such as yo-yo have been studied in many researches. This discrepancy is considered to be originated from the difficulty in the measurement of the rotation. In case of yo-yo, although the high-speed rotation of a rotor is observed as well, but still its speed is relatively lower than the case of button spinner. Moreover, the centroid position of the yo-yo changes in accordance with the rotation of the rotor, and it allows an indirect estimation of the rotation based on the position measurement. Normally, the moving speed of the centroid is not so fast and hence the measurement is not difficult. On the contrary, in case of a button spinner, such movement is not detected, and the indirect manner in the measurement of rotation does not even exist. By introducing a new method to measure the rotation in direct manner, button spinner can be performed as an application in which the rotation control via twisted thread is studied.

Models of Twisted Tread and Limitations

A model of twisted thread is required to clarify the dynamics of system and to control the rotation based on the analysis. In the field of computer graphics, a simulation of the trans-

formation of flexible thread has been a challenging task and dealt with in many researches. Although several researches came from the practical needs for surgical thread simulation in virtual reality [31], most of them have been studied in general attention to produce a realistic animation with the physical interaction [32, 33].

For example, In [32], a physics-based model to simulate thread dynamics is presented. This model is founded upon Position Based Dynamics, which is suggested by [34]. The purpose of the model is to handle the collision and the contact of thread, and is expanded by considering the stiffness and bending with various constraints regarding contact, friction, and torsion. The simulation result that is performed by this model shows plausible visualization with their knotting examples. However, the simulation requires considerable computing time. In fact, it runs at 70 fps, and the twisting of thread itself is not considered.

In regard to the modeling of the twisted thread, in the research of [24], the geometrical physics of twisted pair of thread that is focusing on the transmission characteristic has been modeled in kinetostatic form, as well as the dynamic model. The model is validated by the simulation and the result from experiment, in which the length of thread is changed according to the twisted angle of thread under certain content load, and they showed an excellent matching between the simulation and experience. [22] suggested an expanded model of [24], where a pair of twisted thread is not contact each other at the end of twisting. In case of Godler's model, it has more generalized form than the model suggested by [24]. Also, the simulation and the experiment results in [22] also strongly supports the correctness of the model, and it is easy to notice that the equation in [24] is the particular solution of the one equation in [22]. However, more generalized model is required to formulate the twisting of the threads in the button spinner. In comparison with two aforementioned models, button spinner shows different feature in that it uses two pairs of the twisted thread and the both ends of the pair of thread are separated and opened. In addition, the direction of the twisting is switched periodically with the oscillation of the rotation of the rotor, in case of button spinner. Therefore, new tread model to explain the twisting in button spinner is required, and the new model should equip the expanded shape from the models suggested by [24] and [22]. Also, the new model can be verified by comparing the simulation result with aforementioned two models' results under the same condition, in order to show that it has more generalized form.

Expected Applications

The principle of twisted thread can be applied for several practical applications, in which the rotation of rotor via twisted thread is actively exploited. First of all, development of a

new type of shaker can be anticipated. Contrary to the conventional shaker, the new type of shaker that is designed with the principle of twisting thread mechanism can have less mechanical parts, and can more softly operate owing to the flexible feature of the thread. Additionally, less vibration and less friction loss with small amount of heat release are the expected characteristics. Furthermore, the machine tools such as flexible grinder and drill can be considered to be possible applications, in that the shock produced by an impact can be suppressed by the thread transmitter. Lastly, the principle of twisted thread can be applied to a motion converter which produces high-speed rotation from a normal speed of linear motion. Since it requires only a few pairs of twisted thread, this kind of application is expected to reduce the cost to construct a system.

1.2.3 Rotation Control via Bending

Bending Thread and Applications

Bending of thread can be also used to acquire the high-speed rotation of a rotor from linear motion. For example, when the thread is fixed on any surface of the rotor at its end and is wound up several turns around the rotor, the yanking hand motion at the other end of the thread makes the rotor rotate at high speed. This sort of rotation has been exploited in a variety of applications ranging from a practical equipment such as the rope-pull starter for internal combustion engines [35], to even some toys such as a rubber band powered airplanes [36] and also to a toy top [37]. Since these applications require no delicate control to rotate the rotor but the unique mechanical structure of them plays a important role, many related literatures are found as patent applications rather than research papers.

On the other hand, yo-yo, one of the most popular [38] and historic [39] hand toy which is related to the rotation control via bending thread, requires well-planed operation for the playing. Actually, playing a yo-yo is not an easy task even to human, unless one has an experience of playing it before, in spite of its simple mechanism for playing. This has drawn many researchers' attractions to dive into the study of playing yo-yo with the robotic manipulator.

Many researches have been reported about robotic yo-yo playing [40–45]. In the research of [40], the simplified dynamics model of yo-yo was suggested with its well-defined schematic illustration, and playing a yo-yo was formulated as an optimal control problem. In [41], a method to decide the shape of hand motion with constraining of the boundary conditions was suggested. In addition, they performed the robotic yo-yo playing with visual feedback control using their control scheme that is based on the discrete time formulation.

In case of [42, 43], H. Jin studied about the yo-yo dynamics as focusing on the bottom collision which causes the energy loss during the flight of the yo-yo. Additionally, they discussed the optimized moment for pulling upward, and suggested the method to determine the magnitude of the acceleration for the motion. In the research of [46], the author also gave attention to the energy loss that is occurred at the bottom state of the yo-yo playing. In order to reduce the such energy loss, he suggested a proper hand motion generated in on-line, where the energy loss is compensated according to the dynamics equations that are solved in real time. In [47], the robotic yo-yo operation with a three-link manipulator was performed based on the analysis of human motion. In case of [48], a high-skilled yo-yo operation which is called long-sleeper was realized with a robot arm.

Conventional Robotic Yo-yo and The Limitations

Although aforementioned methods have contributed to the robotic yo-yo playing and the rotation control of a rotor, still many of them show following limitations: Firstly, they performed a robotic yo-yo playing based on the position feedback, not based on the rotation itself. This is because the direct measuring the rotation angle of the rotor during the dynamic motion of yo-yo is difficult with the conventional measurement methods. Therefore, the dynamics of yo-yo was rewritten for the centroidal position of yo-yo under the geometrical constraints according to the length of thread. Secondly, in the previous methods, not only the dynamics models itself for playing yo-yo are complex, but also they require many hypotheses in order to keep the models valid. For example, those models lose their validity unless the motion of playing yo-yo is performed in quasi-static as well as in stable condition. Furthermore, unrealistic features are required as hypotheses, as the models consider that the thread cannot be bent and the wound thread on the rotor axle is uncluttered at all the times, which will not occur in actual experimental condition. Therefore, if there occurs some fluctuations at any place and at any time, the stable condition applied as premise to those models can be broken. Finally, since the control scheme is closely linked to the dynamics model, conducting the accurate system identification is required in advance and model-dependent control with its modeling error is compelled.

As an alternative method in order to play a yo-yo beyond the limitation, the rotation control focusing on the rotation angle of the rotor is promising. Direct measurement and feedback of the rotation angle itself with high-speed vision-robot system is anticipated to take less influence from the fluctuation of the dynamics model than the case of the indirect method that is based on the estimation of the required information.

1.3 High-speed Vision-Robot System

1.3.1 Concept and Applications

As an approach to simplify the complicated model of the robotic manipulation of thread, the introduction of high-speed vision-robot system is considered to be a promising method. A high-speed vision-robot system consists of three main parts: A machine vision camera, computer for image processing, and the robotic manipulator. The machine vision camera in this system captures a visual scene at high speed, such as 1,000 Hz, and the computer is for the image processing in order to acquire the visual information. Also, the robotic manipulator operates at the same control frequency with the capturing frequency of the camera. Since the operation frequency of each part of the system is synchronized with the frequency of the entire system at very high speed, it is guaranteed that a cycle of control loop finishes within very short time intervals, such as 1 millisecond in the above case, by high-speed operation. Therefore, within the short time interval, any complex motion that can be encountered during the high-speed dynamic manipulation can be analyzed into simplified linear motions, and it makes the control of the system easy. Moreover, not only for the dynamic manipulation, but also for the case of a target system which includes flexible objects and for the case where the model is presented by complicated dynamics with uncertainties, the manipulation can be handled with the simple linearization. Thus, this feature is advantageous for the high-speed robotic manipulation of flexible object. Actually, for recent two decades, there have been made many efforts to expand the conventional robotic manipulation into the more dynamic scene by adapting the high-speed vision-robot system.

Namiki et al. suggested a hierarchical control architecture for high-speed visual servoing in [49]. In their research, three layers consisting of servo control, planning, and adaptation, are designed so that a series of object manipulation tasks such as throwing, grasping, and handling can be performed with high-speed active vision and dextrous robotic hand and arm. Senoo et al. developed the visual servo-ing scheme in order that more dynamic robotic manipulation can be applicable, as shown in [50–53]. They realized robotic batting and ball throwing with high-speed vision-robot system which embedded two active vision system in order to measure the three dimensional position of a ball. Murakami et al. also succeeded in robotic catching of a high-speed ball which is thrown by a baseball pitching machine, using the same system [54, 55].

While the aforementioned works focused on the dynamic manipulation of a solid object, Yamakawa et al. used high-speed vision-robot system to handle flexible object such as a rope and a piece of cloth [56–59]. By linearizing the transformation of one or two dimensional

flexible object, they performed the shape control of the ribbon that is used in rhythmic gymnastics, and conducted the high-speed folding of a piece of cloth only with simple PID control. Their works strongly imply that the high-speed vision-robot system helps to simplify and is able to solve the problem regarding rotation control via thread.

1.3.2 Structure Design

Several types of high-speed vision-robot system can be suggested according to the composition of the subordinate elements. For example, whether or not the camera is stationary or actively movable, and according to what types of robotic manipulator is available, can be independently selected as an element for the composition. In this research, a stationary camera and a robotic hand with three fingers are applied to the experimental equipments. The system layout is shown in Fig. 1.4 and the details of each element is given as following.

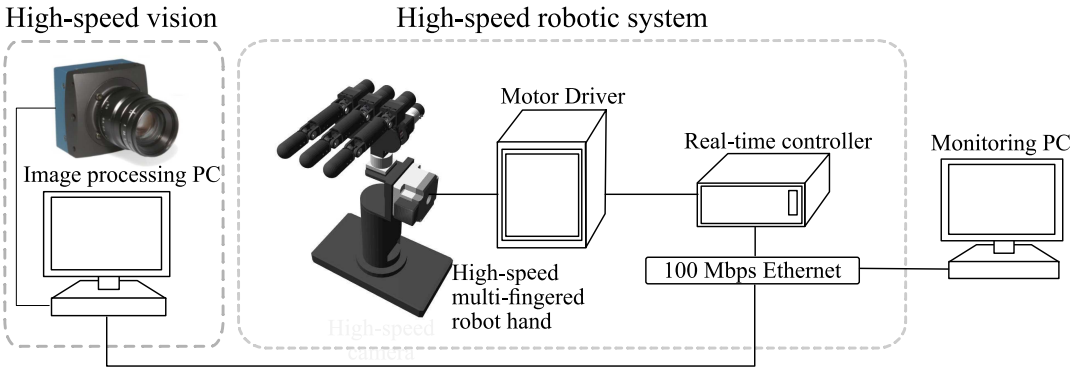

Fig. 1.4 The system layout of the high-speed vision-robot system

High-speed Machine Vision

EoSens is a machine vision camera that can capture images at extremely high frame rates, developed by Mikrotron GmbH [60]. The model used in this research is MC1363, which has Camera Link interface and is adaptable in capturing a colored scene. The maximum capturing speed is 506 frames per second (fps) at 1.3 megapixel resolution (1280 $\times$ 1020 px). The possible capturing speed of this camera can be increased by decreasing the set value of the resolution, for example, 1,860 fps available at VGA mode (640 $\times$ 480 px). Therefore, MC1363 has a good matching with the real-time controller that has a 1,000 Hz

(a) MC1363 (b) FL3-U3-13Y3M-C

Fig. 1.5 High-speed cameras for machine vision

Table 1.1 Model specifications of two high-speed cameras

Model	MC1363	FL3-U3-13Y3M-C
Resolution	1280×1024	1280×1024
Frame Rate	506 FPS	150 FPS
Chroma	Color	Mono
Sensor Type	CMOS	CMOS
Readout Method	Global shutter	Global shutter
Pixel Size	$14 \times 14\,\mu m$	$4.8 \times 4.8\,\mu m$
Lens Mount	C-/F-mount	C-mount
Data Width	8/10 bit	-
Quantum Efficiency (% at 525 nm)	-	61
Interface	Camera Link	USB 3.0
Dimensions	$63 \times 63 \times 47\,mm$	$29 \times 29 \times 30\,mm$

of operation frequency, as described in the later part. Recently, according to that the USB 3.0 is widely adopted as a standard, portable usb 3.0 camera also started to be used for the high-speed image capturing, together with the general-purpose use. FL3-U3-13Y3M-C is a high-speed USB 3.0 camera by PointGrey Research Inc [61]. This camera can capture monochrome images at 150 fps with 1.3 megapixels, and at 450 fps in VGA mode. Although its capturing speed is lower than the aforementioned machine vision camera, the features such as low-cost and the easy-to-use are counted as attractive points, particularly under the condition that multiple cameras are required. For this reason, the high-speed USB 3.0 camera was used when building a high-speed distributed camera network in this research. The major specifications of the two models are described in Table 1.1.

High-speed Robot Hand

In this research, the same structure of high-speed multi-fingered robot hand made by Namiki et al. in [Namiki, 2003 IROS] is adopted, although a small modification was added. This robot hand has three fingers and eight joints as shown in Fig. 1.6, and was designed to have following features: light weight, high speed with high acceleration, and high positioning accuracy. To achieve these features, a specially designed actuator which has high power density and backlash-less structure with harmonics gear was developed and adapted. Since each joint of the robot can rotate 1.8 degrees per 1 millisecond, the robot hand shows excellent performance with the real-time controller that operates at 1 kHz.

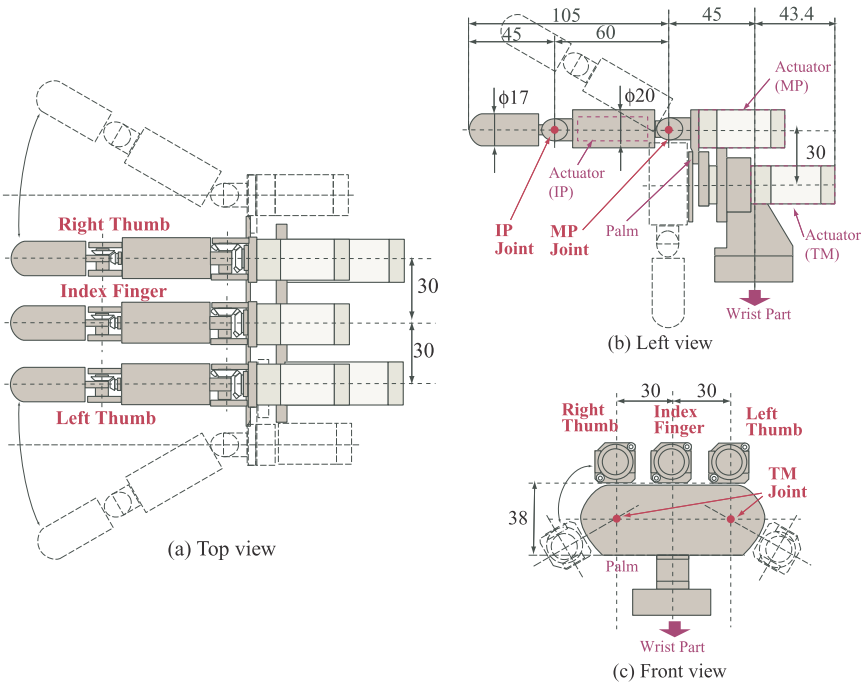

Fig. 1.6 High-speed robotic hand by Namiki [49] was used for the robotic manipulation task. Its high-speed motion with high acceleration and the backlash-less positioning are the core factors of the high-speed vision-robot system.

Real-Time Controller

The real-time controller plays an important role to synchronize the operations of the high-speed vision and the high-speed robot hand, at the high rate system frequency. The modular system developed by dSPACE GmbH [62] is a reasonable solution to arbitrate the high-speed vision and the robot system, since it consists of a dedicated processor and many

expandable I/O board, and is easy to communicate with the host computer for sending the commands and monitoring the results. The control program can be managed with Matlab [63] environment which runs on the host computer, and it helps easy the system development and maintenance.

1.4 Purpose and Outline

The purpose of this research is to control the robotic manipulator in order to regulate the rotation of a rotor as a part of certain rotary system which includes flexible thread as a medium for power transfer. In this system, the rotation has following features: (1) non-linearity in dynamics and (2) the movableness of the rotation axis. In fact, these two features give rise to two problems when controlling the robotic manipulator. First of all, non-linearity due to the flexibility of the thread requires unidirectional control strategy. Secondly, the movableness of the rotation axis demands new method to measure the rotation angle. Therefore, these two crucial problems have been mainly discussed in the following flow.

In this chapter, the background and the purpose of the works were described. The next chapter will discuss a new measurement method for the rotation of a rotor, named 'visual encoder', which is based on the vision-based method and is able to handle the movableness as well as the fluctuation of the rotation axis. As representatives of the conventional measurement methods, two types of visual encoder methods will be introduced. These two types of visual encoder can be separately applied to the measurement condition according to the relative orientation of the sensor to the direction of the rotation axis. In chapter 3 and 4, visual encoder will be verified with two task examples of robotic manipulation: button spinner and yo-yo. Robotic button spinner in chapter 3 is a manipulation example that is related to the power transfer through twisting of thread and the perpendicular type of visual encoder. Robotic yo-yo in chapter 4 is the other example for the power transfer through the bending of thread and the parallel type of visual encoder. Chapter 5 will present the occlusion problem in case of using the visual encoder method, and its solution by using high-speed distributed camera network will be described. In chapter 6, the expected applications and the future works, such as the expansion to visual servo-ing, will be discussed. Overall summary is described in chapter 7.

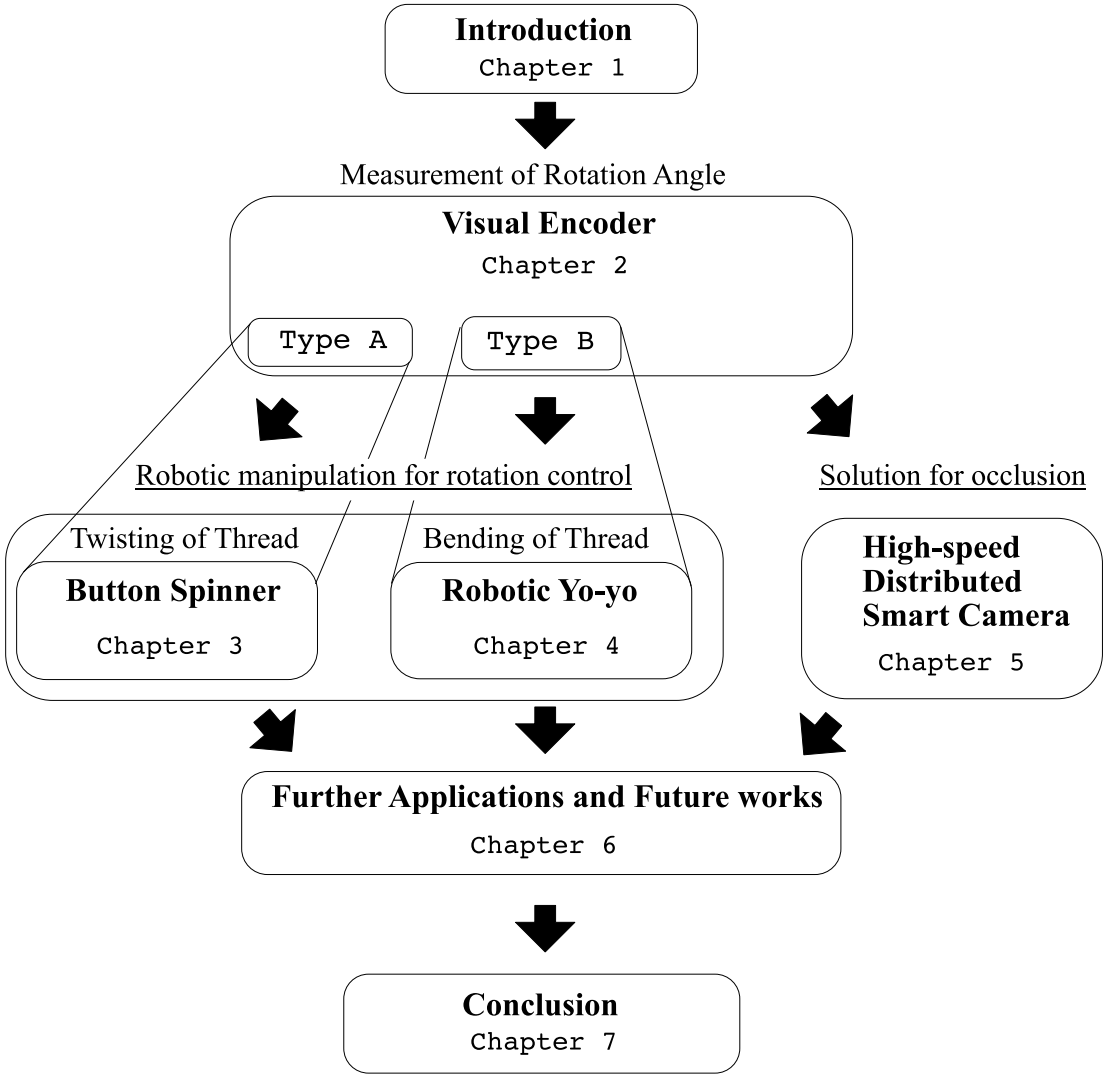

Fig. 1.7 Outline of this research

Chapter 2

A New Rotation Measurement Method: Visual Encoder

The conventional measurement methods for the rotation angle of a rotor, such as the rotary optical encoder, have excellent measurement resolution and accuracy, while its installation and usage are rather limited to the exclusive equipments which have a fixed rotation axis. An alternative method for the rotation angle, which provides more flexible measurement manner, is required for the expanded applications such as remote measurement, robotic manipulation, and so on. In this chapter, 'visual encoder method' is suggested as the alternative method, the most parts of which are published in the author's previous works [1].

2.1 Measurement of Rotation Angle

2.1.1 Conventional Rotary Encoders

As mentioned in previous chapter, the rotor has played an essential role in the many mechanical systems. Therefore, how to control the rotation of the rotor accurately and stably has been one of the most important problems. Understandably, since the feedback control is required to get the desired control result, the measurement quality of the rotation angle becomes a crucial factor. For this reason, various types of rotary encoders to measure the rotation angle have been developed for past several decades. As Dimmler et al. gave a good summary in [9] regarding the encoder types and its features, optical type of rotary encoder has been broadly used among the conventional encoders. The advantages of the optical encoder come from its ability of easy signal processing and high resolution. That's why the

[1] This chapter is rewritten based on the contents in author's published paper [64]

optical encoder is preferred for the primary sensor of many actuators, such as the servo motors. However, in spite of the advantages, the optical encoder also has structural limitations which come from its installation style and the mechanism. For example, the photo sensor as the angle reader must be mounted close to the disc on a rotor in order to allow only small tolerance to the relative position between them. This explains why most of encoders are embedded in the servo actuators to restrict its sensing area to the inside of the encoder.

Then, what will happen if the limitation is broken by separating the sensing part from the actuator volume? It is expected that more flexible applications will be possible by the remote sensing, which leads to the reduction of the weight of the actuators, due to the separation of the sensing part and the actuating part. For instance, a robot arm having multiple links can be controlled without the conventional encoder by introducing the remote sensing method.

2.1.2 Vision-based Methods

Recently, the computer vision has been used for visual tracking of an object [65], with the techniques such as SIFT [14] and SURF [15]. Since the vision-based method is applicable to the object which is moving relatively far from the observer, this method is more suitable for the applications aforementioned. Many researches focusing on the rotation measurement of a rotor using vision-based method have been also reported [21, 18, 17, 19, 20]. Kwon et al. suggested a high resolution angle-sensing mechanism using a gradient color track and RGB sensor [21]. Suzuki et al. reported the measurement method for small-rotation-angle at very high resolution, in the accuracy of 0.4 arcsec [18]. Li et al. measured the rotation angle of a rotor using calibration pattern with spot array [17]. Kadowaki et al. measured the rotation angle of flying golf ball using one-line scanner [19]. Watanabe et al. reported their angle-position measurement method based on the high-speed image processing, and showed that the rotation angle of sphere-shaped marker can be detected at up to 1,200 revolutions per minute (rpm) even under the free motion of the axis of rotation [20]. Above researches have each strong point on following features: cost-effectiveness and easy employment [21], high resolution [18, 17], the fast motion of target object [19], and the ability of detecting high rotation speed and the robustness [20], respectively. However, because of the image processing cost, it was difficult to achieve the high resolution, the ability of high-speed rotation, and the robustness against the fluctuation of the rotation axis, simultaneously.

2.1.3 Visual Encoder as Alternative Method

To overcome the limitations of aforementioned methods, an alternative measurement method of rotation, named as 'visual encoder', is introduced. Visual encoder is able to detect the rotation angle of a rotor in more dynamic environment, using high-speed vision and RGB color pattern aligned on the rotor. Visual encoder shows many advantageous features of aforementioned methods: non-contact, high-resolution, high-speed detection, and robust measurement which is resistant to any free motion and fluctuation of the axis of rotation. Each feature is not new, however, the combination of them can generate new possibilities, since these features can bring the expandability and flexibility of the vision-based method to conventional encoder system, or vice versa. This chapter explains three main parts: the principle of the visual encoder, the solution to improve the measurement resolution, and the experimental verification to confirm the performance of the visual encoder. In the experiments, the maximum measurement speed that is capable by the visual encoder and the measurement resolution of the suggested method is verified, and the robustness of the visual encoder against the fluctuation of the rotation axis is proved in dynamic condition.

2.2 Principle of Visual Encoder

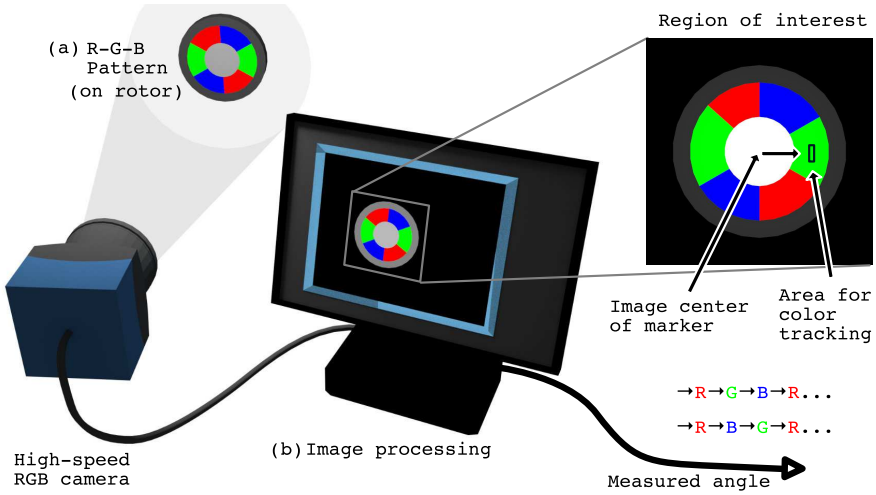

Fig. 2.1 Concept of visual encoder. (a) The shape of marker is based on the disc of the optical encoder but R-G-B colors replace the repeating transparent-opaque pattern. (b) Rotation angle of rotor is measured by the vision-based method. Tracking of the image center of the marker keeps the position of the color detecting point unique. [64]

A combination of the typical disc pattern of the optical encoder and the method based on vision that is attained by the high-speed vision system is the major conception of visual encoder. The RGB pattern on the rotor and high-speed RGB camera that reads the consecutively switching colors in the RGB pattern while the rotor rotates are the two elements of the visual encoder, as shown in Fig. 2.1. Although the visual encoder accommodates the basic design concept of changing pattern in the ordinary optical encoder, it shows different feature in the method of recognizing of the rotation. First of all, the read-out position on the disc is required to be unique in the coordinates with respect to the photosensor, for defining the pattern's rotation on a disc. Since the typical type of optical encoders have steadfast distance between the photosensor and the disc center during the rotation, it is not an issue. On the other hand, in case of visual encoder, it is the image processing which determines the unique point for the measurement, and the fidelity of this process is enhanced by the high-speed vision system. Additionally, before applying the disc pattern which is adapted in the typical optical encoder to the case of visual encoder, it is required to adjust the pattern itself in order to make it recognizable by the camera vision.

2.2.1 Pattern Design by Modifying Optical Disc

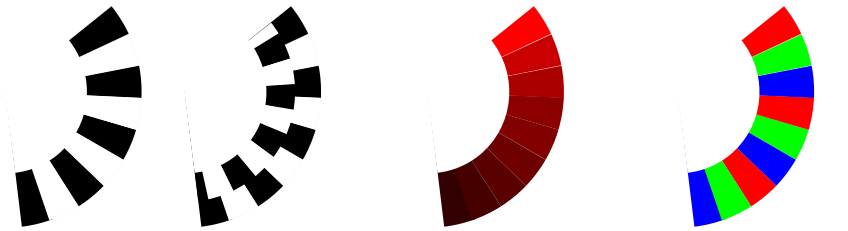

Fig. 2.2 Pattern design of disc. (a) The pattern used on incremental optical encoder. 2-phase type is generally used to detect the rotating angle and the direction of rotation. (b) The color-gradient type. Reflection model of light is needed to measure the accurate rotation angle. (c) Switching RGB type. The structure of 3 states allows detecting of the direction of rotation, as well as the rotation angle. [64]

As shown in Fig. 2.2, there are various types of pattern in order to detect the rotation angle. The 1-phase incremental type that switches between transparent and opaque slit along the outer corner of the optical disc is the simplest pattern. In this type of pattern, the signal from photo sensor shifts between two state, high and low voltage level, according to whether or not the light ray is able to transmitted through the slit. Therefore, the optical

encoder works as calculating the rotation angle using the known number of slits on the disc. The direction of rotation, however, cannot be recognizable in this case, since the changing phase between those two states is independent of the direction of rotation. Hence, incremental pattern with 2 phases is necessary in order to detect the direction of rotation. In case of visual encoder that is developed in this research exploits a color pattern replacing the typical optical pattern, and consists of three basic colors: red, green and blue (RGB). On the circumference of the disc accommodates these three colors in sequence, and the RGB vision camera is placed to capture the reflected light from the disc. In this case, it is possible to detect not only the rotation angle of the disc but also the direction of rotation simultaneously, as taking advantage from the fact that switching RGB color pattern shows one-phase as well as three states. Although it follows the same manner to calculate while it calculates the rotation angle from the counted number of changing states, detecting the sequence of changing color makes it possible to recognize the direction of rotation at the same time. Unlike the case of optical encoder and color-gradient model [21] which exploit the intensity of light in order to measure the rotation angle, switching RGB type does not require the reflection model, because changing three basic colors directly represent the state of the rotation. Moreover, switching RGB color pattern features the robustness against lighting condition which influences surrounding brightness, in that three basic color components are at all times observed by camera, and it only requires comparison among three colors to define the dominant color. In fact, as RGB color space is converted into the HSV color space where a sort of normalized color hue represents the color properties, which decreases the influences from the brightness of light.

2.2.2 Two Types of RGB Marker

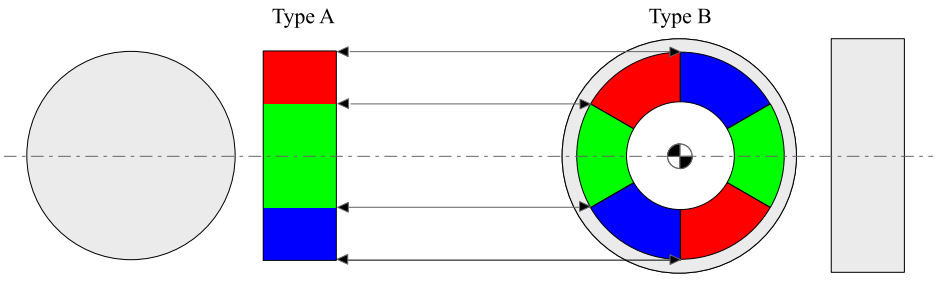

Fig. 2.3 Two types of RGB marker

In this research, two different types of switching RGB patterns for the visual encoder are exploited. As shown in Fig. 2.3, type A accommodates the switching RGB pattern at

the circumference of the rotor, where the rotation axis is perpendicular to the direction of the camera. In this case, the RGB patterns are prepared in a strip, to be attached along the side of the rotor. Visual encoder of type A is adapted in the button spinner. On the other hand, in type B, the switching RGB pattern is located on the surface of the rotor, where the rotation axis is parallel to the direction of the camera. Type B visual encoder is attached on the surface of yo-yo. Although these two types of visual encoders show different features in structure and the direction of the rotation to the camera, both types share identical principle in that one type can be considered to be a projection of the other type.

2.2.3 Angle Measurement by Vision-based Method

Based on the vision method, the rotation angle of a rotor is measured using visual encoder, and comprises following two major parts: (1) The matching between the color disc and the camera sensor, (2) Color extraction at the detected point in order to calculate the rotation angle. Following two chapters explain these two parts in detail, and the entire process is described in Fig. 2.4.

Position matching of camera sensor and the color disc

From the geometrical point of view, the intersecting point of surface plane of the rotating disc and the rotation axis in three dimensional coordinate is projected onto the centroidal point of the disc in the image plane. The centroid of the disc works as a basis of the coordinates while tracking the rotation, since the centroidal point is uniquely defined. Performing the object extraction using the background subtraction, binarization, and calculation of the image moment from the binary image is the simplest way to obtain the position of the centroid in the image. In order to avoid any complexity in the object extraction, black background can be applied.

The distinctive disc pattern that is newly developed in this research can be recognized easily by camera vision and can be extracted from the black background, because it comprises three basic colors, which are represented by unique hues. The hue values of red, green and blue, respectively, are near 0 (or 360), 120 and 240 degrees. Also, the saturation of these basic colors show very high in HSV color space. Since the central area of the disc is white color, the pixel intensity of the center can be exploited as an alternative basis to shorten the calculation cost. From the image thresholding, the binary image can be easily obtained, after capturing the image. Then, the centroidal point $\mathrm{C}(x_c, y_c)$ is calculated from the binary image as shown in Eq. (2.1).

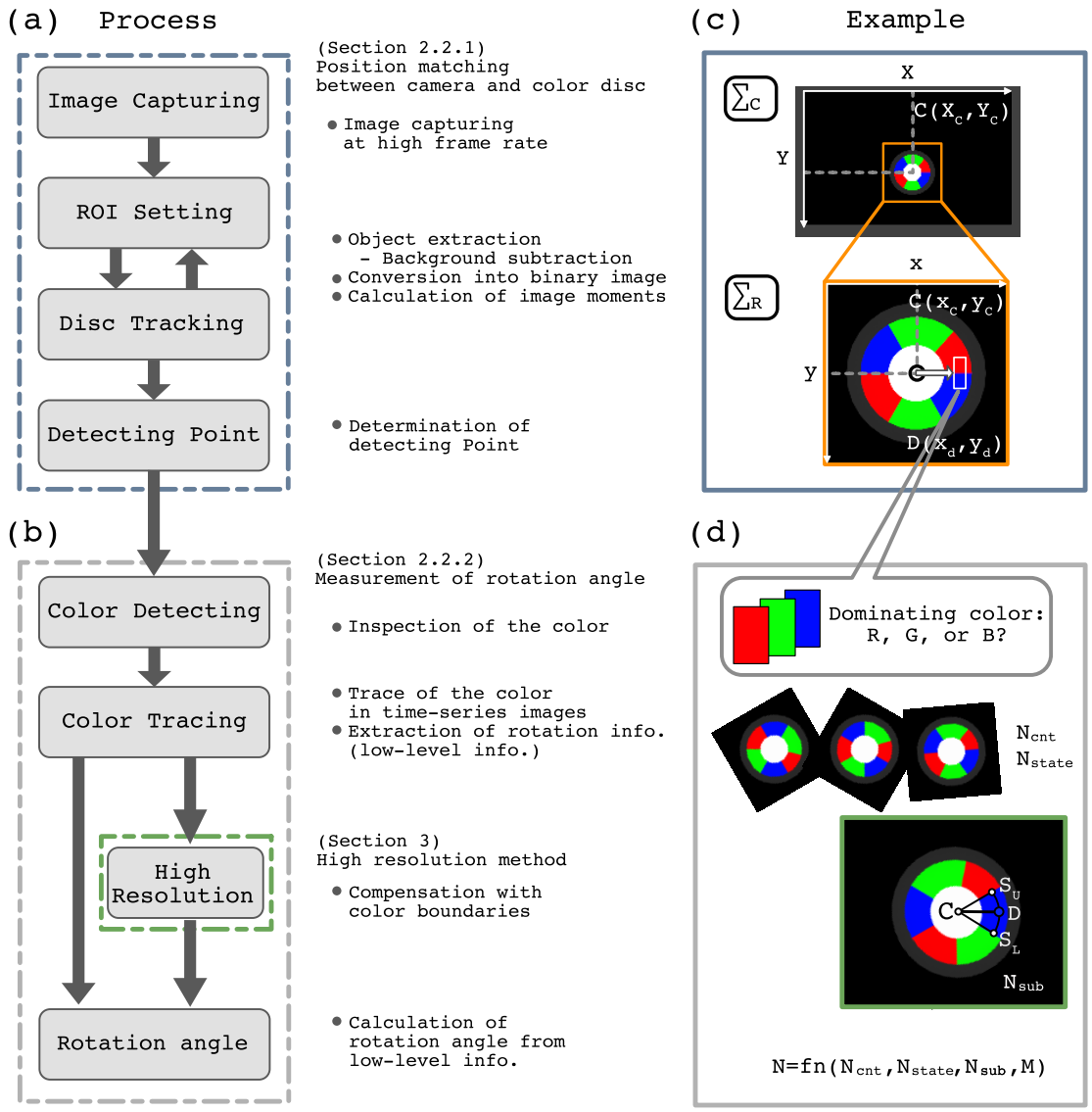

Fig. 2.4 Flow from image capturing to the calculation of the rotation angle. (a) Determination process to keep the position of detecting point unique. A pixel shifted from the centroid of the object area in the image plane is inspected to detect the dominant color on itself. ROI is set to reduce the calculation cost in order to increase the sampling rate. (b) Extraction process to acquire the rotation variables. N_{cnt} and N_{state} indicate the number that the rotor rotates in turns and sub-turns, respectively. High resolution method can be used to enhance the measurement resolution of the rotation angle and N_{sub} is the variable for the process. The rotation angle N is calculated from N_{cnt}, N_{state} (and N_{sub} in case of high resolution). (c) Example of (a). (d) Example of (b). [64]

$$\mathrm{C}(x_c, y_c) = \left(\frac{\mathrm{M}_{10}}{\mathrm{M}_{00}}, \frac{\mathrm{M}_{01}}{\mathrm{M}_{00}} \right) \tag{2.1}$$

where M_{pq} indicates the image moment of order $(p+q)$ when p and q are non-negative integers. M_{pq} can be calculated as in Eq. (2.2), when $\mathrm{I}(x,y)$ is the intensity of pixel (x,y) in the image coordinates.

Since zero or one is applied to $\mathrm{I}(x,y)$ in the binary image, the result from Eq. (2.1) refers to the centroid.

$$\mathrm{M}_{pq} = \sum_x \sum_y x^p y^q \mathrm{I}(x,y) \tag{2.2}$$

The line-scanning from the centroidal point determines the detecting point $D(x_d, y_d)$ for the detection of color. Cartesian coordinates which is translated from the image coordinates with the translation of its origin to the centroidal point $C(x_c, y_c)$ is chosen as the base coordinates in order to detect the rotation. To determine the two color boundaries on the scanned line, line-scanning is carried out from $C(x_c, y_c)$ along the X direction in the image coordinates. As shown in Fig. 2.1, it is reasonable to choose the center point of the two boundary points as the detecting point. By detecting and tracking the color on the detecting point $D(x_d, y_d)$, the rotation angle of the rotor is measured.

Measurement of rotation angle using visual encoder

Visual encoder features quite simple mechanism in measuring the rotation angle, as illustrated in Fig. 2.5. Let N_{cnt} and N_{state}, respectively, be the counters that show the number of revolution the disc rotated and the number of color blocks passed through. The number of color blocks that are arranged along the disc's circumference is represented as M. The direction of rotation is recognized when the color read by detecting point switched, since the RGB color blocks are sequentially arranged. For instance, in case the sequence of the color block follows R $\rightarrow$ G $\rightarrow$ B and this sequence is defined as forward direction of rotation, the switching color read by detecting point such as B $\rightarrow$ G $\rightarrow$ R is recognized as reverse direction of rotation. Therefore, N_{state} simultaneously counts up or down by one, according to the direction of rotation recognized by the detecting point. In case N_{state} is equal to M, N_{cnt} increases or decreases by one according to the direction of rotation while N_{state} resets to zero, because it implies that the disc finished one revolution. Eq. (2.3) shows the calculation of the rotation angle of the disc.

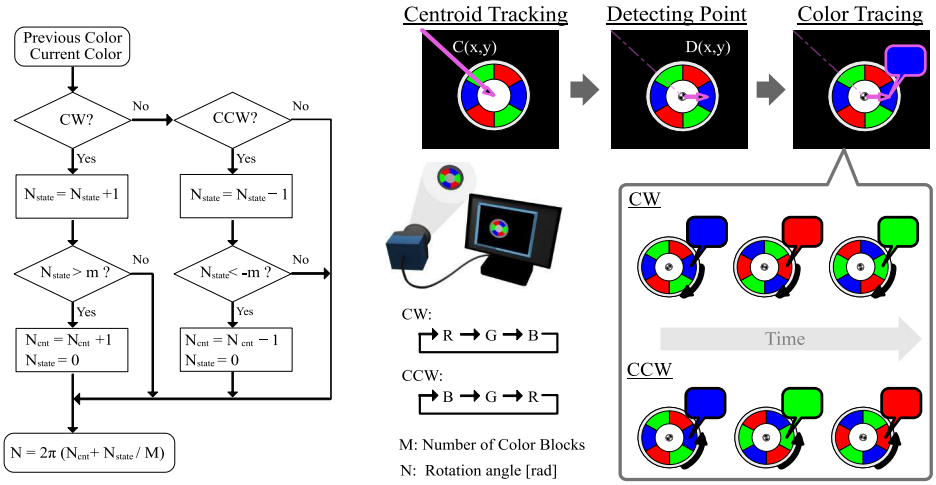

Fig. 2.5 Calculation of the rotation angle for visual encoder

$$N\ [\text{rad}] = 2\pi\{N_{cnt} + (N_{state}/M)\} \tag{2.3}$$

Note that the term M in the right side determines the measurement resolution. Therefore, higher measurement resolution is guaranteed by enlarging M , and the $1/M[rev]$ is equal to the actual resolution. Theoretically, in accordance with the purpose of user, M can be designed so long as the color printer resolution allows. Empirically, however, in many cases the limitation in the sample rate of camera vision confines M up to certain limited value. In order not to misrecognize the direction of rotation, it is not allowable to detecting point to skip the color block. Namely, sequential colors as arranged originally should be read between the consecutive frames by the detecting point in a sample time, the frame rate for the camera vision. Therefore, the maximum speed of rotation for the rotor, V_{max}, is the determined by the frame rate, and the rotation angle can be measured by the visual encoder as shown in the Eq. (2.4).

$$V_{max}\ [\text{rpm}] = \frac{Q\ [\text{frame/sec}]}{M\ [\text{frame/rev}]} \times 60\ [\text{sec/min}] \tag{2.4}$$

where Q refers to the frame rate of the camera, and the number of color block M is the minimum requirement to avoid skipping in detection. The higher Q permits the lower M in case of constant V_{max}, since Q influences proportionally to V_{max}. For this reason, high-speed camera is applied to the visual encoder system in order to attain the high resolution. For example, in case a high-speed camera providing with 1k fps as a frame rate and the V_{max} desired is equal to 1,000 rpm, the resolution $(1/M)$ is $1/60$. As shown in Fig. 2.6, higher

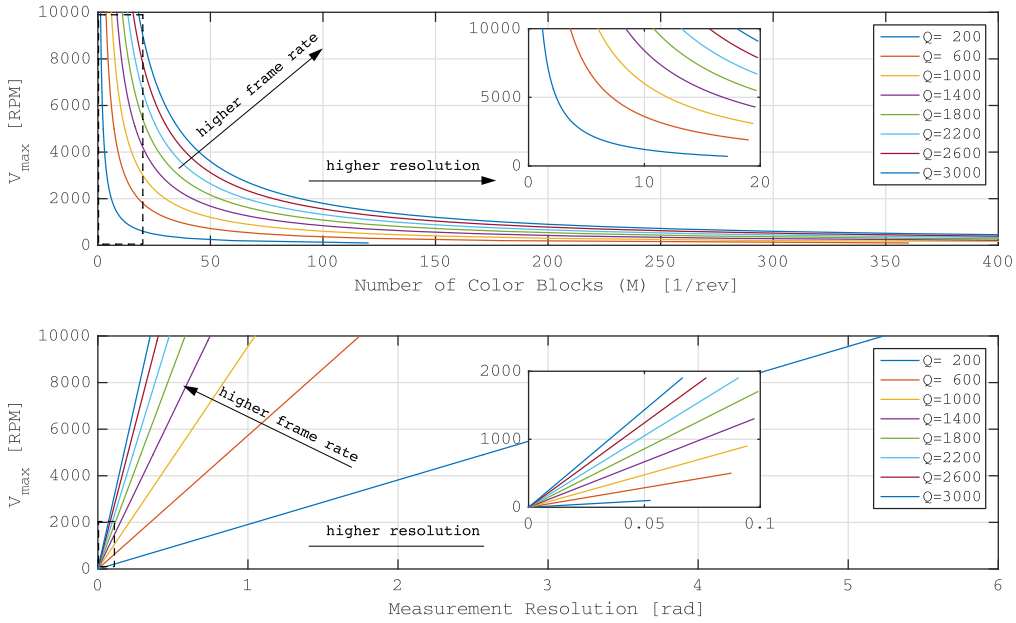

Fig. 2.6 The relation between M and V_{max} when Q varies. M is the number of color blocks on the disc, and V_{max} is the maximum rotation speed of the rotor that visual encoder can measure the rotation. Q represents the frame rate of the camera (fps) used in visual encoder. The higher Q helps to get the higher resolution in measurement of the rotation angle.

Q apparently contributes to achieve the higher resolution. Users can exploit the map of $M - V_{max} - Q$ in choosing the parameters when they design the visual encoder.

2.3 High Resolution Method for Visual Encoder

In the previous example where $Q = 1k$ [fps] and $V_{max} = 1,000$ [rpm], the resolution was $1/60$ revolution, which corresponds to 6 degrees. In fact, the resolution of $1/60$ revolution is very low and hard to be accepted in many cases, even though there exists a trade-off between the measurement resolution and the maximum speed in case of fixed frame rate of camera. Therefore, in order to enhance the resolution, the compensation method is required. Here, a high-resolution method (HR) which searches the color boundaries of both forward and backward directions is suggested. First of all, an imaginary curve is drawn at the current detecting point, and it approximately overlaps to the trajectory of the position on the disc drawn in the past, with the anticipated trajectory in the future. The imaginary curve draws an arc, in case the image plane of the camera vision is almost perpendicular to the axis of rotation. As shown in Fig. 2.4 (d), consider that the centroid $C(x_c, y_c)$ is located on

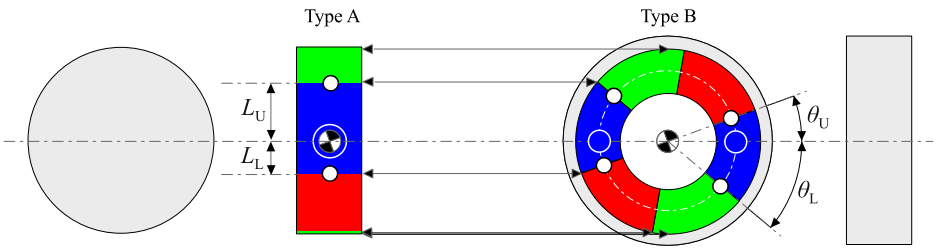

Fig. 2.7 High-resolution method for two marker types

the center of the arc drawn by the detecting point $D(x_d, y_d)$, and the $S(x_s, y_s)$ indicates the searching point. In this case, the three points are related as described in the following matrix equation.

$$\begin{bmatrix} x_s \\ y_s \end{bmatrix} = \begin{bmatrix} \cos\theta & -\sin\theta \\ \sin\theta & \cos\theta \end{bmatrix} \begin{bmatrix} x_d - x_c \\ y_d - y_c \end{bmatrix} + \begin{bmatrix} x_c \\ y_c \end{bmatrix} \tag{2.5}$$

where θ $(-2\pi/M < \theta < 2\pi/M)$ is the angle between $\angle SCD$.

The color determined on $S(x_s, y_s)$ is inspected as θ is changed from zero to the upper limit, until the color is switched from the detected color on $D(x_d, y_d)$. Let the position be $S_U(x_{su}, y_{su})$ and the angle be θ_U. Also, $S_L(x_{sl}, y_{sl})$ and θ_L are determined by the identical process for lower limit of θ. Eq. (2.6) can be obtained by modifying Eq. (2.3), with θ_U and θ_L.

$$N[\text{rad}] = 2\pi\{N_{cnt} + (N_{state}/M) + N_{dir}(\theta_U/(\theta_U + \theta_L))/M\} \tag{2.6}$$

where N_{dir} varies upon the direction of the rotation as following.

$$N_{dir} = \mathbf{sgn}(N_i - N_{i-1}) \tag{2.7}$$

The rotation angle at discrete time i and $i-1$ are described by N_i and N_{i-1}, respectively. The resolution is enhanced by the factor $\theta_U/(\theta_U + \theta_L)$ as noted in the Eq. (2.6). It is reasonable to verify the performance of visual encoder empirically, instead of theoretical evaluation, since this factor is dependent upon the resolution of camera image as well as the size of the color blocks in the image plane. In case of the type A marker, Eq. (2.6) can be modified as following.

$$N[\text{rad}] = 2\pi\{N_{cnt} + (N_{state}/M) + N_{dir}(L_U/(L_U + L_L))/M\} \tag{2.8}$$

2.4 Experiment Results

2.4.1 Experiment Setup

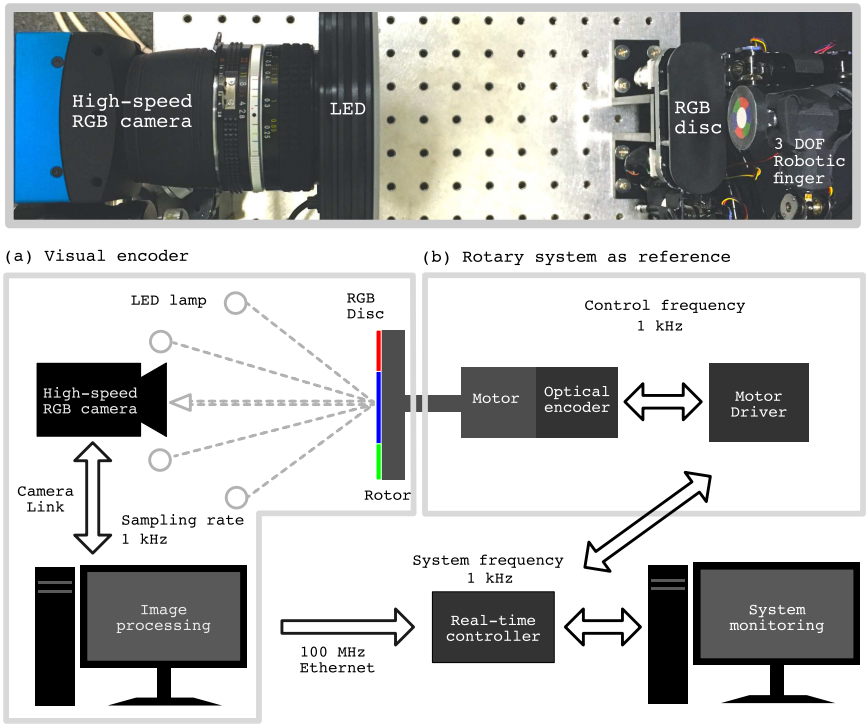

Fig. 2.8 Testbed of visual encoder with real-time controller. The whole parts of this system work at 1 kHz, as both of the sampling rate and the control frequency. (a) Visual encoder with high-speed camera of 1,000 fps. (b) Reference system with optical encoder. [64]

In order to verify the performance of the visual encoder, two major experiments were conducted. The first experiment verifies the performance of visual encoder, under the same condition of the conventional encoders where the rotation axis is fixed. In the second experiment, the rotation axis is intendedly fluctuated rather than fixed, and the rotation angle of visual encoder is measured to prove the robustness of the visual encoder. With the previous conventional optical encoders, the condition of second experiment has not been able to be dealt with. Fig. 2.8 describes the testbed that is built for the experiment, and it consists of the visual encoder and the reference rotary system. The visual encoder system comprises a high-speed camera, a rotary disc, and a PC in order to process images. A high-speed RGB camera (Mikrotron EoSens MC1363) with the camera-link interface is applied to the actual

system and images are taken at 1,000 fps with 400 $\times$ 600 pixels resolution. Within 1 millisecond, the image capturing through high-speed camera and the image processing via PC were accomplished, and via 100 Mbps of ethernet the calculated rotation angle was shared using a real-time controller. The PC accommodates Intel Xeon E5-2609 processor of 2.4 GHz base frequency, and adapted Windows 7 as an operating system. The color pattern is printed and attached to the surface of the rotary disc, and the camera is placed to face the disc. In both experiments, identical numbers of color block ($M = 6$) are applied. In order to secure enough brightness to the measurement system, around the camera lens placed the a ring-type LED lamps for supplying sufficient light.

To detect the referential rotation angle of a rotor, the typical servo actuator consisting of an optical encoder and an electric motor is adapted. dSpace, a real-time controller, is connected to the motor driver which controls the rotary system. The real-time controller works as operating at 1 kHz of the system frequency and receives the measured rotation angle from the visual encoder via 100 Mbps ethernet. The frequency of receiving was 1 kHz as well and the real-time controller synchronizes the entire processes at the system frequency.

Since the visual encoder is a sensor based on the counter of incremental type, the stability of measurement is significant. If there occurs a mistake in counting for any reason, it causes the measurement error and this continues and accumulates from the moment of failure, except for the case where the error is removed by adapting other references, for example the Z-phase of the optical encoder. Moreover, as the rotor rotates faster, it shows the higher probability of failure, and the motion blur appears between successive colors in the visual encoder which makes it look blended. Applying the high-speed camera, however, can resolve such problem by reducing the motion blur as well as the failures in counting.

2.4.2 Accuracy Verification at Various Speeds

Two kind of experiments are conducted to verify the measurement stability and the accuracy of the visual encoder. In the first experiment, various rotating speeds were kept constant while the rotation angle of the rotor is measured. In the second experiment, the speed of rotor rotation is accelerated to the maximum speed.

Rotation at Various Constant Speeds

In this experiment, the rotor experiences both forward and backward rotation for 10 seconds at various constant rotating speed, and the comparison between the rotation angles measured

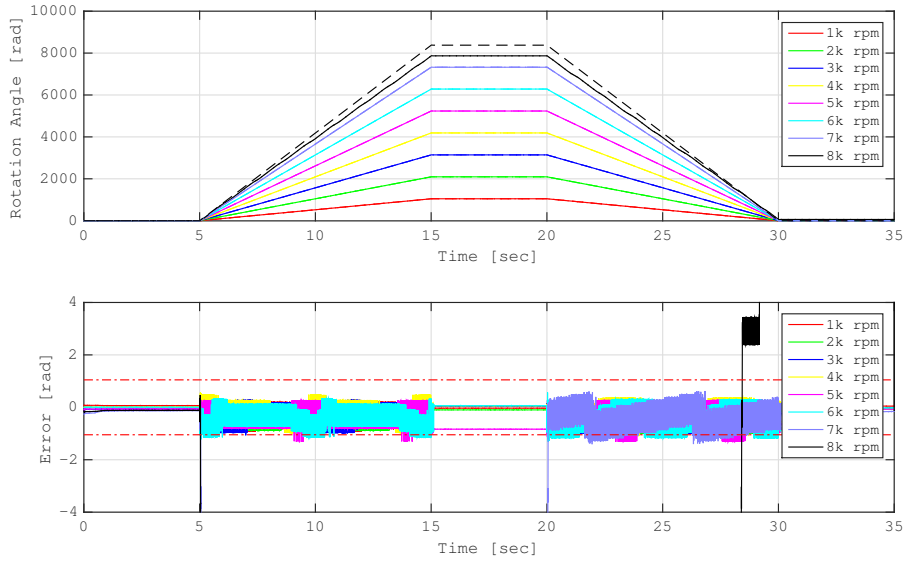

Fig. 2.9 Measurement of rotation angle at constant speed of the rotor. (upper) Each dashed line indicates the reference angle measured by the optical encoder, and each continuous line by the visual encoder, at each rotation speed [rpm]. (lower) Errors between the two measurements. Two red dashed lines indicate the designed resolution. As long as the errors stay inside two lines, the measurement using the visual encoder is stable. [64]

by visual encoder and the conventional optical encoder was conducted. With an increment of 1,000 rpm, the rotation speed is tested from 1,000 rpm to 8,000 rpm. Fig. 2.9 shows the successful measurement of visual encoder up to 7,000 rpm, as it correctly measures the rotation angle within the designed resolution. Each dashed line at various speeds indicates the reference rotation angle as a true value, and the continuous lines show the rotation angle measured by visual encoder in the experiment, which is wholly overlapped to the reference at respective case. The number of color pattern used was six ($M = 6$), and the resolution was equal to $\pi/3$. In the graph of error along time, two red dashed lines indicate the tolerance in measurement. Except for the failed case when the rotation speed is 8,000 rpm, majority of errors exist between two lines.

Rotation with Speed Acceleration

In the second experiment, the rotation speed of the rotor is accelerated up to the maximum speed that is generated by the actuator, 10,000 rpm. To verify the performance of the visual encoder, the visual encoder and the conventional optical encoder read the rotation angle of

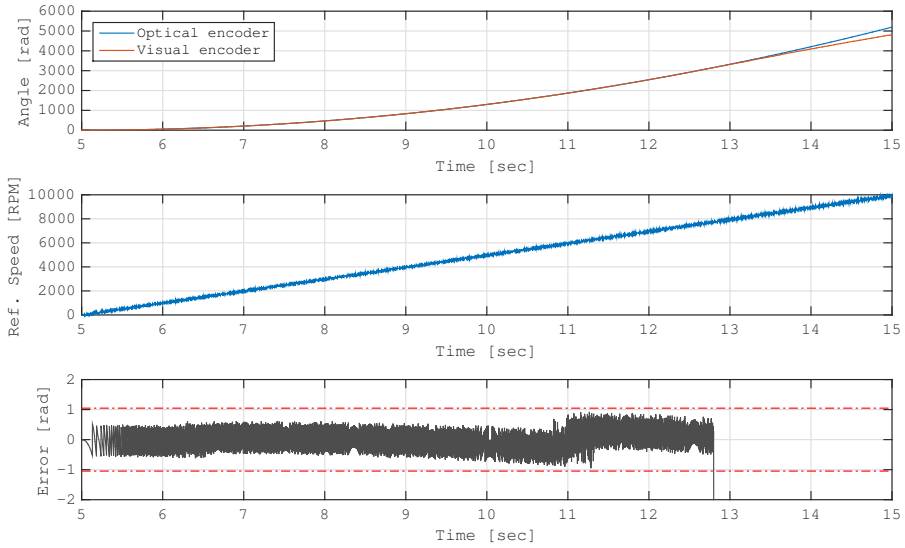

Fig. 2.10 Acceleration test to verify the maximum detectable speed. (upper) The rotation angle measured by the optical encoder (blue) as ground truth, and by the visual encoder (red). (middle) Reference rotor was rotated at constant acceleration. (lower) As the rotation speed is increased, the error can exceed the tolerance at a certain moment (here, at 12.8 sec). This results in the measurement failure (at 7740 rpm). [64]

the rotor, simultaneously. The limitation of speed can be more precisely checked in the result graph, as shown in Fig. 2.10.

During the reference speed is pulled up to 10,000 rpm, at a certain speed the failure in measurement appears. The experimental result showed that the limitation of speed is around 8,000 rpm, unlike the limitation that is theoretically calculated as 10,000 rpm, from Eq. (2.4) in case $M = 6$ and $Q = 1,000$. The reduced limitation in speed is considered to be caused by the motion blur, which mixes the color that hinders detecting point from determining the current color. This kind of problem can be resolved and the maximum speed can be increased by using higher frame rate with shorter exposure time.

2.4.3 Verification of Robustness and High Resolution Method

To verify the robustness of visual encoder again the fluctuation of rotation axis, sinusoidal oscillations are intendedly introduced while measuring the rotation angle, in X and Y direction in the image coordinates. As shown in Fig. 2.11, a circle is drawn by the oscillations as a trajectory of the rotation axis, for the purpose of making the shape of trajectory more complex. In order to draw a circular motion, a robotic finger equipped with three joints is

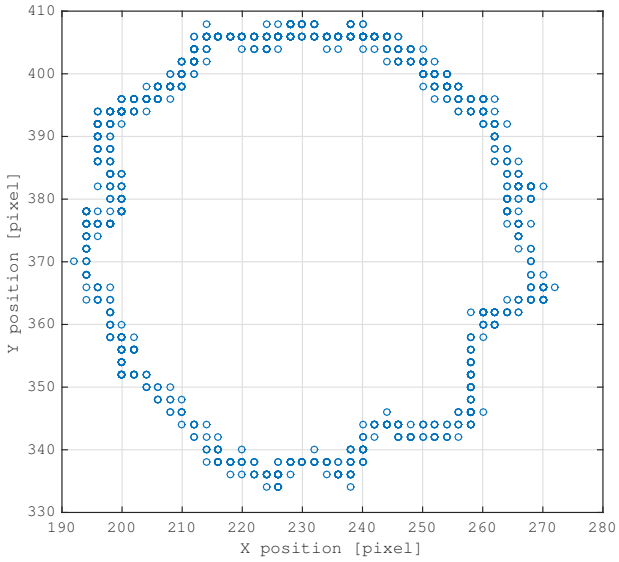

Fig. 2.11 The motion of the rotation axis in fluctuation. When sinusoidal oscillation is introduced in X and Y direction, the trajectory of the rotation axis draws a circle. The amplitude and the frequency were 5 mm and 1 Hz, respectively. The fluctuation in the motion was intentionally generated, to test the robustness of the visual encoder. [64]

adopted, and the visual encoder is attached on the robotic finger tip. The amplitude and the frequency of oscillation in the experiment, respectively, were 5 mm and 1 Hz. With the identical condition applied in the previous experiment, visual encoder measured two rotation speeds of the rotor: 1,000 rpm and 6,000 rpm. Fig. 2.12. shows the result of measurement when the rotation speed was 6,000 rpm. Note that all the errors stay inside the measurement tolerance, which verifies the correct work done by visual encoder even with the disturbance such as motion and fluctuation.

Also, the red line in Fig. 2.12 represents the result from the verification of high resolution method (HR). Although the quantization error exists in case of normal measurement method (blue line), the magnified view in the upper graph shows that HR includes less of such error, suggesting that HR contributes to the reduction of quantization error. Table. 2.1 shows the comparison between two experiment results that are conducted with HR and normal measurement. In high resolution method, the measurement error was notably reduced and the resolution of measurement is improved by more than 10 times. Fig. 2.13 shows the consecutive images that are taken in actual experiment and applied to the image processing for the HR.

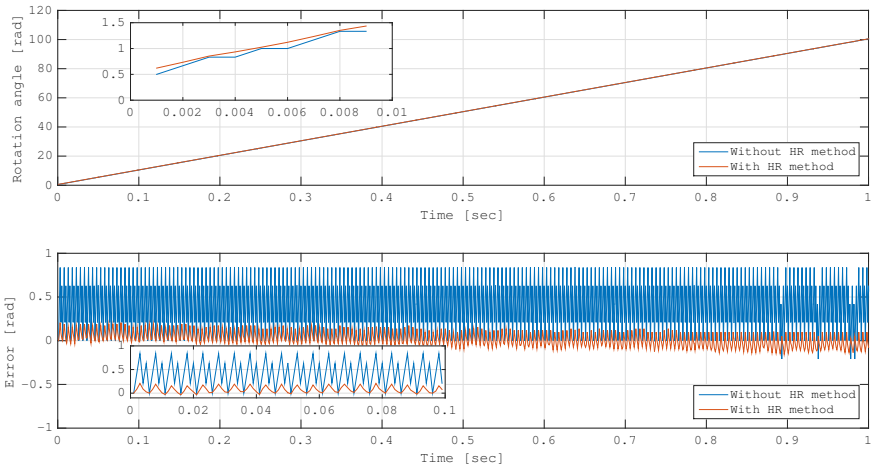

Fig. 2.12 Rotation angle and the measurement error during the motion shown in Fig. 2.11. (upper) The rotation angle of the rotor measured by the visual encoder, at 6,000 rpm. Magnified graph shows that the high resolution method improved the measurement accuracy. (lower) The measurement error was substantially reduced by the high resolution method. [64]

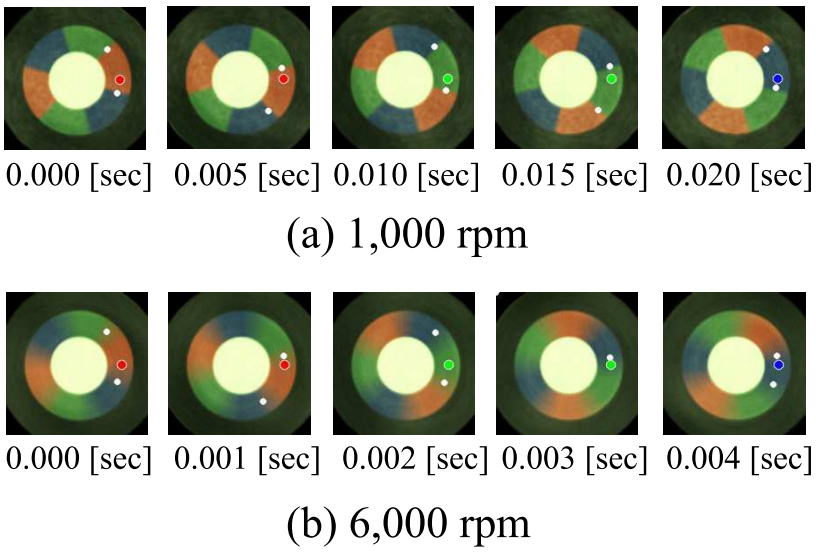

Fig. 2.13 Sequential images of color pattern on the disc in image processing. Images were taken at the rotation speed of (a) 1,000 rpm and (b) 6,000 rpm, respectively. A color-filled dot indicates the detecting point, and two white dots represent S_U and S_L in section 2.3. [64]

Table 2.1 Performance of high resolution method (HR). [64]

Rotation speed [rpm]		with HR [rad]	without HR [rad]
1,000	mean	-0.0499	-0.4388
	std.	0.0197	0.3048
6,000	mean	0.0187	0.4147
	std.	0.0777	0.2978

2.5 Discussion

2.5.1 Advantages of switching RGB pattern

The switching RGB pattern is superior to the other alternative patterns, as shown in Fig. 2.2, in terms of the robustness against the change of the external lightning condition. Consider that the brightness of environmental light fluctuates and the intensity of measured color also varies during a measurement, as shown in Fig. 2.14. In this case, when using the monochrome or the color gradient pattern, the threshold level for the signal processing is required to be adjusted according to the change of brightness. Otherwise, the measurement error will be increased, as shown in Fig. 2.14 (B) and (C). On the other hand, since the switching RGB pattern exploits the hue in HSV color space which maintains the same value, as long as the color of light is not changed, it does not require any adjustment of threshold intensity regardless of the current brightness of the light, as shown in Fig. 2.14 (D) and (E). Therefore, more reliable measurement is guaranteed when using switching RGB pattern than using monochrome or color gradient pattern.

In addition, the switching RGB pattern contributes to accurate calculation of the centroid of the rotor which affects the position of the detecting point, and reduces the measurement error occurred from the misestimation of the current detecting point. Particularly, this feature plays a significant role in the case of the color markers in type A, as mentioned in 2.2.2, where the rotation axis of the rotor crosses the optical axis of the camera perpendicularly. As shown in Fig. 2.15, in the case of the monochrome pattern, since the black region in the pattern cannot be distinguished from the background region, the centroid of the rotor acquired by calculating image moment from the binary image varies depending on the rotation of the rotor. This fluctuation of the centroid results in the potential measurement errors caused by the misreading of the detecting point, which is remarkable at high-speed rotation. However, in the case of using switching RGB pattern, the region of rotor can be easily recognized and extracted from the black background, and there has no such side effect as in monochrome pattern.

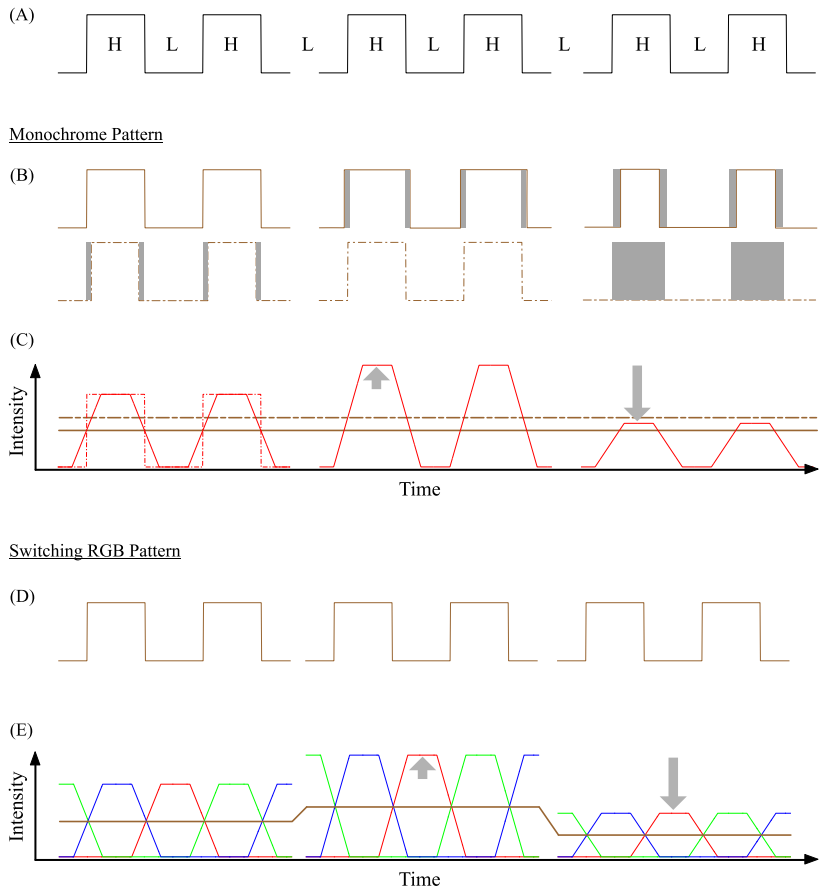

Fig. 2.14 Influence of environmental light. The intensity of measured signal varies according to the brightness of the environmental light. (A) Digital signal as ground truth. **Monochrome pattern**: (B) The signal estimated by the corresponding threshold intensity. The gray region indicates the estimation error. (C) The intensity of measured signal and the threshold level (brown lines). The slope of intensity is generated by the motion blur at the boundary of adjacent two pattern blocks. **Switching RGB pattern**: (D) The signal estimated by the hue level. (E) The intensity of the RGB colors and the apparent threshold. The apparent threshold level is automatically adjusted.

2.5.2 Camera specification and performance of visual encoder

The performance of the visual encoder method is closely related to the camera specification, such as the shutter speed and the resolution of image sensor (or camera resolution). The influence of the shutter speed appears in explicit form, as shown in Eq. (2.4). On the other hand, the camera resolution affects the measurement resolution in indirect form when applying the high-resolution method. The latter term in Eq. 2.6 includes the angle parameters such as θ_U and θ_L, which are directly affected by the discrete pixel distance from the

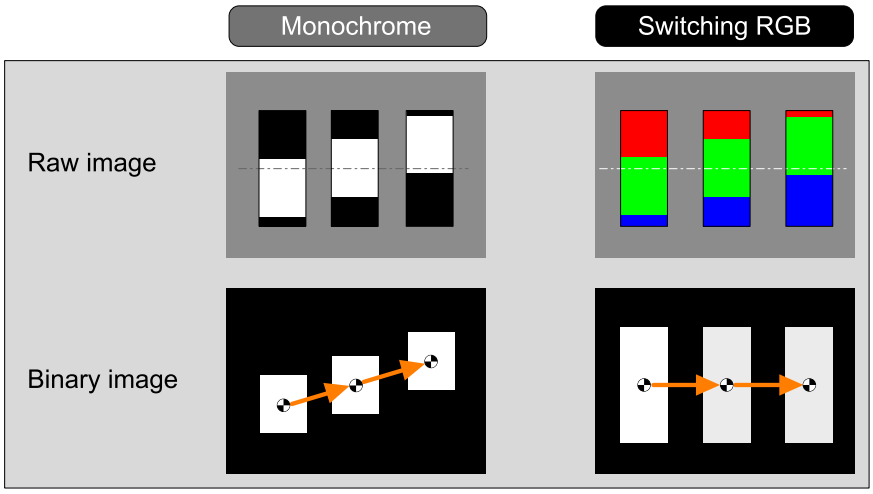

Fig. 2.15 Marker types and calculation of the centroid of a rotating marker

detecting point to the boundary points, and from the centroid to the detecting point in the calculating process. Therefore, the measurement resolution of the high-resolution method is proportional to the camera resolution. Strictly speaking, the coarse resolution of the visual encoder method represented by $1/M$ is also influenced by the camera resolution, especially when the marker size in a camera image is small and the huge number of color patterns are used. For this reason, the marker size and the camera resolution should be carefully considered. However, for the general use, if the reciprocal of the distance from the centroid to the detecting point in pixel unit is less than $1/M$ as a minimum condition, visual encoder method works as expected.

2.6 Summary

A new measurement method, 'Visual encoder' is introduced as a newly developed method for measuring the rotation angle of a rotor with a high resolution in this chapter. Also, the performance of visual encoder is proved with experimental verification. In principle, visual encoder is founded on the conventional optical encoder and the vision-based method, and is equipped with the strong points of both methods: non-contact, high-resolution, and robustness against the motion and fluctuation of the rotation axis. Beyond the simple combination of two existing methods, the visual encoder provides with new possibility to many research fields including the robotic control based on visual serving and the sensing of high speed rotor that is located remotely. Also in the previous works [66, 67], a new robotic manipulation

through flexible thread was able to be performed by applying the principle of visual encoder, even though elementary sensing mechanism and the different type of patterns were exploited. In accordance with the intention and purpose of user, the performance of the visual encoder can be modified by designing the color pattern of the disc. The visual encoder tested in this chapter achieved correct measurement of rotation angle up to about 8,000 rpm in case of fixed rotation axis, and up to 6,000 rpm in real time even under the condition of fluctuating rotation axis. Furthermore, it is confirmed that high resolution method contributes to the improvement of resolution, by more than 10 times compared to the measurement result that is conducted without high resolution method.

Chapter 3

Rotation Control through Thread-Twisting: Robotic Button Spinner

In this chapter, the rotation control of a rotor through the twisting of flexible thread by robotic manipulator is discussed with the geometric model of twisted thread. The twisting of thread has an excellent transmission structure to transfer the power and convert a kind of motion from linear to rotation, or vice versa. Here, the rotation control regarding the twisted thread is studied with the representative application, the button spinner [1]. The visual encoder method introduced in the previous chapter is applied to the feedback control for the rotation of the robotic button spinner.

3.1 Introduction

For robotics communities, the manipulation of objects via flexible objects, such as thread, has been a challenging tasks. In fact, controlling the flexible objects is difficult not only for robots, but even human takes time to achieve, in case of whipping a rod or playing a yo-yo [41, 46]. The difficulty is originated from the fact that flexible objects may consist of different properties such as density and stiffness, which can be changed easily when the external force is applied. In case of thread, for example, it is obvious that even the diameter of the cross section is not uniform throughout the entire length, and is easily changed according

[1] This chapter is rewritten based on the contents in author's published paper [66, 67]

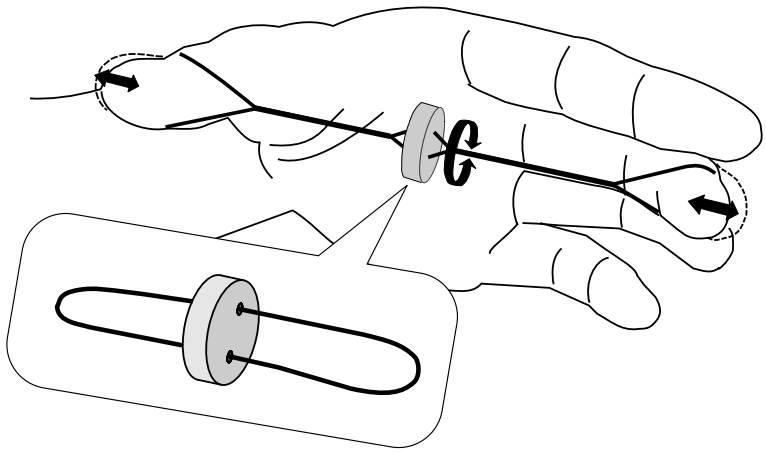

Fig. 3.1 Button spinner (One-handed manipulation) [66]

to the applied tension. Such a non-linearity that appears in the flexible object makes the modeling complicated and inhibit from the determining the control parameters.

However, several attempts [56–58] to solve the problems in regard to the manipulation of the flexible object are reported, as increasing the processing speed of the control system, and as adapting applying high-speed sensor and actuator. Among these strategies, handling the flexible object as a linear system by adapting the high-speed sensing can simplify the complicated non-linear system. For instance, in Yamakawa's research about manipulation of flexible ribbon [58], he suggested the linearly approximated model with short control time to treat the ribbon as a thread-like object. In this work, he proved that constant velocity and high-speed motion are the crucial conditions to make any shape with ribbon. This method is considered to be effective when control the bending of the flexible object itself.

In this chapter, the rotation control of the button spinner is presented as an example task, where the rotor is hung by the thread at the center of the system. Using the visual encoder method shown in the previous chapter, the rotation of the rotor is detected and controlled, as a target object that is rotating high-speed via twisted thread. Before describing the details, the system of button spinner is explained first.

Button spinner is a traditional hand toy, as shown in Fig. 3.1, comprises a button and a thread loop. The button is located at the center of the system, as the thread loop passes through the two holes of the button. To play the button spinner, two finger tips are placed inside each end of the thread loop, and then the thread is twisted by turning the button a few turns. After the initial state is set, pulling two fingers at the same time allows the button to

spin. The repeated periodic motion of pulling and restoring of the fingers keep the button spinning, which continues the playing of the button spinner. Now the button in this system is referred as a rotor, for the generality. The interesting point in the button spinner is that the shape of motion is changed, from linear finger motion to the rotation of the rotor. Practically, from 1 to 2 Hz of linear finger motion produces almost over six thousands rpm (revolutions per minute) of the rotation of the rotor.

In this chapter, although the force feedback is not applied here, firstly the button spinner system is analyzed with a twisted thread model, considering the changes in geometry of the thread and the rotor when the thread is twisted. Then, as a control strategy, the visual encoder method is applied to measure the rotation position and the rotation angle, in order to prove the robustness of the measurement method that does not require accurate model.

3.2 Geometric Model of Twisting Thread

As mentioned previously, the force feedback is not applied here in the manipulation of the button spinner. Instead, the angular position of the rotor is measured using visual feedback, rather than sensing the tension of the thread. However, the estimation of the force is required to design the physical model of the system. Therefore, the tension of the thread from the length of the thread is calculated, based on the general spring model where the force is proportional to the changes in the length of thread. There have been reported many researches regarding simulation models of wire deformation. For example, Servin et al. [33] describes a visual interactive simulation models of wires. Even though the model designed by him works well, it is not fast enough to be applied in the high-speed robotic control. As a compact model dealing with a twisted pair of thread, the researches such as [24] , [26] and [22] were reported. However, these models cannot handle the shape of threads that appear in the button spinner.

Therefore, a novel model for a twisted pair of threads that can be applied to the button spinner is presented here. In order to simplify this model, the following four assumptions are suggested.

- Assumptions

    1. The mass of the thread can be ignored.
    2. The elasticity of the thread can be ignored when determining the geometry of the twist.

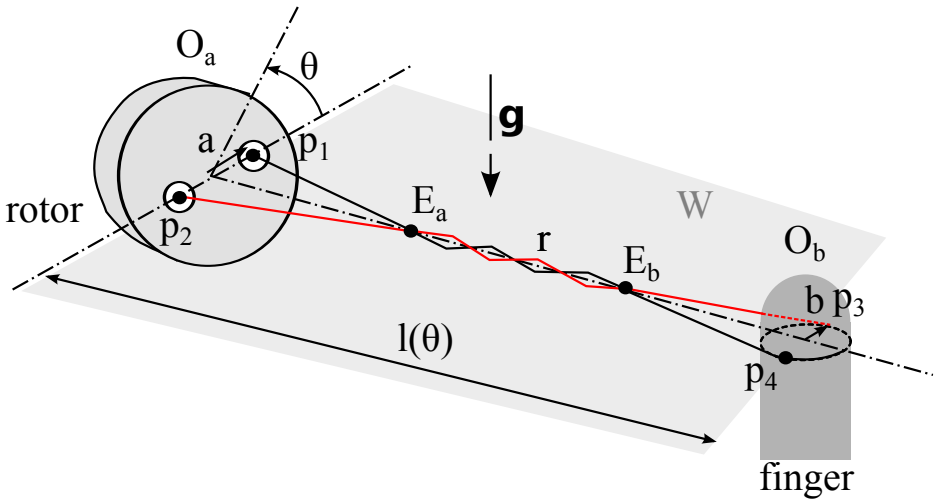

Fig. 3.2 Modeling a twisted pair of threads [66]

3. The shape of the cross section of the thread does not change with respect to the tension.
4. The tension is uniform for the whole length of the thread.

By applying assumptions above, the geometric model for a twisted pair of thread can be introduced as shown in Fig.3.2. Note that O_a and O_b indicate the cross sectional locations of the thread loop where the rotor and the finger tip of the robotic hand contact, respectively. Also, a denotes the distance between the center of the rotor and the hole through which the thread is passing, b indicates the radius of finger tip, and r refers to the radius of the finger tip. In case E_a and E_b represent the two points where the twisting of the thread is finished. Also, p_1 and p_2 denote the points that the thread contact the two holes of the rotor, and p_3 and p_4 indicate the points where the thread contact the finger tip. In this geometry, it is obvious that E_a are on the rotational axis by the symmetry.

Then, consider a plan W containing the rotation axis, which is perpendicular to the gravity vector $\mathbf{g}$, and points $p_i (i = 1 \sim 4)$ are on the W. Note that the centers of the threads almost lie on W. As the thread projected on to the plane W, several virtual nodes n_i can be set on the plane W, as shown in Fig. 3.3. Each point where two threads are crossing correspond to the nodes that are numbered such as $n_i (i = 0, 2, \cdots)$, and the nodes $n_i (i = 1, 3, \cdots)$ indicate the points where the center of the threads are at the distance of $2r$ from each other.

Then, it is obvious that there appear a number of triangles with equal proportions that are formed by p_i and n_i according to the degree of twist. Therefore, a novel triangle model for a twisted thread is suggested here.

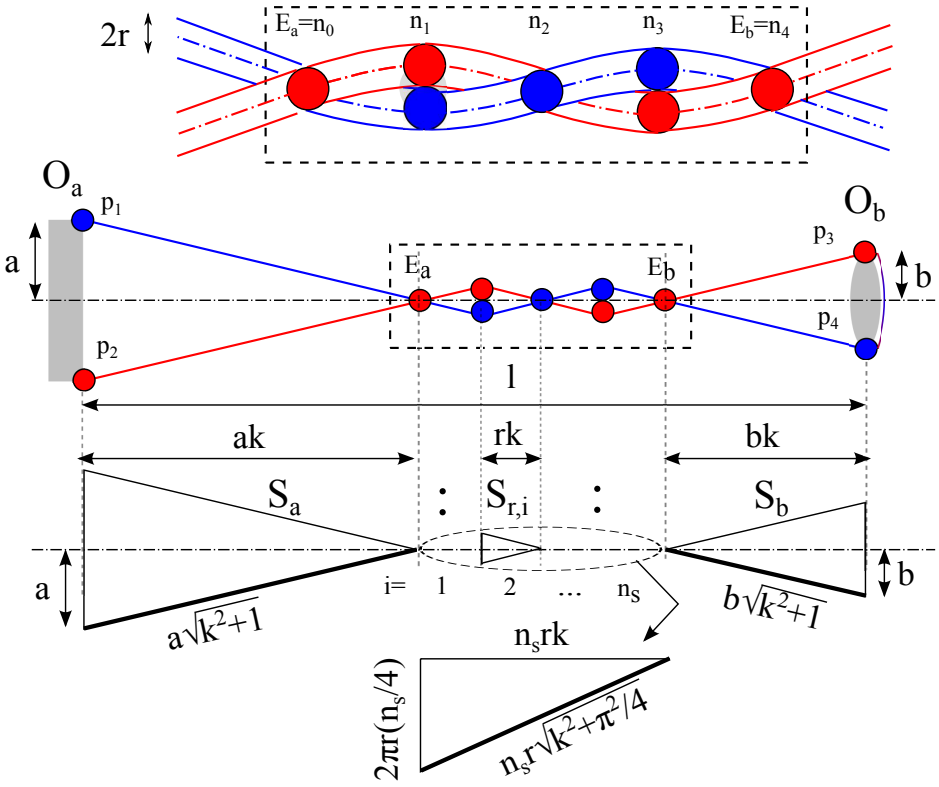

Fig. 3.3 Triangle model of a twisted pair of threads [66]

S_a indicates the triangle $\triangle p_1 p_2 E_a$, S_b indicates the triangle $\triangle p_4 p_3 E_b$ and $S_{r,i}$ shows the triangle determined by the nodes n_{i-1} and n_i in the twisted part of the thread. Let k be a constant of proportionality that indicates the ratio of length to half the height, which is the uniform value for all of the triangles. Then it is obvious that the hypotenuse is $\sqrt{k^2+1}$ times half the height.

Let us define the distance between O_a and O_b is equal to ℓ, then ℓ can be built as:

$$\ell = (a + n_s r + b)k,\ n_s = 4|N| - 2 \tag{3.1}$$

where n_s is the number of $S_{r,i}$ and N is the number of turns of the rotation of the rotor. In this case, k and ℓ can be calculated by using the aforementioned assumptions and by considering the length of the thread when it is not twisted. Let the length L be the distance between p_1 and p_3 (or p_2 and p_3) when the thread is not twisted.

$$L = (a+b)\sqrt{1+k^2} + n_s r\sqrt{k^2+\pi^2/4} \tag{3.2}$$

where the term of $n_s r\sqrt{k^2+\pi^2/4}$ reflects the spiral length of the twisted section in three dimensional space, as shown in Fig.3.3. (Since one revolution generates four triangles of S_r, for given n_s, rotor rotates $n_s/4$ turns.)

The coefficient k can be easily obtained by solving Eqn.(3.2) using a transformation of variables as following:

$$D = At + B\sqrt{t^2+C}$$

where $A=(a+b)$, $B=n_s r$, $C=\pi^2/4-1$, $D=L$, $t^2=1+k^2$ $(all>0)$. Thus,

$$t = \frac{AD \pm \sqrt{(A^2-B^2)B^2C+B^2D^2}}{A^2-B^2}$$
$$k = \sqrt{t^2-1}$$

Note that there exist two solutions for t owing to the square root operation in the transformation from variable k to t. Only one between them is the correct solution. Let the two solutions be t_1 and t_2 $(t_1 \geq t_2)$. In order to evaluate the correct one, consider the situation where A and B are equal (a real possibility). Then,

$$t_{1,A\to B} = \frac{\cancel{(A+B)}D}{\cancel{(A+B)}(A-B)} = \text{UNDEFINED}, \qquad \text{when } A=B$$
$$t_{2,A\to B} = \frac{\cancel{(A-B)}D}{(A+B)\cancel{(A-B)}} = \frac{D}{A+B}, \qquad \text{when } A=B$$

In actual condition, because A might be equal to B, the solution should exist. Therefore, solution t_2 is considered to be the correct solution. Accordingly, from now on, t indicates only t_2.

3.3 Model-based Strategy

3.3.1 Control Strategy

Button Spinner Model

In the button spinner, the tension T generated by the change in length of the twisted threads produces a torque τ that rotates the rotor. Let the component of T that is responsible for the torque be called T_r. Then, using the relation as shown in Fig.3.4, T_r can be calculated as following:

$$T_r = T\cos\alpha\sin\beta \tag{3.3}$$

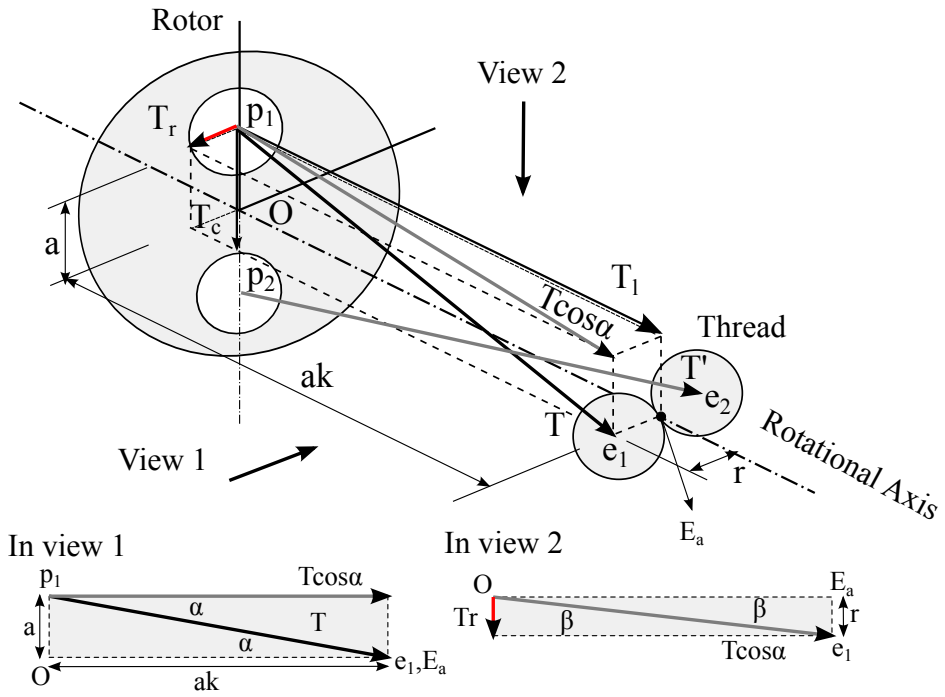

Fig. 3.4 Mechanism of producing torque in button spinner [66]

where α indicates the angle of $\angle p_1 E_a O$, β refers to the angle of $\angle O e_1 E_a$, O denotes the center of the rotor, p_1 and p_2 are the points where the centers of the threads cross the rotor, E_a represents the end point of twisted part of the thread nearest the rotor, e_1 and e_2 indicate the points at which the center of the threads cross the cross sectional plane at E_a. Therefore,

$$\cos\alpha = \frac{k}{\sqrt{1+k^2}}\ ,\ \sin\beta = \frac{r}{\sqrt{a^2k^2+r^2}}. \tag{3.4}$$

Note that the relative positions of the threads is swapped in case the direction of the twist is reversed. Then, reversing of the twist has an influence on the reversing the direction of T_r and τ. Because τ always works against the twist, Eqn.(3.3) is required to be modified as following.

$$T_r = -T\cos\alpha\sin\beta\,\mathrm{sgn}(\theta) \tag{3.5}$$

where θ indicates the angular position of the rotor and $\mathrm{sgn}(\theta)$ is equal to $\theta/|\theta|$ when θ is not zero, which is zero otherwise. Therefore, from Eqn.(3.4) and Eqn.(3.5)

$$\tau = T_r a = -Ta\frac{k}{\sqrt{1+k^2}}\frac{r}{\sqrt{a^2k^2+r^2}}\mathrm{sgn}(\theta)$$

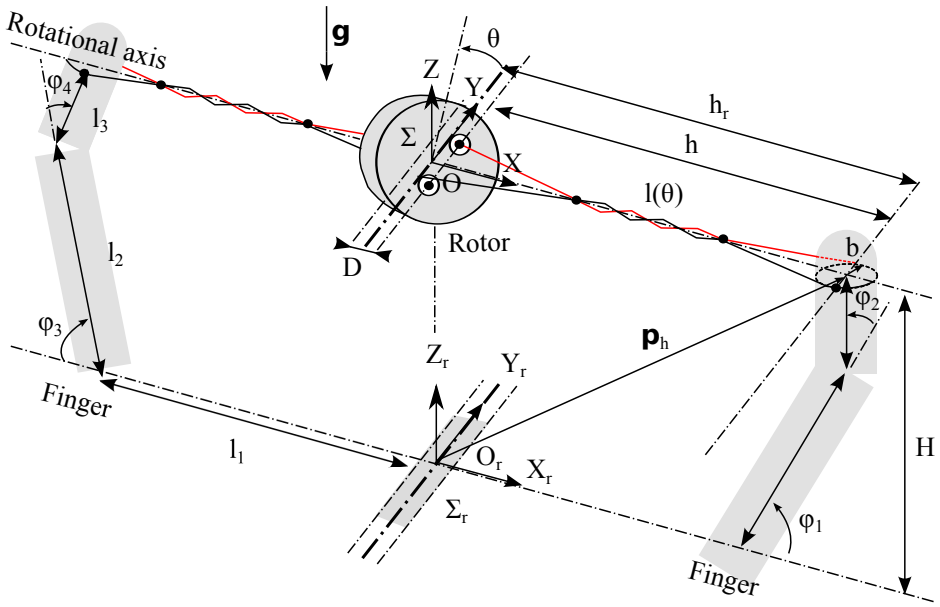

Fig. 3.5 Button spinner on robotic hand [66]

Now the model for the button spinner can be designed as shown in Fig.3.5. Let the coordinates of the robotic hand be $\Sigma_r(O_r - X_rY_rZ_r)$ and some other coordinates be $\Sigma(O - XYZ)$, which has identical orientation with Σ_r but at a distance H along the Z_r-axis direction. If it is assumed that the rotation axis of the rotor lies on the X-axis and the motion of each finger tip is confined to this axis, the motion of the rotor can be described as following:

$$J\ddot{\theta} = \tau - D_r\dot{\theta} \tag{3.6}$$

$$= -Ta\frac{k}{\sqrt{1+k^2}}\frac{r}{\sqrt{a^2k^2+r^2}}\mathrm{sgn}(\theta) - D_r\dot{\theta}$$

$$= K\mathscr{F}(h-\ell)aF_n - D_r\dot{\theta} \tag{3.7}$$

where J indicates the moment of inertia of the rotor about the X-axis, D_r denotes the coefficient of viscous friction, K refers to the thread's spring constant, $\mathscr{F}(x)$ represent the function that produces x in case $x \geq 0$, which is otherwise zero, and h indicates the distance from the rotor to each finger tip along the X-axis in the direction of Σ, F_n represents the factor in order to convert T to T_r, which is calculated as $F_n = -\frac{k}{\sqrt{1+k^2}}\frac{r}{\sqrt{a^2k^2+r^2}}\mathrm{sgn}(\theta)$. Considering D as the thickness of the rotor, and the position of the finger tip in X-axis as h_r, h is equal to $h_r - D/2$. Then, the tension T is proportional to $h - \ell(\theta) = (h_r - D/2) - \ell(\theta)$.

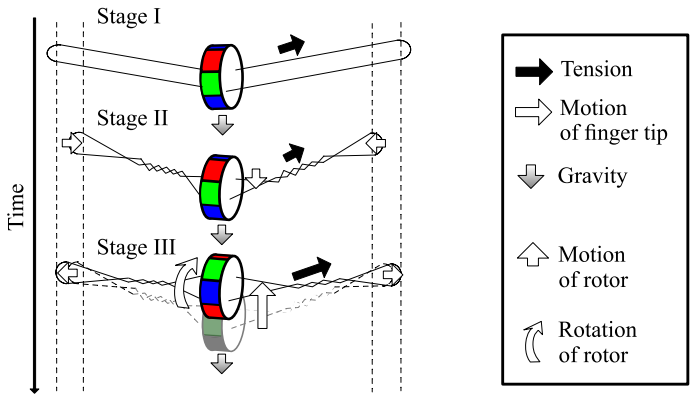

Fig. 3.6 Motion in button spinner (early stage) [67]

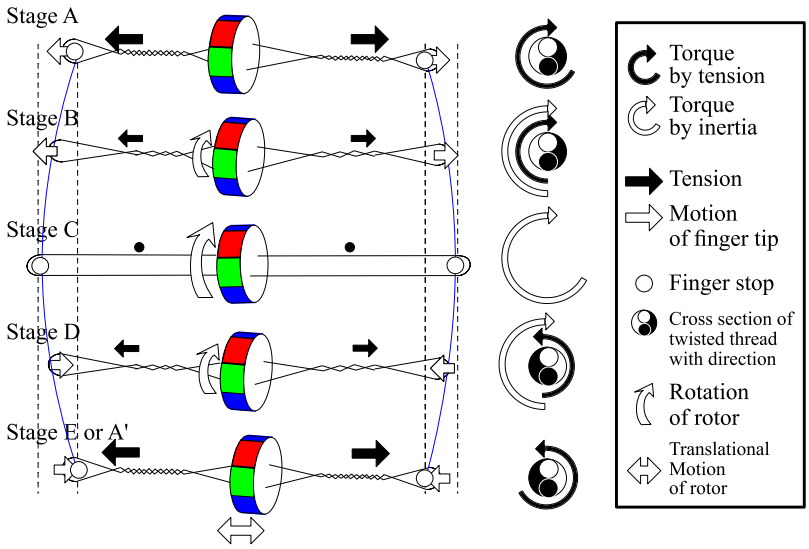

Fig. 3.7 Motion in button spinner (general stage) [67]

Therefore, h_r is a value that is controllable in the button spinner system, and the controller should command the trajectory of h_r considering the motion of robotic finger tips.

Analysis of Motion in Button Spinner

In the previous section, the geometry of the button spinner is precisely inspected, and the twisted thread model is built. Although the model itself is not directly applied as a control strategy, it helps to investigate the applied forces and the movement of the rotor in the system of button spinner. In this section, in order to understand the motion of button spinner

precisely, step-wise analysis of motions that appear during playing the button spinner is described.

There are many sub motions of fingers as well as a rotor to play a button spinner, as shown in Fig. 3.6 and Fig. 3.7. Firstly, the thread is twisted as the rotor is wound a few turns, as an initial state (stage II). Then, the rotor starts to spin as pulling the fingers outside, which makes the thread loop to be stretched (stage III). In this stage, because the gravity acting to the rotor and the direction of the tension that is applied to the thread are coincident with the rotation axis, the center of mass of the rotor is located below the line that connects two fingers. For this reason, there occurs an unstable state of the rotor, and thus the control of fingers should be carefully performed in order to obtain a successful spinning of the rotor. Provided that there is enough twisting in thread, it shows almost linear features among three points, finger tip - rotor - and the other finger tip, where the tension on the thread acts stably, and it decreases the fluctuation of the rotation axis (Fig. 3.7). At the moment that the number of the turns of the rotor is attained the local maximum value (stage A), the twisted thread is started to unwind by pulling the fingers outwards which accelerates the spinning speed of the rotor (stage B). Until the distance between the two fingers reaches the limit due to the fixed length of the thread loop, the speed of rotation increases gradually. When the finger tips reach the limitation, the rotor spins at its maximum rotation speed as the thread is unwound completely (stage C). As it passing the point of the limit, the thread is now started to be twisted again but in the opposite direction, while keeping the direction of the rotation the same as the previous condition, with decreased spinning speed (stage D or A'). In order to prevent energy loss of spinning as well as to maintain the minimum tension of thread not to hang down the rotor, the finger tip is required to be moved carefully toward the rotor. At the point the thread is twisted in maximum and the rotor counts the maximum number of turns, the distance between the two finger tips reaches the local minimum value where the rotor stops its spinning (stage E). After the aforementioned processes are iterated, the system arrives at quite stable state, in comparison with the early stage of button spinner. From analyzing the button spinner controlled by human hand by using the high-speed visual sensing, it is recognizable that a sine wave is drawn by the oscillation of the finger tips, and also the angular position of the rotor traces a sine wave in the time course graph. The parameters such as stroke, amplitude, frequency and the oscillation center are significant effectors in the playing of the button spinner, provided that the movement of finger tips adopts a sine wave as an input trajectory. Therefore, in order to achieve the robotic manipulation of the button spinner, those parameters are extracted from the successful cases and applied to the robotic manipulation.

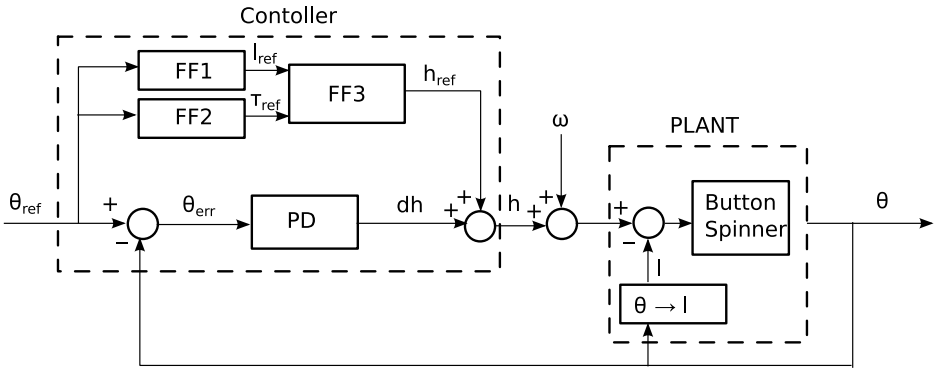

Fig. 3.8 Block scheme of controller for button spinner [66]

Controller Design

PD control is one of the most popular controllers and also expected to be suitable for the button spinner. However, PD control is not suited for unidirectional control. For this reason, it may be reasonable to adopt a feed-forward component to compensate for the unidirectional nature of the system. The control scheme is shown in Fig.3.8. The feed-forward components consist of three blocks: FF1, FF2 and FF3. FF1 converts θ_{ref} to ℓ_{ref} by substituting θ_{ref} into N in Eqn.(3.1), and FF2 to τ_{ref} using Eqn.(3.6) ($\tau_{ref} = J\ddot{\theta}_{ref} + D_r\dot{\theta}_{ref}$). FF3 acquires h_{ref}, the reference of finger position, by substituting ℓ_{ref} and τ_{ref} into Eqn.(3.7) as following:

$$h_{ref} = \ell_{ref} + \frac{1}{aKF_n}\tau_{ref}$$

The control input h can be given by,

$$h = h_{ref} + K_P(\theta_{ref} - \theta) + K_D(\dot{\theta}_{ref} - \dot{\theta}) \tag{3.8}$$

where each K_P and K_D is a gain selected appropriately by trial and error.

The button spinner can be manipulated with h_{ref} alone, as $h = h_{ref}$, if it satisfies the following three conditions: no disturbance, well-defined plant model and initial state for θ corresponding to initial θ_{ref}. Realistically, it is difficult to achieve these conditions. Hence, we should look into the performance of the suggested controller, taking into account the uncertainty of the conditions. To do this, we consider the following two set of simulations: one concerns various initial positions of the rotor, and the other concerns a disturbance d added to the control input h in Fig.3.8. The results are given in section 3.3.2.

3.3.2 Simulation Result

For a button spinner, a sinusoidal curve, as shown in Fig.3.12, is considered as the desired trajectory of the rotor. Therefore, a reference input can be set as $N_{ref} = N_{0,ref}\cos(2\pi ft)$, where $N_{0,ref}$ is the amplitude of the reference function and f is the frequency of the oscillation. Here, let the initial angular position of the rotor be N_0, which also indicates the initial state in the controlled object. A set of simulations was conducted according to the following four cases:

- Case I : FF, $d = 0$, various N_0
- Case II : FF+PD, $d = 0$, various N_0
- Case III: FF, various d, $N_0 = 6$ [turns]
- Case IV: FF+PD, various d, $N_0 = 6$ [turns]

Where FF refers to the case of feed-forward only control and FF+PD refers to the case where both feed-forward and PD control are used. The following parameters are common to all cases: $N_{ref} = 7$, $f = 1$ [Hz], $J = 8.686 \times 10^{-8}$ [kgm^2], $D_r = 5.306 \times 10^{-8}$ [kgm^{2}s^{-1}], and N [turns], as the angular position of the rotor given by θ [rad]$/2\pi$, are used. The coefficient J is calculated using the physical properties of the rotor, and D_r is estimated from the decreasing rate of N. The simulation results are shown in Fig. 3.9 and in Fig.3.10.

From these results, the following are observed: First, the case of FF+PD shows better performance than the case of FF only, in all cases. In case I and II, N quickly approaches to N_{ref}, irrespective of N_0, and the error $N_{err} = N_{ref} - N$ converges to zero as time passes. Second, this control strategy is quite robust. Even when 30 percents of the finger stroke, given by the difference between maximum and minimum of h_{ref}, is added to h as d, it works correctly. Third, the system is more stable when N_0 is smaller than $N_{0,ref}$, and closer to $N_{0,ref}$, which can be easily confirmed in Fig.3.9(d). Finally, in the case of FF, on the other hand, N does not converge to N_{ref} generally, except when N_0 equals to $N_{0,ref}$. In summary, the controller of Eqn. (3.8) is suitable for the button spinner. The parameters used in the simulation are shown in Table 3.1.

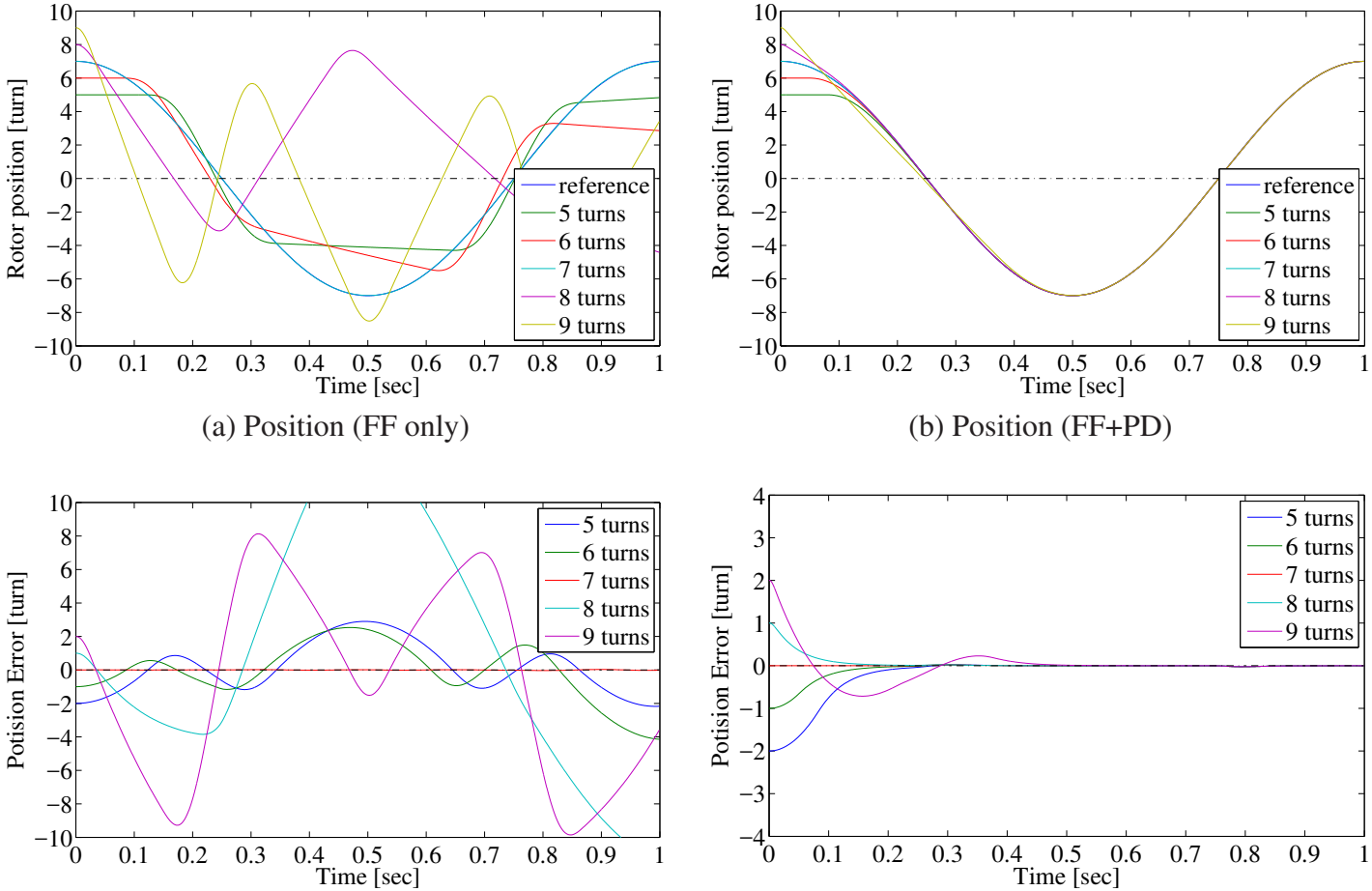

(a) Position (FF only)

(b) Position (FF+PD)

(c) Error (FF only)

(d) Error (FF+PD)

Fig. 3.9 Simulation of controller with variable initial state of rotor [66]

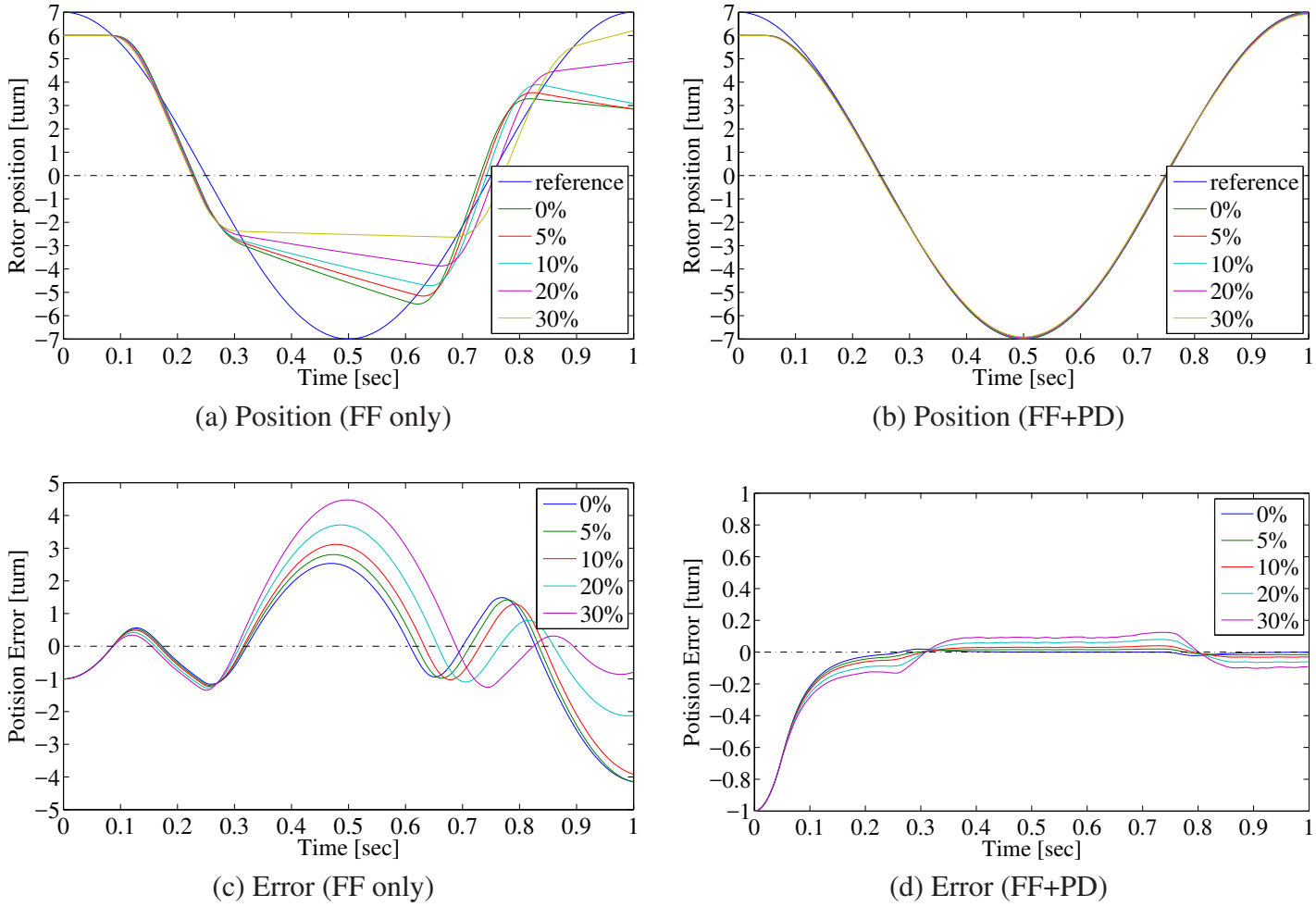

(a) Position (FF only)

(b) Position (FF+PD)

(c) Error (FF only)

(d) Error (FF+PD)

Fig. 3.10 Simulation of controller under disturbance [66]

Table 3.1 Parameters of Robotic Button Spinner

Parameter	Value [mm]	Parameter	Value[mm]
a	3.2	l_1	60
b	2.7	l_2	62
r	0.2	l_3	27
D	5.0	l_{max}	73.6
H	80		

3.4 Reference-based Strategy

3.4.1 Feedforward Control Based on Human Motion

The system of button spinner applied in the experiments mainly comprises two parts: (1) a robotic and with a real time controller and (2) a high-speed camera system, as described in Fig. 3.11. In order to build a high-speed visual feedback loop, these two parts are set to operate at 1 kHz, respectively, and are connected to each other through 100 Mbps Ethernet. For the feedforward control experiment, the camera system works only in recording the rotation of the rotor including the position and the angular position of the rotor, not for the feedback control.

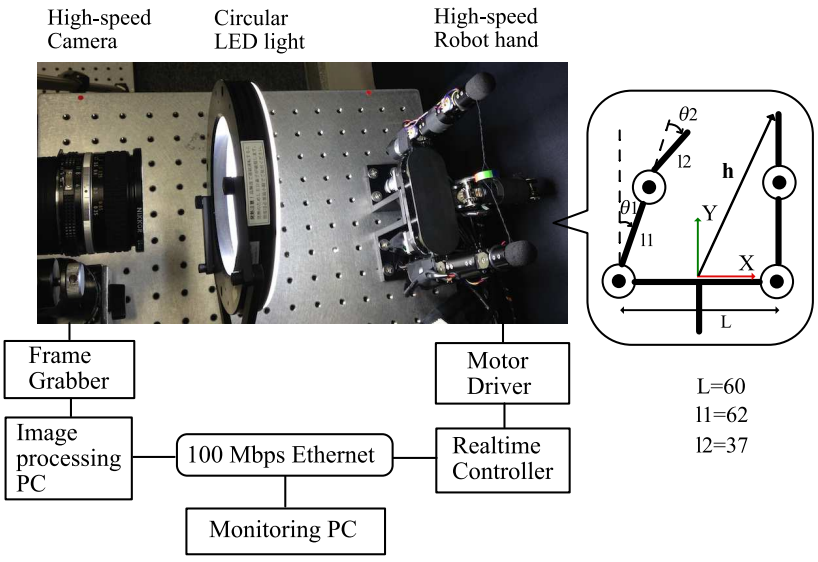

Fig. 3.11 High-speed robotic system and button spinner [67]

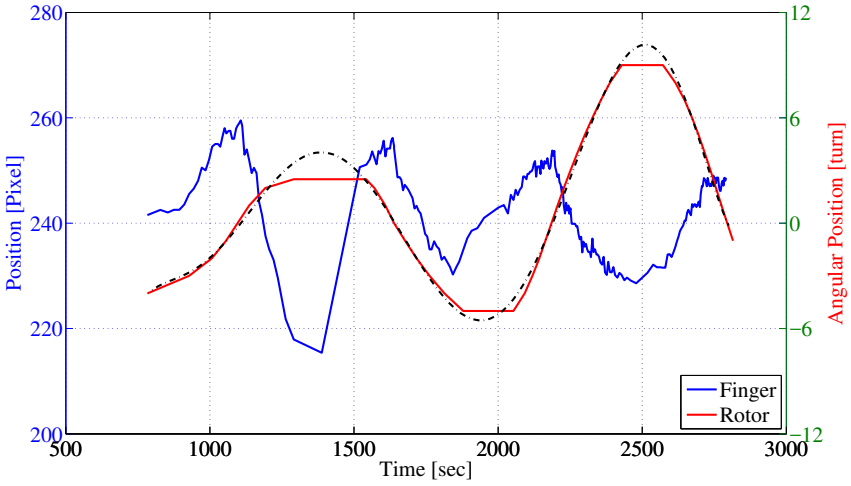

Fig. 3.12 Button spinner by human hand [67]

In order to avoid the difficulty in the accurate system identification due to the nonlinearity of the flexible thread, the control input to play the button spinner is determined based on the human finger motion, as shown in Fig. 3.12. Since the finger motion showed a shape of a sinusoidal wave, the following sinusoidal function was applied as a feedforward control input.

$$\mathbf{h}_{ref}(x,y) = \big(A\cos\{2\pi f(t-\delta)\} + C_{osc}, \quad y_0\big) \tag{3.9}$$

where $\mathbf{h}_{ref}$ refers to the position of the robotic finger tip as the control input, A is the amplitude of the sinusoidal wave, f denotes the oscillation frequency, δ indicates the phase, and C_{osc} stands for the center of the oscillation. As already mentioned, the parameter A, δ, and C_{osc} were determined with the human reference. The calculated term $\mathbf{h}_{ref}$ is converted to the joint angles $\mathbf{q}_{ref}$ as a control input for the robotic hand system, by solving Inverse Kinematics (Fig. 3.13). The basic textbooks such as [68] describe the examples of Inverse Kinematics in regard to the two-link model. In 10 times of trial runs, the robotic button spinner showed 100% of success ratio with the above condition. As it is anticipated, the angle of the rotor does not show the arrangement in the trajectory and the amplitude, which refers to that the visual feedback is necessary in order to control the angle transition favorably. Additionally, it is observed that there occurs a drift of the rotor position, along the rotation axis. However, the motion planning referring to the the human hand motion is proved to work well, and it helps the robotic button spinner manipulation without any detailed model for the target task. With high-speed visual feedback, now the effectiveness of the high-speed robotic system will be shown through the rotation control via the twisted thread.

3.4.2 High-speed Visual Feedback Control

In section 3.4.1, it is confirmed that the robotic button spinner works with feedforward control. Now the visual feedback control is suggested in order to regulate favorable rotation of the rotor and maintain the stability in the rotation axis, based on the control input.

Angular Position Control

The results of feedforward control experiment showed that there are certain conditions that the robotic button spinner is possible. With those results, the control method with visual feedback where the amplitude of sine wave with respect to the rotation angle of the rotor is now suggested. The position of the finger tips is the system input, considering a sine wave to be the proper shape of the input trajectory. In this case, following parameters can be controlled: (1) the position of the center at the oscillating fingers, (2) the stroke of the finger tips, and (3) the oscillation frequency. In fact, the stroke of the finger tip is the only controllable parameter in this task, because the constant oscillation frequency is desirable and the oscillation is influenced by the geometrical limitations due to the fixed thread length. The optimal timing to alter the stroke is considered to be the moment when two finger tips are located the most remote position from each other at every turn during the oscillation, since the maximum distance between finger tips are determined.

As shown in Fig. 3.13, the new stroke using the proportional control in which the control input is taken as the error between the reference and the observed amplitude is fed back. Since the sine wave in the experiment is relatively long compared to the control cycle, only proportional control is applied to modify the stroke of $\mathbf{h}_{ref}$, even though PD control is generally applied in many applications using high-speed visual feedback when generating $\mathbf{h}_{ref}$. Since the y coordinate of $\mathbf{h}_{ref}$ is fixed in the given task, it is sufficient to consider the

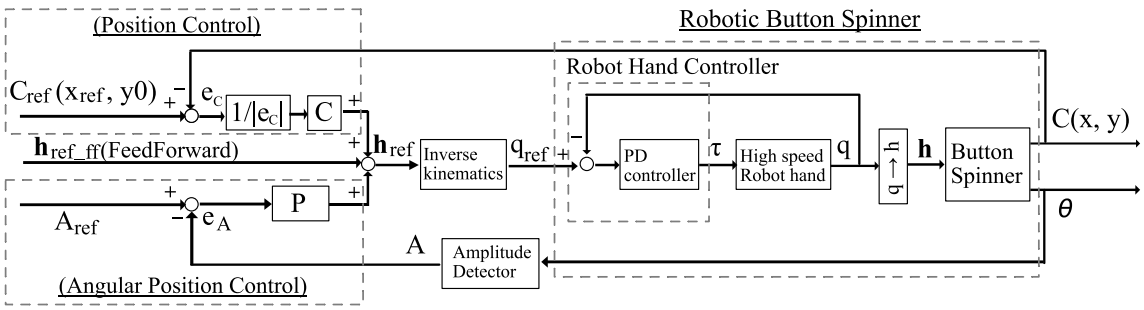

Fig. 3.13 Block diagram of control system for button spinner [67]

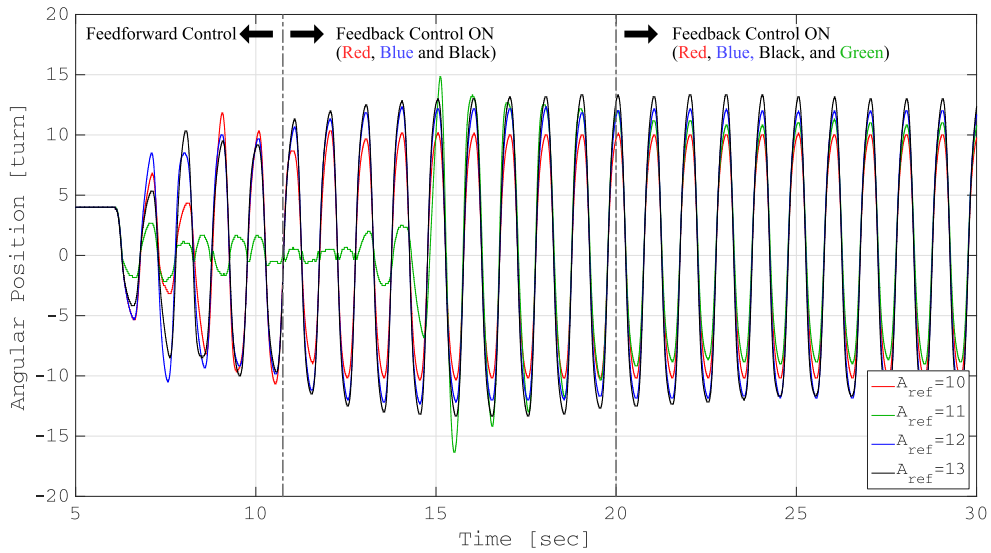

Fig. 3.14 Angular position control with various reference [67]

x coordinate, h_x, alone. The control input is as following.

$$h_x = K_p(A_{ref} - A)\cos\{2\pi f(t-\delta)\} + C_{osc} \tag{3.10}$$

where K_p indicates the proportional control gain, A_{ref} refers to the desired amplitude, and A is the current amplitude estimated from the measured rotation angle of rotor θ.

Fig. 3.14 shows the results. Except for the slow response speed, the amplitude is controlled correctly in accordance with the designated value. Such a slowness in the response speed is considered to be inevitable, due to the non-linearity of the flexible objects.

Position Control

The button spinner can move along the rotation axis as it slides on the thread, because the rotor is suspended by the thread that passes through the holes of the rotor. Moreover, the tension of thread applied to the both sides of finger tips is difficult to maintain, and the rotor is likely to slide at the moment when the thread is pulled. Here, with the visual feedback, the position of the rotor is controlled to be constant on the thread, as the position of the finger tips are shifted by the control. The shifting of the finger, in this case, is tend to influence the tension of the thread, which causes that the rotor moves against the intention. Therefore, in order to compensate the error, a constant control in which the direction with a constant gain is fed back without the feedback of the size of position error is tried as shown in Fig.

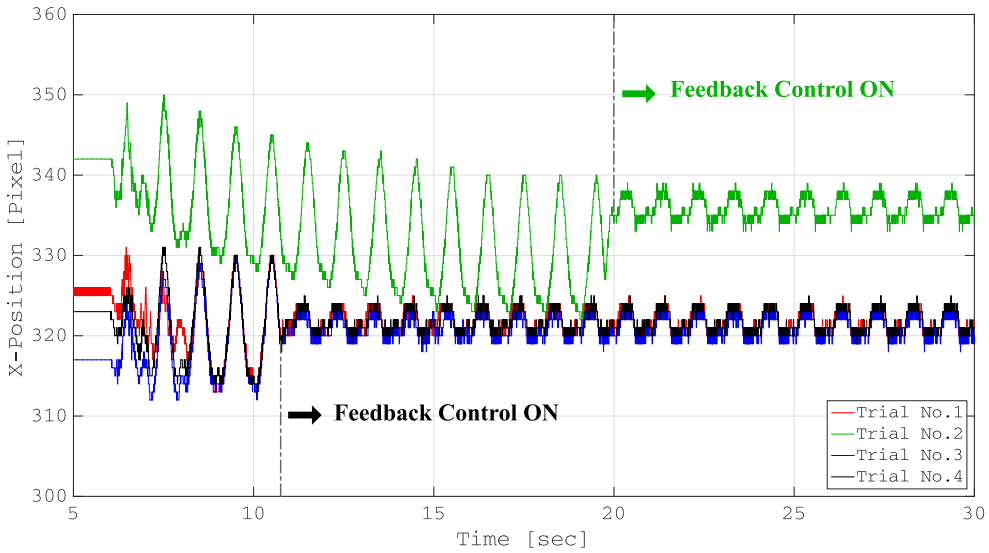

Fig. 3.15 Rotating axis control with high-speed visual feedback [67]

3.13. In high-speed system, it takes advantages in that the cycle of control is short enough for catching the dynamic system, just the same as in static condition. Hence, provided that the constant value is small enough, the tension is not changed fast and it contributes to the stability in the non-linear system which includes flexible objects. The control input is as the following.

$$h_x = A\cos\{2\pi f(t-\delta)\} + \frac{C_{ref} - C(x,y)}{|C_{ref} - C(x,y)|}C_{osc} \tag{3.11}$$

where C_{ref} is the desired position of the rotor, $C(x,y)$ indicates the measured centroid of the rotor. Fig. 3.15 shows the data acquired from the experiments.

When with feedforward control, there occurred a drift along x direction of the rotor around 20 pixels, while the experiment result with the visual feedback control restricted the drift or the control error within 5 pixels, which is only 0.8 mm in actual dimension. It is notable result in that the control law worked great even though the control law itself is apparently simple.

Rotation and Position Control

Here, with high-speed visual feedback control, the rotation of the rotor and its angular position are controlled simultaneously. The control input is as the following.

$$h_x = K_p(A_{ref} - A)\cos\{2\pi f(t-\delta)\} + \frac{C_{ref} - C(x,y)}{|C_{ref} - C(x,y)|}C_{osc} \tag{3.12}$$

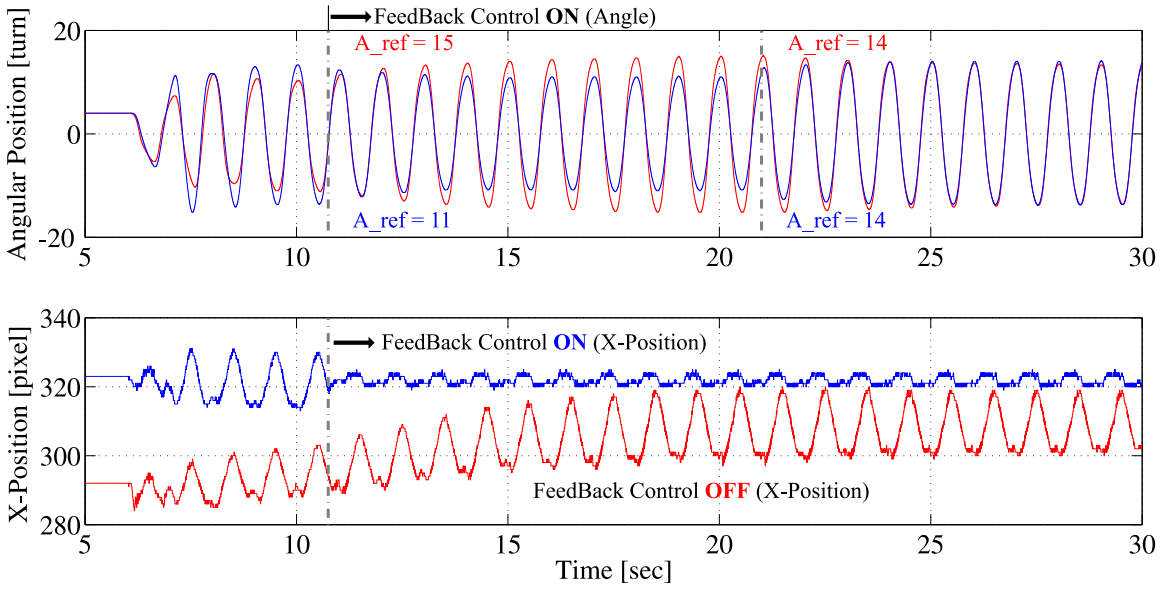

Fig. 3.16 Manipulation of button spinner with high-speed visual feedback [67]

The high-speed sensing and manipulation help to the task possible, although there is no system model, regardless the non-linearity of the system. As described in 3.16, the results show that the experiment is conducted successfully.

3.5 Summary

In this chapter, the robotic button spinner with high-speed control system comprising high-speed vision and manipulator is demonstrated, as an example task of the manipulation of rotating object through the twisted thread. The visual sensing method is introduced as a novel measurement method, in order to measure the center of mass as well as the angular position of the rotating object at high speed, and it is proved that this novel method is able to work at high rotation speed at 6,000 rpm, even under the condition of fluctuating rotation axis. The motion of button spinner when conducted by human is analyzed using visual sensing system, and the parameters are extracted to apply to the feedforward system.

Finding a rough but stable condition for the system to work the feedforward control was the first step of the control strategy, and then the error between the reference and the controlled value are exploited for compensation in high-speed visual feedback. In consequence, as intended the strategy worked well, and it is proved that the high-speed visual sensing and feedback control contribute to the simplicity of the model even under the condition of many limitations, without any sophisticated model. From the experiment results in the button

spinner, it is showed that the position of the rotor along the rotation axis can be controlled within 1 mm, and the rotation of the rotor can be controlled in the order of sub-turn.

The twisted thread in the button spinner shows interesting feature as a power transfer structure, in that is periodic linear motion can be transformed into the high-speed rotating oscillation, without any rigid body transmitter such as a gear wheel. This flexibility of the twisted thread can lead to the various uses, since it enables the rotating motion in a floating state with uncomplicated structure and low cost. Furthermore, the robustness of the control system is improved by the stable manipulation of the high-speed rotation. To optimize the parameters for the robotic button spinner control as well as to devise the power transfer structure for the applications in the industrial field are the next steps of this research in the future.

Chapter 4

Rotation Control through Thread-Bending: Robotic Yo-yo

In this chapter, the problem about the rotation control of a rotor through bending of flexible thread will be discussed. The external force is applied to the perpendicular direction to the rotation axis, and the force produces the torque to rotate the rotor as much as the amount of the multiplication of the force and the arm length, which is from the centroid of the rotor to the point of application. The most remarkable feature is that the rotation axis is movable in any direction, and rather fluctuates, due to the flexibility of the thread and the free end. Visual encoder method can be exploited to measure the rotation of the rotor in direct manner, and it will help the control of the rotary system which assumes abundant non-linearity. Yo-yo can be an appropriate example for aforementioned problem.

4.1 Introduction

Yo-yo is a popular hand-toy that can be played by the rotation of a rotor through thread-bending. The rotor of yo-yo consists of two thick discs connected by an axle, the one end of a thread is fixed on the axle. The purpose of the playing yo-yo is to continuously rotate the rotor with vertically linear motion of hand where the other end of the thread is fixed. Playing yo-yo consists of following 6 steps. Firstly, the free-end of the thread is grabbed by hand. In this step, normally the thread is knotted to make a circle to be held by a finger. The second step is to wind up the thread fully around the axle of the rotor, and grasp the rotor by hand. The third step is to release the rotor until the thread is fully unwound and even almost stretched in length, as holding the thread during the free falling of the rotor. The fourth step is to retrieve the rotor as rapidly pulling the thread upward using wrist snap. Then, in the

next step, the thread is now rewinding backward. The final step is to grasp the rotor again by hand when the thread is fully wound up. These basic six steps are repeated throughout the playing, regardless of various playing techniques of yo-yo.

Despite its simple structure, playing yo-yo contains many dynamic motions of the rotor: The high-speed rotation of a rotor, the periodic switching in the direction of the rotation, the oscillation of the centroid of the rotor along the direction of gravity, and an unintended spinning of the rotor around the longitudinal direction of the thread. Although human can manage and handle these motions for achieving successful playing of yo-yo after the repeated practice, playing yo-yo by robot is still considered as a difficult task. The main reason of the difficulty comes from the nonlinear features of thread, such as flexibility and stretchability, and those features should be counted when modeling and controlling the yo-yo system: The deformation of the geometric shape of thread affects the modeling, and the unidirectional power transfer via thread influences to the controlling. Since the power transfer is also affected by the deformation of thread, especially by the thread-winding around the axle of rotor, the winding of thread should be described as accurately as possible. However, the earlier works regarding robotic yo-yo in [40–45] used simplified winding models where the thickness of thread is neglected, and inevitably include large modeling error in order to relate the rotation angle of rotor with the wound length of thread. Even in other works [46, 69] where the thickness of thread is considered, the significant amount of modeling error remains as described later. Since the conventional robotic yo-yos has used the winding model of thread to design the controller, it is expected that the modeling error affects the control itself. Moreover, even if an accurate model was found, the system identification for the model should be accompanied. However, generally speaking, the nonlinearity of thread disturbs the accurate estimation of the system parameters. For this reason, alternative control scheme to perform robotic yo-yo with less model-dependency is required and the introduction of the high-speed visual feedback system with visual encoder method can be a solution. The consideration of the existing winding model for yo-yo and a new control scheme based on the rotation-angle feedback are discussed here.

4.2 Modeling of Yo-yo

4.2.1 Yo-yo Dynamics: Rotation and Translation

When playing yo-yo, the rotor shows a motion with 6 degree-of-freedom (DOF): Three of them are linked to the position of the centroid, and the other three are related to the rotation

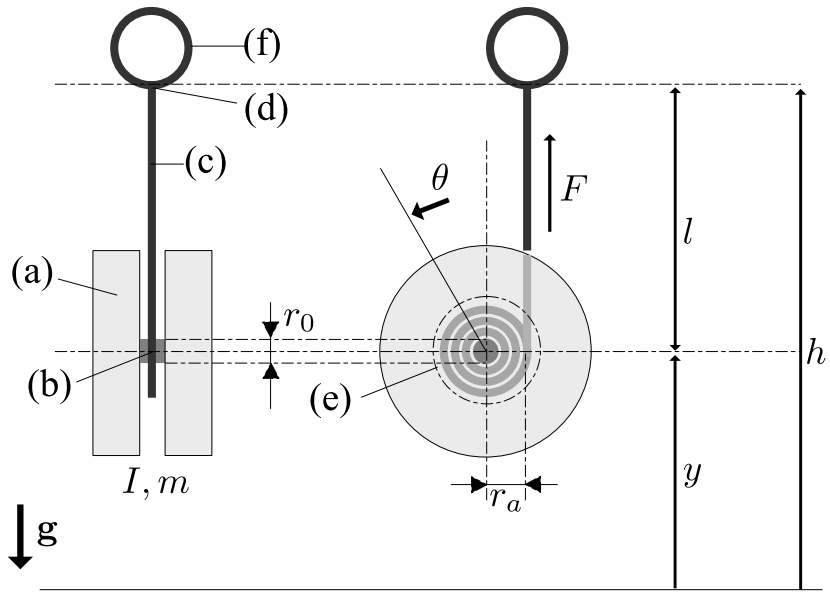

Fig. 4.1 Schematic illustration of yo-yo. (a) the rotor of yo-yo consisting of two thick discs and an axle. (b) axle. (c) thread. (d) position of a finger tip or a hand. (e) wound thread around the axle. (f) a loop of thread as a manipulation handle

of the rotor in three dimensional space. However, since only the vertical motion and the rotation of the rotor around the axle are considered significantly meaningful in the entire motion, only the two corresponding DOF, regarding the vertical position and the rotation angle of the rotor, play roles as the main parameters and the rest of them are treated as a kind of disturbances [46]. Let the two main parameters be y and θ, respectively, as shown in Fig. 4.1.

In this case, the motion of the rotor can be modeled for the two parameter as following.

$$\begin{aligned} I\ddot{\theta} + D\dot{\theta} &= -r_a F \\ m\ddot{y} &= F - mg \end{aligned} \tag{4.1}$$

where I is the inertia, r_a is the moment arm, F is the force via thread, D is a drag coefficient, m is the mass, and g indicates the gravity. Note that r_a is a function of θ, and y is a function of θ, r_a and h, when h indicates the hand position in vertical axis. In related works, since θ was not the parameter that can be observed in direct manner but y can be easily measured, θ should be calculated from the relation between y, r_a and itself. However, since r_a is also the parameter that cannot be directly measured, it should be calculated from the winding model

of the thread. Several winding models of yo-yo were suggested with some assumptions. In [41] and [43], r_a was regarded as a constant value under the assumption that the diameter of thread can be ignored. Let's define the constant value r, which is same with the diameter of the rotor's axle. Then, if L is the length of thread at the moment when it is fully stretched and l is the length of the unwound part of the thread, the relations of L, h and θ can be described as following.

$$l = h - L + r|\theta| \tag{4.2}$$

Although this assumption makes the equations simple, it cannot correctly reflect the actual conditions. In [46], Zlajpah suggested more realistic model for r_a by using the Archimedes spiral, which is found in [70, 71]. According to his model, r_a is calculated by following equation.

$$\left.\begin{aligned} l &= h - L + r_a|\theta - \pi/2| \\ r_a &= (r_0 + r_e(|\theta| - \pi/2))\text{sign}(\theta) \end{aligned}\right\} \quad \text{for } |\theta| \geq \pi/2 \tag{4.3}$$

where r_e is the effective radius of the string. As shown in Eq. (4.3), the winding model is too complicated to be linearized in simple manner. The author solved these sequential equations in order to obtain its simplified formulation with boundary conditions at the bottom height, and explained the yo-yo playing with the compensation of the energy loss caused by the impact at the bottom. An on-line generated hand motion for yo-yo playing that is suggested by the author, is based on a clear theoretical background and actually worked well as shown in the experiment results [46]. However, the on-line generated hand motion always requires the accurate identification of the model's parameters, such as mass and the moment of inertia of the rotor. Actually, the height of the rotor, which is required to be fed back to controller, is likely to be influenced by the disturbance. Therefore, in case the wound thread around the axle of the rotor is uncluttered or the unwound part of the thread during the play forms an angle with the direction of gravity, the hand motion following this model that is based on the height of the rotor can cause considerable error, and the error may hinder the control from generating the optimal trajectory for the successful yo-yo playing.

4.2.2 Thread-Winding model

Archimedes spiral [71] is often used to describe the winding coil of a rope. This spiral is generally explained by the following equation in polar coordinates.

$$r = a + b\theta \tag{4.4}$$

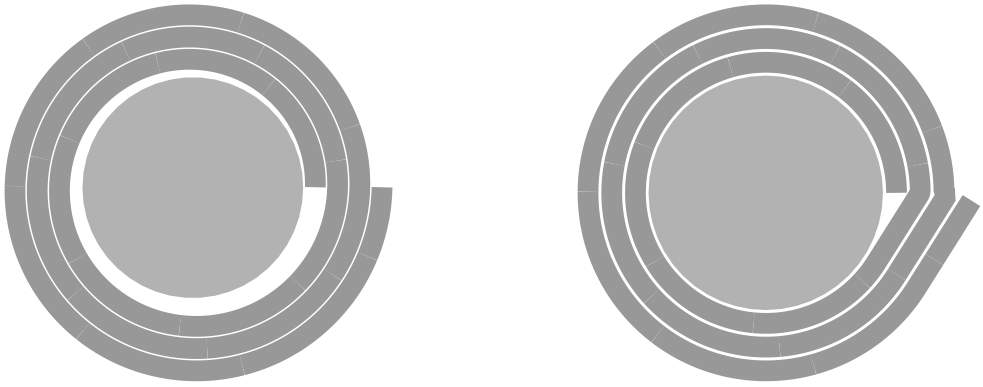

(a) Archimedes Spiral (b) Realistic Winding

Fig. 4.2 Winding models of thread

where a and b are the parameters to determine the initial position of the coil and the distance between adjacent threads, respectively. In [46], the model of thread-winding based on the Archimedes spiral was used too. However, Archimedes spiral cannot accurately describe the actual thread-winding of yo-yo because of the existence of the axle, as shown in Fig. 4.2a. The shape of the winding drawn by the Archimedes spiral in Fig. 4.2a, which is calculated by Eq. 4.4, generates a gap between the axle and the thread. However, in the real world, the gap hardly exists due to the tension of the thread, and thus it is considered as a modeling error. Therefore, in order to reduce the modeling error, a new model for the winding is suggested here as shown in Fig. 4.2b and Fig. 4.3. The thread in the suggested model shows two different bending states: linear and curved shape. Basically, the loop of the thread around the axle is stacked evenly. However, since there occurs an interference between the adjacent turns of the wound loop, the region where the thread is linearly stretched by the tension of the thread appears. Above two states are distinguishable at the boundary angle θ_c that can be acquired from the simple geometry as following.

$$\theta_c = \arccos\left(\frac{r_a + r_e}{r_a + 3r_e}\right) \tag{4.5}$$

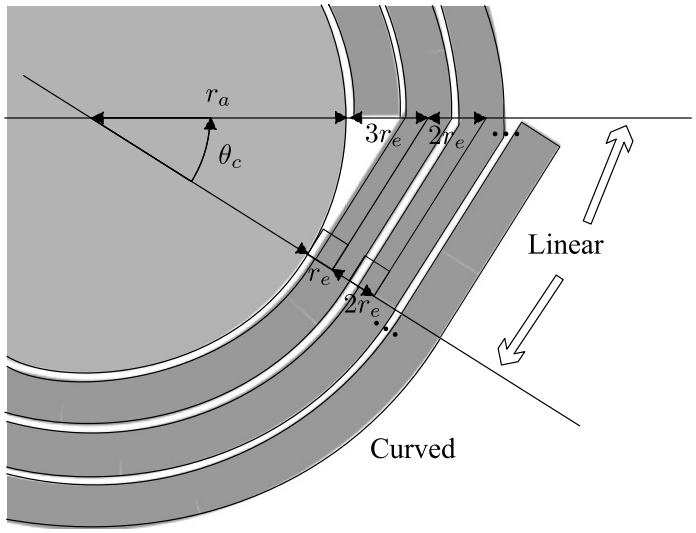

Fig. 4.3 The geometry of the wound thread around the axle in yo-yo. (The magnified view of 4.2b)

Then, the length of wounded thread, l_w, is calculated as in Eq. (4.6).

$$l_w(\hat{\theta}) = \begin{cases} r_N\hat{\theta} + \sum_{i=0}^{N-1} r_i\{(2\pi-\theta_c)+\tan\theta_c\} & \text{if } \hat{\theta} \le (2\pi-\theta_c), N>0 \\ r_N\{\hat{\theta}+\tan(\theta+\theta_c-2\pi)\} & \\ +\sum_{i=0}^{N-1} r_i\{(2\pi-\theta_c)+\tan\theta_c\} & \text{if } \hat{\theta} > (2\pi-\theta_c), N>0 \end{cases} \tag{4.6}$$
$$l(\theta) = h - L + l_w(\theta)$$

where $N = \lfloor \theta/2\pi \rfloor$ refers to the number of thread loop, $\hat{\theta} = \theta - 2\pi N$, and $r_i = r_a + r_e(1+2i)$ indicates the radius related to each thread loop.

As shown in Eq. (4.6), this winding model of thread contains a strong non-linearity. Accordingly, exploiting this equations in an application is quite complicated. Moreover, even in case where the non-linearity is negligible, the model as in Fig. 4.2b includes many unrealistic assumptions as followings: Firstly, the diameter and the length of the thread is considered to be constant. Secondly, the winding status of the thread is always uniform throughout the entire figure. Thirdly, the wound loops are layered without any clutter. Therefore, almost all the thread models developed so far seem to be difficult to completely avoid modeling errors. This is the reason why the simpler equation Eq. (4.2) is preferred in the robotic manipulation problems. Fig. 4.4 shows the actual modeling error estimated by the computer vision. The height of the rotor y and the rotation angle θ in Fig. 4.1 were measured from the video which is recorded by high-speed vision. The height y is used to calculate the

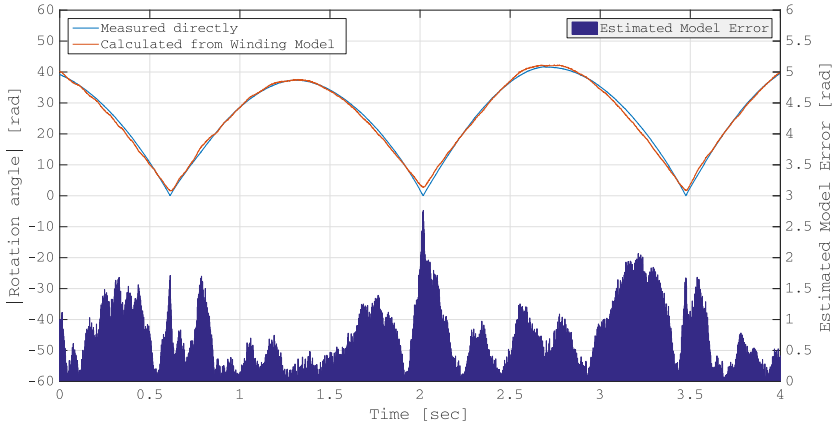

Fig. 4.4 Modeling error of the thread winding model in the yo-yo playing

estimated rotation angle and the modeling error was acquired by comparing the estimated rotation angle with above θ. As shown in Fig. 4.4, the considerable modeling error was observed in actual yo-yo playing.

However, in case the rotation-based control is performed instead of the position-based control, the robotic yo-yo playing can be handled as much easier problem. When the frame of reference is set on the centroid of the yo-yo, the rotation of the rotor of yo-yo is described by simple equation as in Eq. (4.1). The thread is wound up around the axle of the rotor and the infection point of its geometrical shape plays a role as the point of application of the force via the thread. r_a is the same length to the distance between the centroid of the disc and the point of application. Since this term depends on the rotation of the rotor, the torque changes under the constant tension of thread. Therefore, directly adjusting the tension of thread by using simple PD or PID controller with the rotation information feedback is expected to reduce the control error that is caused by the modeling error.

4.3 Control Strategy

4.3.1 Yo-yo Focused on Rotation

As mentioned previously, the model-based control strategy shows its limitation when the system modeling cannot be performed accurately. In yo-yo, the easy-transformation and the nonuniform features of the thread can hinder the accurate modeling. Moreover, in the conventional position-based control scheme, the measurement error regarding the height of the rotor of yo-yo cannot be ignored due to the swing motion of the thread. Therefore,

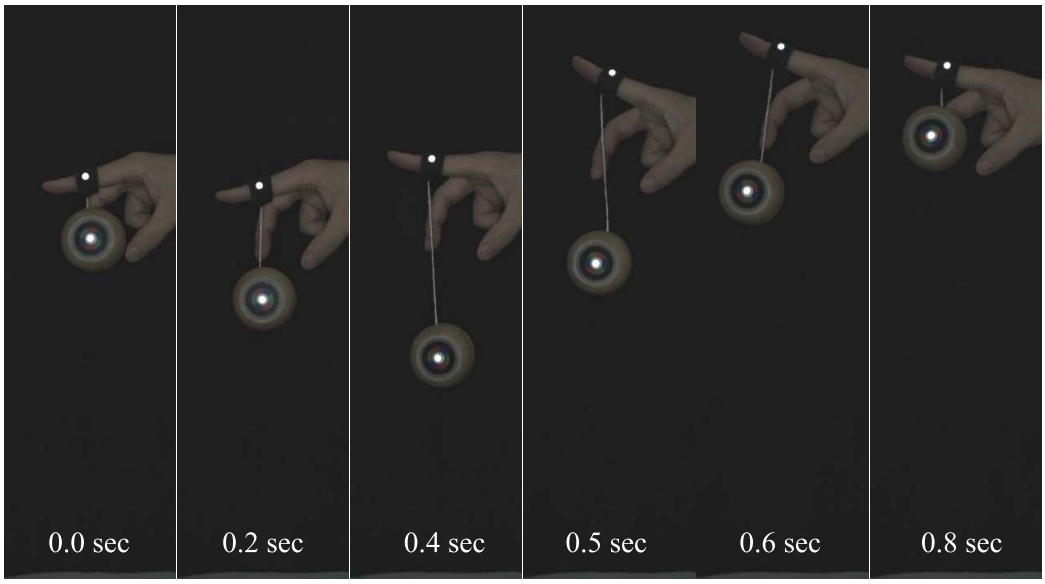

Fig. 4.5 Human's yo-yo playing captured by a high-speed vision. An RGB color marker and a retroreflective marker ball are attached on the rotor of the yo-yo and the finger tip, respectively, to assist the vision-based analysis.

an alternative control scheme which is less influenced by the aforementioned disturbances is required, and the rotation-based control scheme is considered as the desirable control scheme.

In yo-yo, the rotation of the rotor is a core motion, and the control of the rotation is a hidden task, as well as the up-and-down motion control of the rotor. Since the measurement of the rotation angle does not much depend on the winding condition of the thread and the swing motion of the thread, the rotation-based control is expected to be more suitable for the yo-yo playing. The rotation angle of the rotor of yo-yo can be easily measured by the visual encoder method with the high-speed vision-robot system.

4.3.2 Analysis of Yo-yo Played by Human

The hand motion for the yo-yo playing is limited to simple up-and-down motion. In playing yo-yo, the start timing of the yank-up motion, the hand stroke, and the monotonic trajectory of the hand are considered as the crucial parameters that determine a successful playing of yo-yo. The data about successful yo-yo playing by human hand can be exploited to estimate the characteristic of above parameters. Fig. 4.5 shows the motion of the yo-yo that is recorded by a high-speed video camera, when human plays the yo-yo. This recorded motion

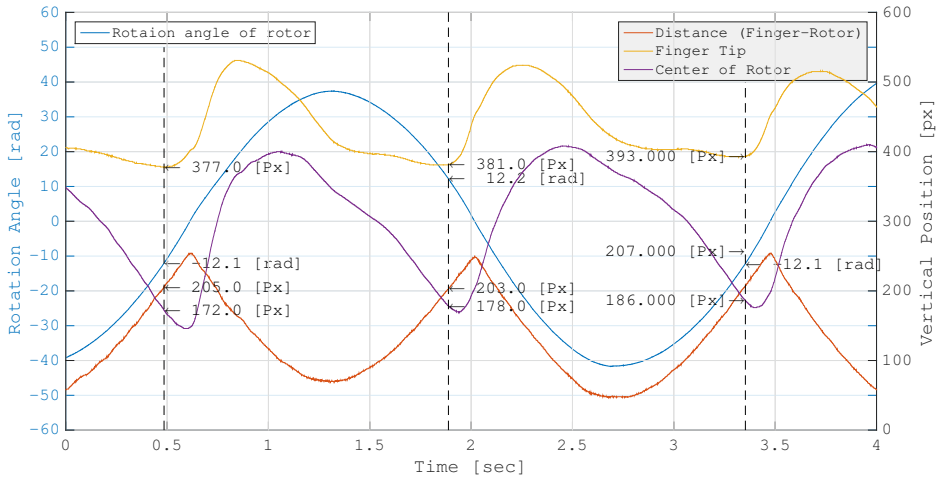

Fig. 4.6 Human hand motion during the yo-yo playing. Each dashed line indicates the moment that the upward motion of the finger tip (yellow line) starts. It precedes the bottom state of the rotor.

is analyzed with an image processing and used to calculate following four parameters: the rotation angle and the height of the rotor, the height of finger tip, and the distance between the finger tip and the center of the rotor, which characterize the yo-yo playing, as shown in Fig. 4.6. As pointed out in many literatures [40, 41, 46], the upward motion of the hand occurs before the rotor reaches to the bottom state where the rotation angle of the rotor is zero. The positions in time are marked with the dashed lines. The highest state of the finger tip is achieved after the impact that is occurred from the thread to the rotor. Therefore, between the lowest and the highest positions of the finger tip are connected with a smooth monotonic curve which has an inflection point.

4.3.3 Timing Control using Visual Encoder

Taking into account above analysis result, the trajectory of the hand can be planed as shown in Fig. 4.7 . Determining the appropriate moment that the thread to be pulled upward, as shown in dashed lines in Fig. 4.6 and (B) in Fig. 4.7, is considered to be very important. It is difficult to find the time in the case of the position-based control due to the modeling and measuring errors. However, if the visual encoder is applied, the timing can be easily and accurately determined, because the zero angle which indicates the bottom state of the rotor can be directly detected. As mentioned above, the time at which the upward hand motion starts should be located before the moment when the impact occurs. Therefore, the starting time can be determined with a time margin. It is shown in 4.6 that the margin

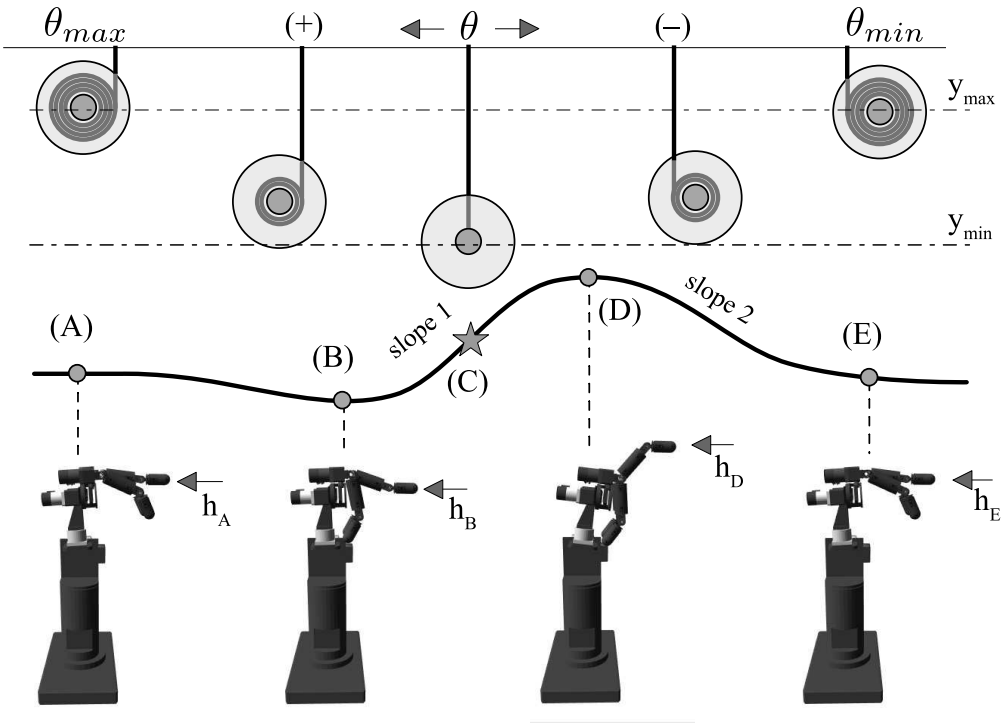

Fig. 4.7 Motion planning for yo-yo.

with the prepared yo-yo is equal to about 12 radians. The next important issue that should be considered carefully is how to produce the trajectory between (B) and (D) in Fig. 4.7. Generally, the biggest acceleration of the hand motion is required to be advanced before the impact at (C), in order to maximize the efficiency of the energy compensation against the energy loss caused by the impact or the friction. The impact position (C) is represented by the inflection point between (B) and (D). There are several methods to draw the trajectory [41, 46], and here a monotonic curve consisting of two Gaussian curves is used for the hand motion. For the simplicity, let the curve (A)-(B) be a line and locate (E) as the same height of (A) ($h_A = h_B = h = E$). When the local time t is reset to zero at every (B), the height of the hand h is determined as in Eq. 4.7.

$$h = \begin{cases} (h_D - h_B)\exp(-\alpha(t-\tau)^2) + h_B & \text{if } t \leq \tau \\ (h_D - h_B)\exp(-\beta(t-\tau)^2) + h_B & \text{if } t > \tau \end{cases} \tag{4.7}$$

where two parameters α and β determine the half width of the Gaussin curve. α sets the curve (B)-(D) and β does the curve (D)-(E) in Fig. 4.7.

Table 4.1 Parameters for Yo-yo Simulation

Parameter	Value	Parameter	Value
R	$0.03\,\mathrm{m}$	M	$0.0479\,\mathrm{kg}$
I	$2.156\times10^{-5}\,\mathrm{kg\,m^2}$	r_e	$0.0001\,\mathrm{m}$
L	$0.2\,\mathrm{m}$	r_a	$0.003\,\mathrm{m}$
h_B	$0.49\,\mathrm{m}$	h_D	$0.56\,\mathrm{m}$

4.3.4 Simulation Result

The simulation result of the yo-yo playing via the rotation-based feedback control is shown in Fig. 4.8. The time interval in this simulation is synchronized to the system frequency of the high-speed vision-robot system, as 1 ms (1 kHz). The blue line indicates the actual parameters and the red line represents the references. The sinusoidal oscillation of the rotation angle implies the correct rotation of the rotor, which leads the successful playing of the yo-yo.

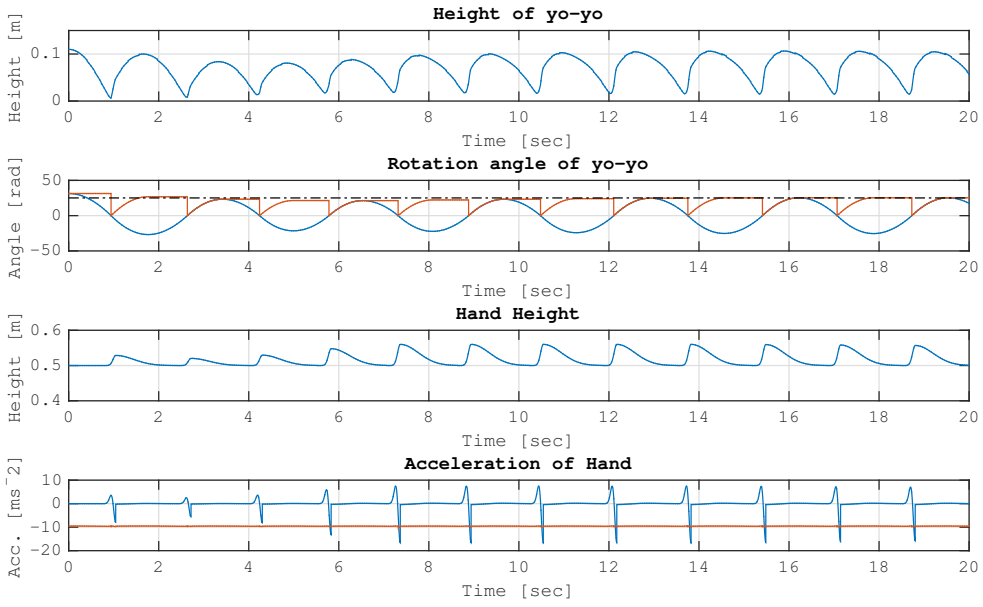

Fig. 4.8 Simulation of yo-yo based on rotation feedback

(a) Yo-yo with RGB marker

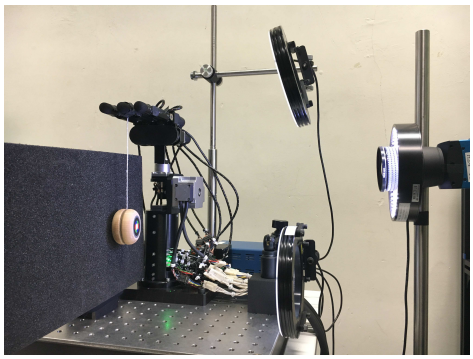

(b) Robotic yo-yo system

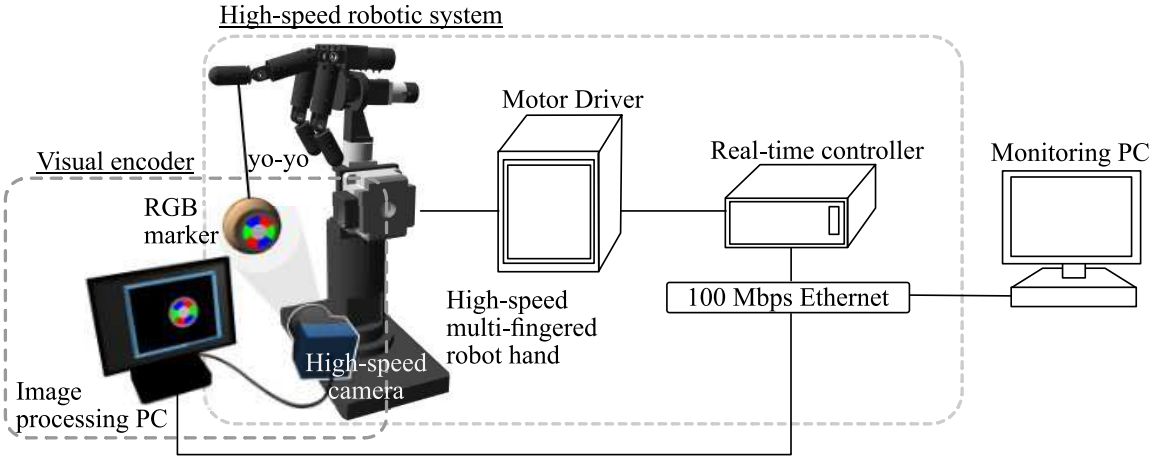

(c) System layout of high-speed vision-robot system

Fig. 4.9 Experiment setup for the robotic yo-yo playing

4.4 Experiment Setup

A yo-yo is prepared for its robotic playing and an RGB marker is attached on the surface of the rotor to measure the rotation angle by the visual encoder method, as shown in Fig. 4.9a. Since, the six color blocks are used for the RGB color marker, it is expected that up to 8,000 rpm of the rotation of the rotor can be measured by the visual encoder method. The maximum rotation speed is considered to be enough to use for the yo-yo playing.

Here, two type of tasks are performed. The first is the releasing and catching motion and the second is continuous playing of the yoyo. The controller as shown in Fig. 4.10 is used for the two tasks where the wave generator is designed differently depending on the task. The details are discussed in section 4.5.

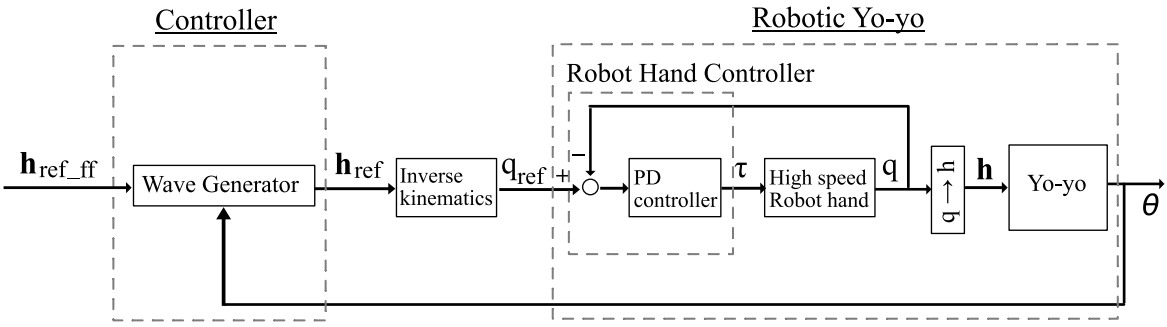

Fig. 4.10 Yo-yo controller based on the rotation feedback

4.5 Robotic Yo-yo Playing

The wave generator in Fig. 4.10 has its local timer to create the desirable hand trajectory as described in Eq. (4.7), and the timer is reset according to current rotation angle measured by the visual encoder. Therefore, at first, the threshold angle ($\theta_{(B)}$ in Fig. 4.8) which resets the timer should be determined. Then, the other parameters such as α, β, τ, $(h_D - h_B)$ in Eq. (4.7) should be found too. Since the determining of the parameters is not the easy process, the parameter tuning based on the yo-yo playing by human is helpful.

In this section, the two representative yo-yo playings, 'releasing and catching' and 'continuous playing' are performed with the hand trajectory made with the human reference.

4.5.1 Releasing and Catching

The 'releasing and catching' of the yo-yo is most basic skill required to play yo-yo. This skill consists of following sequential motions: grabbing, releasing, yanking-up, and catching (grabbing) of yo-yo. Since the grabbing, releasing and catching is not the interesting point of this research, the yanking-up motion is discussed mainly.

Fig. 4.11 shows the experiment result when the robotic yo-yo was played with the hand motion based on the human reference. The hand trajectory h is generated by the wave generator as the shape in Fig. 4.10. It is calculated from Eq. (4.8).

$$h_{ref} = \begin{cases} (h_D - h_B)\exp(-\hat{\alpha}(t-\hat{\tau})^2) + h_B & \text{if } t \le \hat{\tau} \\ (h_D - h_B)\exp(-\hat{\beta}(t-\hat{\tau})^2) + h_B & \text{if } t > \hat{\tau} \end{cases} \qquad (4.8)$$
$$t = 0 \qquad \text{if } \theta < |\theta_B| \text{ and } t > t_w$$

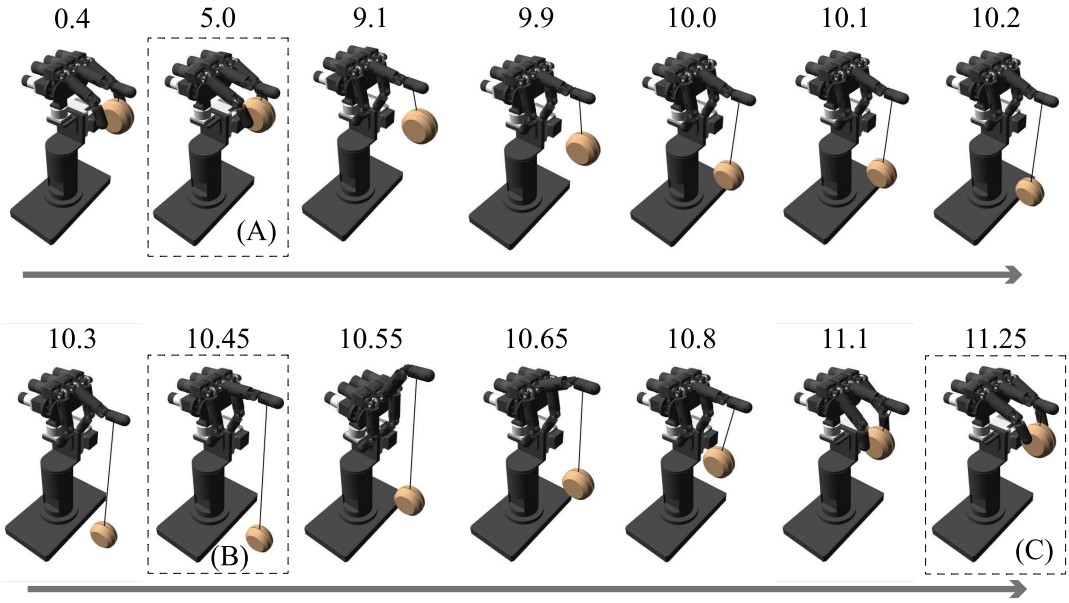

Fig. 4.11 Time course sequential motion of releasing and catching of yo-yo. The upper numbers show the event time in second. (A), (B) and (C) indicate the moment of releasing, reaching the bottom state, and catching, respectively.

where the hat mark is added to the parameters that is acquired from the reference of the yo-yo playing by human. The $\hat{\alpha}$ and $\hat{\tau}$ are adjusted to get the bottom impact during the yanking-up motion of the hand, and the h_D and h_B are determined as to have the maximum stroke by considering the working range of the robot joints. The threshold angle θ_B (in Fig. 4.8) that is used to reset the local timer in the wave generator and the other threshold angle θ_C that is used to determine the moment at which the catching motion starts, are also determined from the analysis of human motion. t_w indicates a time to wait the next time reset event and is adjusted with the $\hat{\alpha}$.

As shown in Fig. 4.11, the successful yo-yo playing for 'releasing and catching' is performed with the above hand trajectory in Eq. (4.8). The figures are drawn to help the understanding about the motion, based on the actually acquired data.

4.5.2 Continuous Playing

In comparison with the 'releasing and catching', 'continuous playing' is considered as more complicated task because there is no stopper such as the catching motion, between consecutive releasing motions. In 'releasing and catching', the maximum stroke of the hand motion is used to maximize the energy compensation via the yanking-up hand motion, and the sur-

(a) Guide wall (b) Guide tip

Fig. 4.12 Two different guided systems for yo-yo

plus energy can be absorbed when the rotor of yo-yo is caught by the hand. However, in 'continuous playing', the surplus energy produced by each yanking-up motion may cause the impact between the rotor and the hand, in case the rotor is excessively pulled upward. Therefore, the energy compensation should carefully treated by controlling the maximum stroke, $h_D - h_B$ in Fig. 4.7. The provided energy and the tension of thread via the yanking-up motion of hand are proportional to $\ddot{h}$, the acceleration of the hand in the vertical direction, and $\ddot{h}$ is proportional to $h_D - h_B$ as shown in Eq. (4.8). Hence, the h_D in Eq. (4.7) can be modified as following.

$$h_D(\theta) = H_0 + K_P * (\theta_{ref} - max(|\theta|)) \tag{4.9}$$

where H_0 indicates the initial height of h_D, K_P is the proportional gain, and the θ_{ref} refers to the desirable maximum amount of winding of the thread.

Moreover, the rotor of yo-yo can be turned around according to the stretched thread, when the rotation speed of the rotor is slow. The turning motion is regarded as a disturbance, and it may hinder the detecting of the rotation angle of the rotor, causing the occlusion problem. In order to focus mainly on the rotation of the rotor, two guide equipments such as the guide wall and the guide tip are prepared and applied when playing yo-yo, as shown in Fig. 4.12.

With Guide Wall

The robotic yo-yo based on the rotation feedback was performed with the guide wall as shown in Fig. 4.12a. The control input h_{ref} was acquired for the timing control by using Eq. (4.8) and Eq. (4.9). The result is shown in Fig. 4.13. Although the periodic oscillation

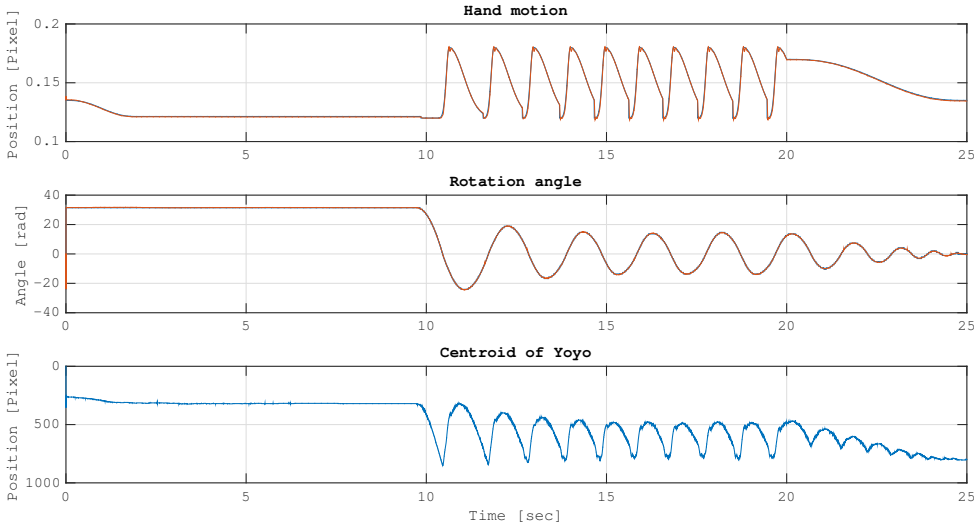

Fig. 4.13 The yo-yo playing with a guide wall

in the rotation of the rotor was achieved, the amplitude was smaller than the desired value. The center height of the rotor, y was also lower than the initial releasing height.

The amplitude and the height of the rotor are considered to be decreased by the friction loss between the surfaces of the rotor and the wall. However, in spite of existence of the friction loss, the rotor of yo-yo rotated normally, as shown in Fig. 4.13.

With Guide Tip

To reduce the friction loss, a small guide tip, which is made of a piece of thin plastic film, was designed and attached on the finger tip of the robotic hand instead of the guide wall. Unlike the guide wall, the guide tip contacts with the rotor only the area near the finger tip, and thus contributes to the reduction of the friction loss. Actually, the unwanted turning of the rotor around the direction of gravity still happens near the finger tip, when the rotor is wound fully and the rotation speed of rotor is close to zero. However, if the rotation of the rotor is controlled as intended and the maximum number of winding is regulated, it is expected that continuous playing of yo-yo is possible avoiding above disturbance. Fig. 4.16 shows the experiment result.

As expected, the rotation angle of the rotor and the height of the rotor were clearly regulated during the rotation control. Although automatic tuning of the parameters such as $\alpha, \beta, and \tau$ in Eq. (4.7), is still required, it is proved that the suggested rotation control based on the rotation-feedback is effective for the rotary system, in which the bending of flexible

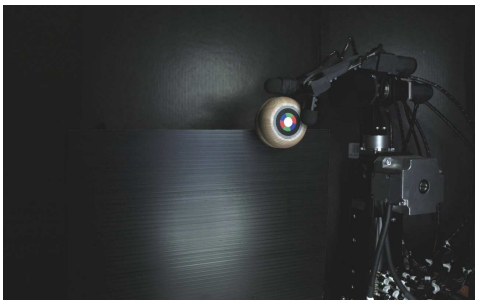

(a) t = 0.00 [sec]

(b) t = 0.40 [sec]

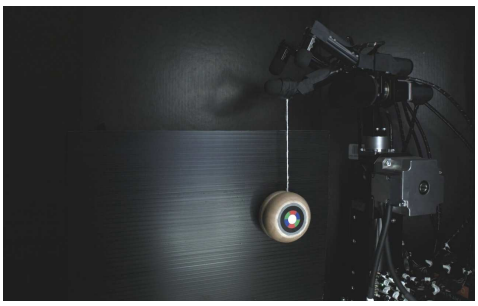

(c) t = 0.53 [sec]

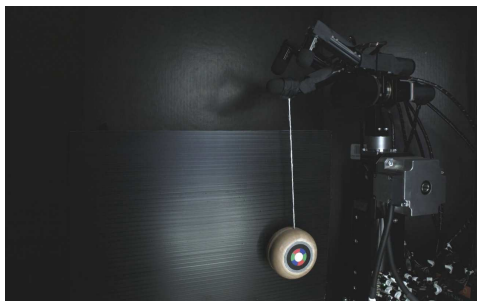

(d) t = 0.63 [sec]

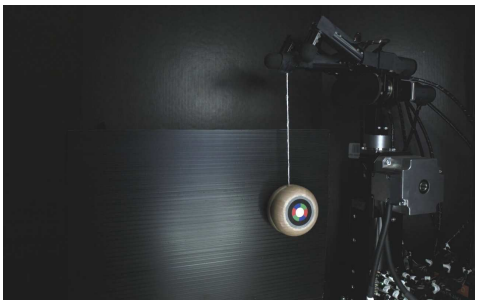

(e) t = 0.70 [sec]

(f) t = 0.77 [sec]

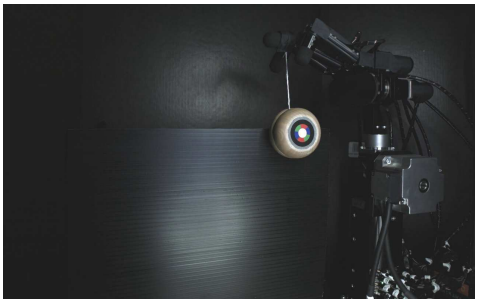

(g) t = 0.93 [sec]

(h) t = 1.33 [sec]

Fig. 4.14 Snapshot of robotic yo-yo with a guide wall in local time

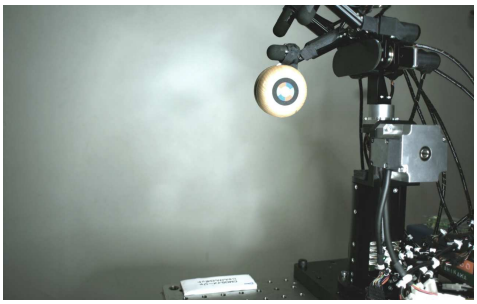

(a) t = 0.00 [sec]

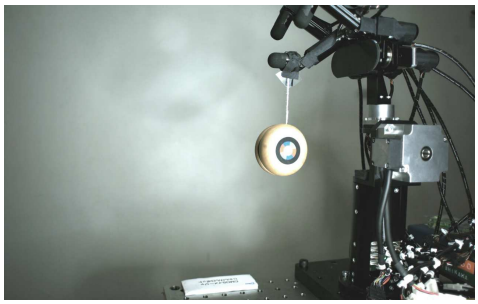

(b) t = 0.37 [sec]

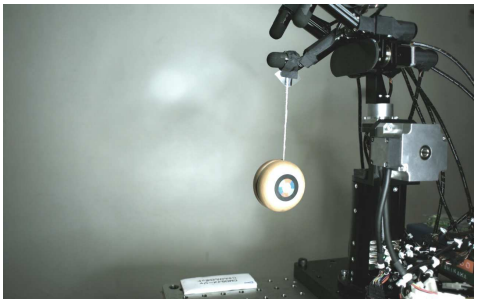

(c) t = 0.50 [sec]

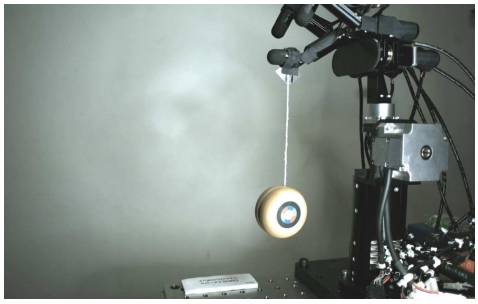

(d) t = 0.60 [sec]

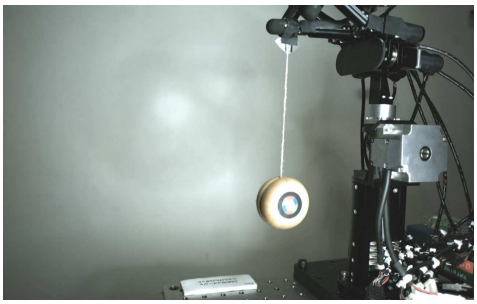

(e) t = 0.70 [sec]

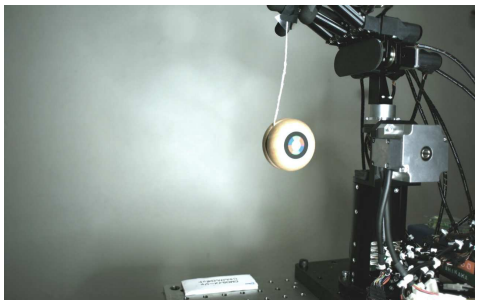

(f) t = 0.77 [sec]

(g) t = 1.00 [sec]

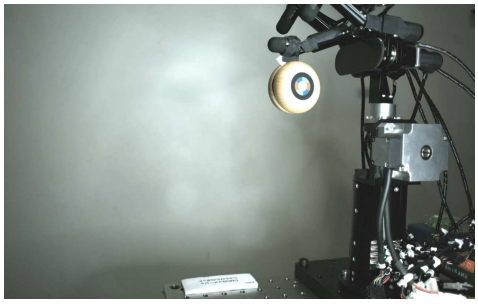

(h) t = 1.40 [sec]

Fig. 4.15 Snapshot of robotic yo-yo with a guide tip in local time

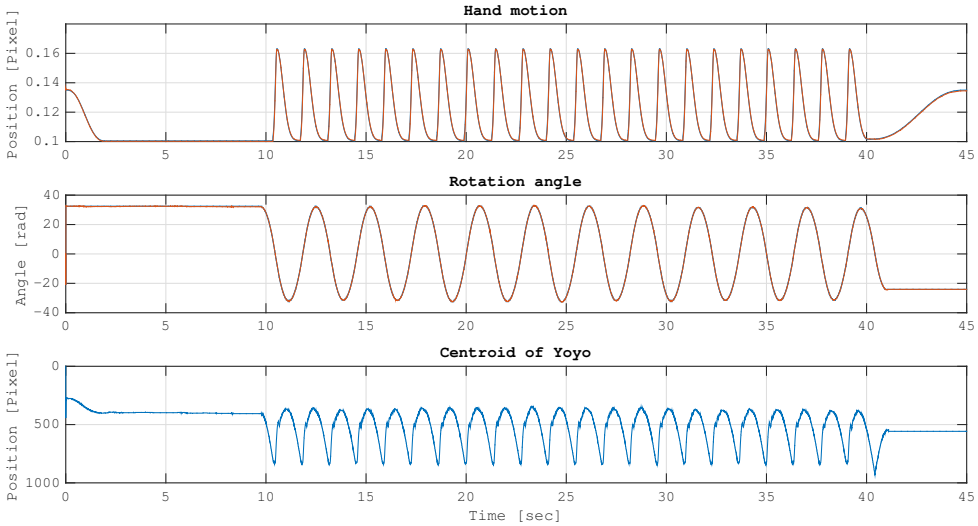

Fig. 4.16 The yo-yo playing with a guide tip

thread transfers the power to rotate the rotor in fluctuating condition. This control was possible by introducing the visual encoder method and the high-speed vision-robot system.

4.6 Summary

In this chapter, the robotic yo-yo was played as an application in which the rotation of the rotor via the bending of the flexible thread is controlled. The robotic yo-yo is not a simple task due to the aspects of the high-speed rotation of the rotor, the fluctuation of the rotation axis, and the nonlinear characteristic of the flexible thread. The effectiveness and the efficiency of the employment of high-speed vision-robot system with the visual encoder into above problems were studied as following.

First of all, the accurate winding model of thread around the axle of yo-yo was suggested and compared to the conventional winding model, such as Archimedes spiral. The modeling error of the winding was experimentally evaluated with the vision-based analysis, and it was proved that the considerable modeling error is inevitable. Secondly, the yo-yo playing was analyzed and the hand trajectory was proposed, focusing on the rotation of the rotor instead of the translational motion of the rotor. Finally, the two robotic yo-yo playings, ‘releasing and catching’ and ‘continuous playing’,were performed successfully with the proposed hand motion.

Chapter 5

High-speed Distributed Camera Networks for Visual Encoder

In this chapter, as a solution to avoid the occlusion problem of the visual encoder method, a structure to build a high-speed distributed camera network is introduced [1]. This structure based on the Message Passing Interface (MPI) and Real-Time Clock (RTC), includes multiple high-speed camera nodes and shows the sufficient performance in the time synchronization between the camera nodes. Because the properties such as 'easy to build' and the 'convenient to use' are the main concepts of the suggested structure, the high-speed distributed camera network can be used for many practical camera applications as well as for the visual encode method.

5.1 Introduction

Camera technology has made rapid progress as shown in the surprising performance of the built-in cameras of recent smartphones. Actually, most cameras commercially available a few years ago offer relatively lower shutter speed, such as 30 Hz, when capturing an image. However, recently marketed smartphones generally provide with high shutter speed, such as a few hundreds of Hz, as allowing users a new experience in photographing. Therefore, recording a slow motion of a flying ball or capturing an instant moment when a water drop collides became available techniques not only for the experts but also for the users with the smartphones in their hands. In fact, price lowering and the speed increasing of camera itself contributed to this trend that even the smartphones in everyday life are equipped with such

[1] This chapter is rewritten based on the contents in author's published paper [72]

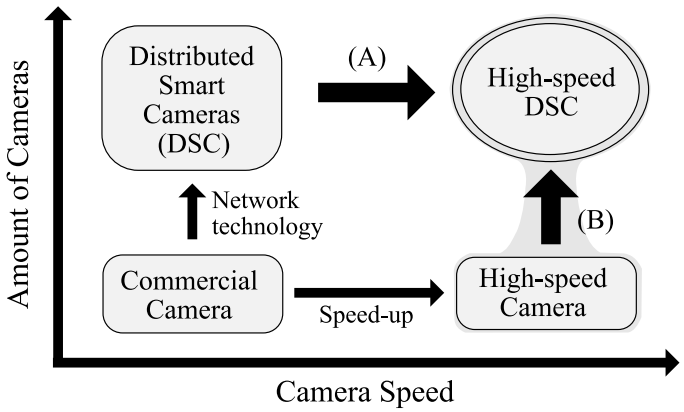

Fig. 5.1 Concept for high-speed distributed smart cameras (H-DSC) [72]

high-speed camera. Therefore, a novel network system comprising the high speed cameras that are able to capture an image at very high frame rate, such as hundreds of Hz close to 1 kHz can be suggested, in order to conceive a distributed smart camera (DSC) [73] for solving the occlusion problem in using visual encoder. In this chapter, the promise of a DSC with high-speed camera is described, and the way to build a system as well as the scheme for the verification of the system performance are considered. Not only as a traditional multi-camera system but also as a DSC, the simple system developed in this research can be treated, if each camera node processes the obtained information from its vision at a moment, and only the extracted feature information is shared across the system.

The most common example of DSC can be found in a surveillance camera system [74] mostly for monitoring the places near the camera, specifying the target object detected by the camera, and tracking any moving object appears in the camera view. Among the above functions, tracking an object is able to cover from the object which is moving relatively slowly, such as a walking human, to the object which is moving fast, such as running automobile on a highway. In addition, also in factories, DSC plays a role as an inspector that is able to automatically track and check the products on the conveyer belts which are flowing rather rapidly. Therefore, adapting high-speed camera into the DSC can increase the speed of the inspection and improve the productivity of the entire manufacturing system, by achieving the high inspection frequency. (A in Fig.5.1)

Capturing the dynamic scene by using high-speed camera, which the existing cameras are not capable of, can help users to estimate the object or surroundings that moves fast. Precisely speaking, the ‘high-speed’ is usually defined as the speed around 1 kHz. However, the ‘high-speed’ defined here indicates the order of hundreds Hz in capturing speed and the shorter imaging time than recognition time of human eye, since this order of speed is

far faster than the cycle of normal recognition, 25 Hz. As an application, there has been reported a research that the trajectory of the fast-moving object is reconstructed in 3 dimensions using mono high-speed camera, as suggested by Noguchi et al. [75] showing a novel approach as well as excellent result. However, because of the short exposure time and the fast shutter speed, their methods show a limitation, since the target object is required to repeat the movements following the designated path until the system collect enough data points for the reconstruction of the trajectory in high-resolution. In contrast, in case a DSC is adapted in the above application and install multiple distributed cameras on the path, only one movement of the target object along the designated path guarantees to gather enough data points for the reconstruction in 3 dimensions, which enhances the system efficiency. (B in Fig. 5.1)

As mentioned above, when the high-speed camera and the distributed smart camera system are applied together at the same time, it helps the performance enhancement of the existing application systems that are not concurrently accommodate these two features. Accordingly, the convergence of high-speed camera and DSC is a highly desirable direction of development, for both DSC and high-speed camera. However, only with the simple combination of these two features, users cannot conjure up the desired result, because of the limitation of 'high-speed'. Therefore, the verification of the unexpected errors which might occur when the two structures are combined is required. In this chapter, the required features for the verification of the convergence system, where DSC and high-speed camera are combined, are suggested, and the system structure which meets the conditions is described. In addition, the results of performance with the suggested system is presented.

5.2 High-speed DSC

5.2.1 Restriction by High-speed

The capturing frequency in DSCs such as common surveillance camera system does not play a role as a significant restriction, due to the slowness of the system. Such systems allow the images to be captured below 30 Hz and they are synchronized among all network cameras at those frequency, which is easily achievable with current hardware level. However, in order to build a H-DSC by combining high speed cameras and the DSC, time is required to be more precisely controlled in this case. For example, consider that all the cameras in a H-DSC capture images at 1 kHz, as the captured result are synchronized with other cameras in the network. In this case, the time allowed by system for each camera node to

finish capturing as well as synchronizing the images are only 1 ms. If 2 ms are consumed by some cameras in the entire camera network for a certain task, it is failed to achieve in gathering and processing the required data set that is supposed to be finished within 1 ms. Accordingly, some data of the advanced time span are required to be recognized and processed as current data, in the next given time. In order to avoid this kind of undesirable messed-up, it is carefully considered whether or not each process of all camera nodes can be finished in very short time span, which is determined by the processing time. That is to say, it is significant issue in H-DSC to synchronize the processes in accurate time, and thus the time synchronization is required to be guaranteed in order that each node of H-DSC should finish the designated processes in a precise short time span. Since it is closely related with this time synchronization, the real-time feature at high-speed is dealt with as an interesting topic in a H-DSC.

The 'real-time' precisely indicates the feature of the system where it is able to secure that a designated process should be completed within a fixed given time span, in any case. In this chapter, the 'real-time' [76] is defined as the condition where all entire camera nodes connected in DSC complete their given tasks within desired time span at software level. The soft-real-time is described as "a statistical distribution of response time is acceptable" [76]. The time interval is considered to be short enough in order to cover the variety in the processing time. In the system which is equipped with the real-time feature as above, if the camera system has a fast processing cycle, synchronization is not an issue to worry about. The real-time is referred to the same with the synchronization, due to the restriction of high-sped.

Therefore, as shown in Fig.5.2, a H-DSC is suggested which can be built easily with simple structure founded by Message Passing Interface (MPI) and Real Time Clock (RTC), proving that this system shows valid real-time feature by examining the processing time in both camera node level as well as the entire system level. Firstly, a summary of MPI and RTC will be descried below.

5.2.2 MPI & RTC

MPI [77, 78] denotes the Message Passing Interface, which is applied to a system comprising massively parallel computer networks. The performance of MPI has been qualified through many applications for recent 20 years, mostly in the simulation by super computers such as the interaction between galaxies in space [79, 80] or the collisions of atoms [81]

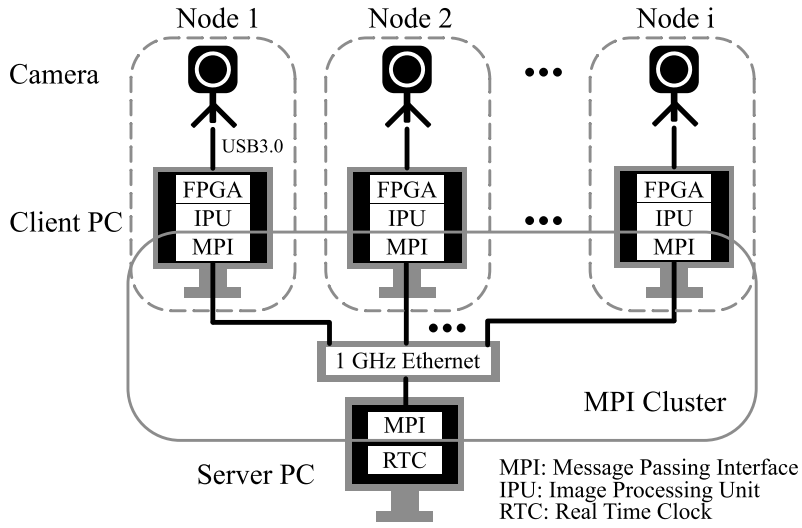

Fig. 5.2 Configuration of the H-DSC based on MPI [72]

where a large amount of calculations are required. In such simulations, MPI has played a role in managing the communication that is required between its calculation nodes.

MPI shows following features that are practical in the construction of H-DSC. First of all, MPI is equipped with a network of many calculation nodes connected in parallel. Secondly, MPI enables the data transfer to be fast and efficiently, since it supports the functions for broadcasting as well as gathering the data between node and the sub nodes. Lastly, MPI is proved to guarantee a stable transfer of data in a huge-scale of the calculation system.

Exploiting above beneficial features, it is easy to build and operate system nodes in a hierarchy with a structure that is consisting of two levels. In this structure, as the nodes of higher level handles the data processing as a post image processing and the entire system control, the lower-level nodes focus on the camera managing and the image processing. Based on this structure, while the processed data is transferred from the lower-level to higher-level node, the raw image data are not shared between lower-level and the higher-level node. This feature contributes to speed-up of the entire system and helps to maintain the real-time processing owing to the stable control of the nodes.

RTC is an acronym of Real Time Clock and is a built-in a computer processor, which can generate the periodic time signal at up to 8,096 Hz (in case that OS is Ubuntu Linux). By Adopting the signal as a trigger for starting the data broadcasting in MPI, it is possible to set a loop with a cycle that is far shorter than a millisecond.

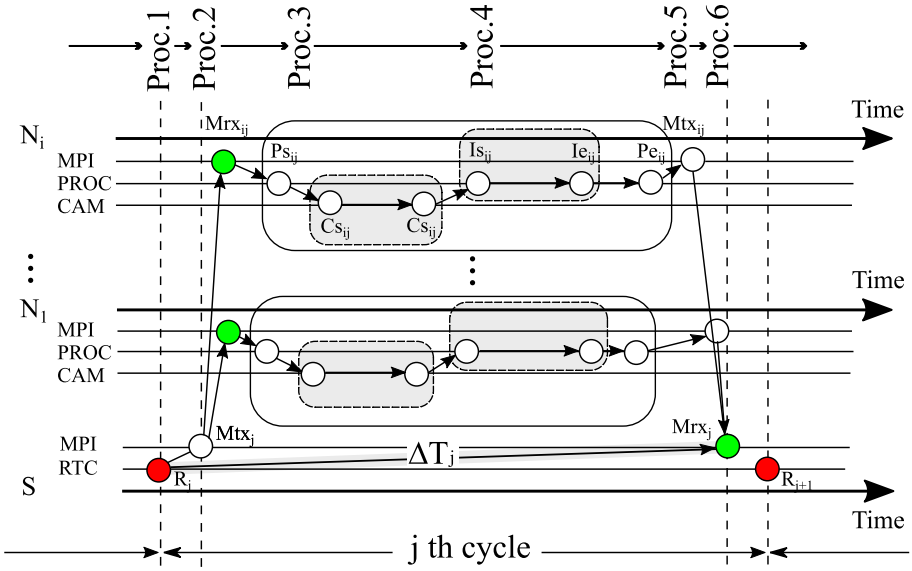

Fig. 5.3 Processing structure in suggested H-DSC. S and N represent server and calculation nodes, respectively. Here, C, P, I and M indicate camera capturing, processing in node, image processing and MPI Tx/Rx, respectively. The subscript 's' signifies the start of a process and 'e' for the end of the process. Index *i* indicates a node number and *j* for a certain processing cycle. Periodic trigger generated by RTC determines the processing cycle. Each event has its own time variation which has an effect on the real-time feature of the whole system. [72]

5.2.3 System Configuration

As shown in Fig.5.2, a H-DSC of a simple structure that is based on MPI and RTC is constructed. The H-DCS has a hierarchical structure where a server computer as a higher-level node plays a role in controlling camera networks and the three client computers handle respective camera and conduct image processing as lower-level nodes. A Gigabit Ethernet Switch makes a network between the server and the clients, and the high-speed cameras that are linked to the client computers can capture an image up to 450 Hz using USB 3.0 connection.

As shown in Fig.5.3, H-DSC performs a following sequential process in one cycle time: Proc. 1. Using RTC per a certain cycle time, the server computer generates a tigger signal. Proc. 2. After the trigger signal is fired, via MPI broadcasting the start signal is transferred to all client computers. Proc. 3. Arriving the start signal, respective client computer begins to capture image by controlling Field-Programmable Gate Array (FPGA) of high-speed camera, and the image data is loaded to the hardware memory of the client computer. Proc. 4. By lower-level image processing, the higher-level information including the center position

or the pose of the object is extracted from the image data. Proc. 5. Each client computer transfer the higher-level information data as well as the end signal notifying to the server computer that the process is completed. Proc. 6. Server collect the information data from the client computers, and terminate the entire processing in a cycle. The sequence from Proc. 1. to Proc. 6 is repeated.

The image capturing and processing on the entire nodes are guaranteed to be completed within one cycle time, throughout Proc. 2 to Proc. 5 in the suggested structure above. Additionally, the shorter cycle time secures the more accurate synchronization. The cycle time is significantly influenced by following factors: The time span accuracy for the generation of trigger in Proc. 1, the speed of signal transfer from Proc. 2 to Proc. 5, the speed of image capturing in Proc. 3, and the speed of image processing in Proc. 4. The cameras in the system are synchronized appropriately in high-speed condition, in case the time for processing in one cycle is actually proved to be far shorter than the desired time specification. Because normally the speed of image capturing of a camera is almost constantly managed with high accuracy by FPGA, the performance of the entire system is dependent upon the processing time from Proc. 2 to Proc. 4 . Therefore, in order to evaluate the stability of the suggested structure for H-DSC the processing time for above using statistical analysis.

In comparison with the existing system [82], the H-DSC features following distinguished characteristics: First of all, since it is achieved automatically by the system structure using MPI and RTC, there is no extra time for synchronization in H-DSC. In contrast, in case of general camera network, the processing timer is shared among the entire computers including the server and the clients, which is synchronized by Network Time Protocol (NTP) [83, 84] or Precision Time Protocol (PTP) [85], etc., and the stamps on the timer schedules all the processes in camera modules. Secondly, MPI transfer plays multiple roles in timer synchronization as well as in fate transfer, no separated network modules are required. Lastly, since MPI provides with practical functions, performing parallel jobs in massive and maintaining the system such as coding and system operating are very easy to deal with. Owing to these advantageous feature, H-DSC can be open to users who want to adapt distributed camera networks, and the development of technologies regarding DSC is expected to be accelerated.

5.3 Experiment Setup

As shown in Fig.5.4, a server and three clients are prepared to build a H-DSC for the experiments. The experiments consist of two major parts: One part is to measure and verify

the time consumed by each process in section 5.2.3, and the other part is to test actual application via capturing image and tracking object at high speed. In order to measure each processing time, the time stamps in processors are exploited and synchronized in order of nanosecond as all computers run a PTP daemon. A laptop computer with Linux as its OS is used as a server computer, where an Intel i7(3615 QM) quad-core processor of a base frequency 2.3 GHz is built in. Also, the processor for clients computer connected to each camera node is Intel i5 (3317 U) dual core, of 1.7 GHz of base frequency, and Linux is adapted as OS. High-speed USB 3.0 camera are linked to each MPI node, where the images can be captured up to 480 frames per second (fps) provided that the resolution of the image is 640×480.

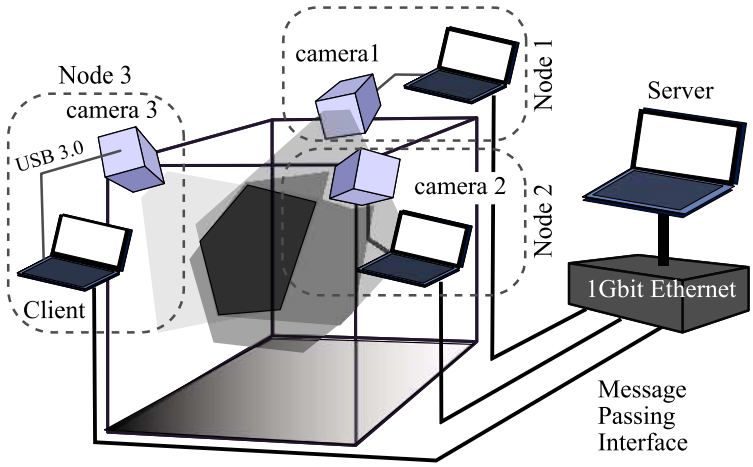

Fig. 5.4 H-DSC used in image capturing and tracking tasks. Three networked cameras are arranged in order to overlap the field of views. [72]

5.3.1 Measurement of Processing Time

While the trigger is generated at 1,000 Hz of frequency, the time accuracy of the trigger signal are measured. The processing time which is defined as $\Delta T_j = Mrx_j - R_j$ is measured as shown in Fig.5.3. Also, in order to estimate the system performance, the descriptive statistics of $\Delta T_j (j = 1, \cdots)$ was computed.

RTC

With very high accuracy, the RTC-based triggering signal can be produced. In case of 1,000 Hz of the trigger frequency, the variety in time generated correspondingly are calculated as $\Delta T_j = R_{j+1} - R_j$, as shown in Fig.5.3.

RTC+MPI

The time taken as transferring data using MPI was measured when RTC activates the start trigger. For checking the time consumed by transfer alone, as soon as it received the trigger signal, immediately each client transmit the priorly determined 4-byte data set.

RTC+MPI+Image Capturing

The whole processing time in one cycle excluding the time consumed by image processing was measured. Since the camera is not able to operate at the frequency higher than 480 Hz, the system is run at 400 Hz of capturing cycle, although 1,000 Hz was the desirable frequency. Also, USB 3.0 is exploited in the experiment, which shows restricted transferring speed, while the type of connection influences the high speed operation. Therefore, capturing at higher frequency can be achievable if the cameras which offer high speed camera link interface are applied.

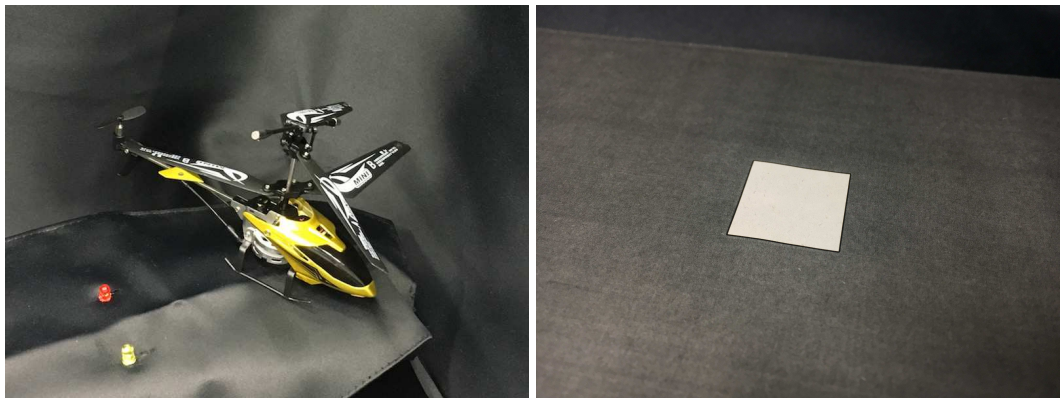

(a) Toy Helicopter with LEDs (b) White Square Marker

Fig. 5.5 Samples used for experiments. (a) A toy helicopter and two blinking LEDs. The blinking is captured as an evidence of the synchronization of multiple cameras. (b) A white square marker printed on a sheet of paper is moved on a desk surface by hand, to determine its position and orientation. The four corners of the square were detected by FAST corner algorithm and P4P problem was solved with the corner points. The marker size is 20x20 mm. [72]

5.3.2 Example of Applications

Following two test are conducted as examples of high-speed image capturing and real-time object tracking.

High-speed Image Capturing

High-speed Image Capturing: Image capturing based on H-DSC is performed as following: (1) Firstly, memory allocation with enough memory space for capturing is conducted in the client computers. (2) Secondly, as an on-line process, the captured images are sequentially loaded to the local memory. (3) Lastly, as an off-line process, the images in memory are saved to the local SSD on the client computer, after completing the entire processes. As a target object, a toy helicopter and two blinking LEDs are used as shown in Fig. 5.5a. The LEDs are controlled to maintain their 'on-state' during the time less than 4 msec so that the turn-on is only captured one or two frames during the blinking. The synchronization of multiple cameras is proved by comparing the frame which shows 'on-state' among the sequential images on each camera view. Due to the limitation of the cameras of the system, the image capturing is performed at the frequency of 400 Hz.

Real-time Object Tracking

As shown in Fig. 5.5b, a small square marker which is printed on a sheet of paper was tracked while it is moved by hand, as a simple example of an object tracking. When the image capturing is complete, the post processing begins as each camera node recognize the four corners of the marker, calculate the center position of the marker, and perform the pose estimation. In real-time, the computed pose data such as the orientation and the position of the marker were transmitted to the server computer. The trajectory of the object position is confined to two dimensions and thus the normal vector is not easily changed, because the square marker is set to move on the plane.

5.4 Result

5.4.1 Timing Performance

Since the designated trigger time is almost equal to the measured trigger time, it is obvious that RTC is able to fire a trigger signal with very high accuracy, as shown in Fig. 5.6. It is only 23 microseconds as mean value (with 4.7. microseconds of standard error) when

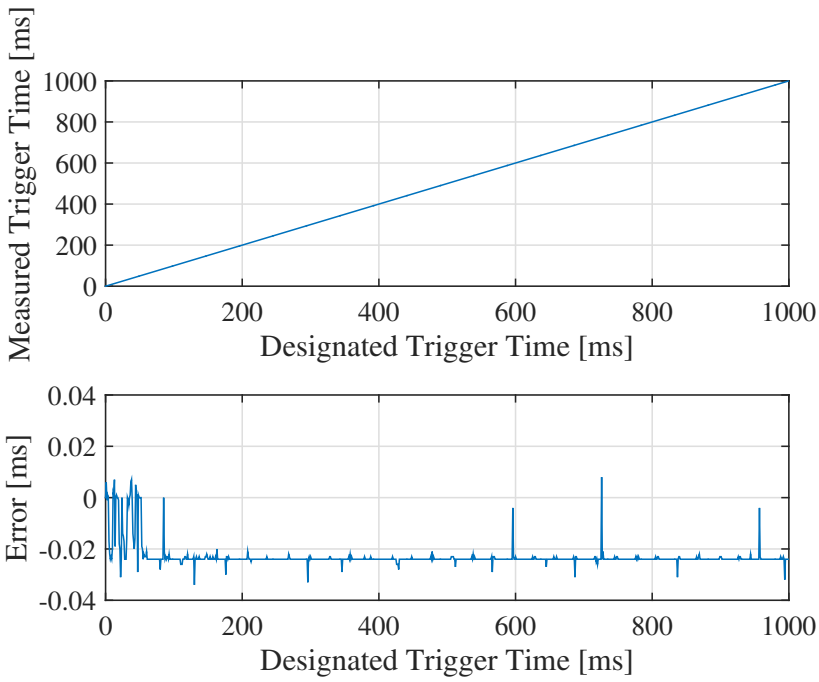

Fig. 5.6 RTC: Time accuracy of trigger signal by RTC. The error between the designated and the measured trigger time was -0.023 ms and 4.7 ms, the mean and standard deviation, respectively. [72]

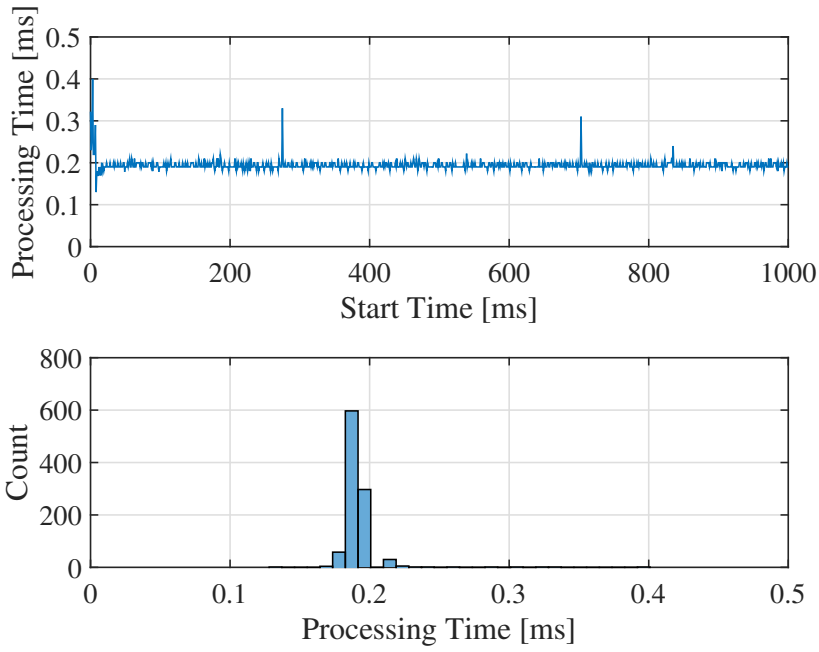

Fig. 5.7 RTC+MPI: Processing time for a cycle of the trigger generation and MPI data transfer. The mean value was 0.19 ms and the standard deviation was 0.0125 ms. [72]

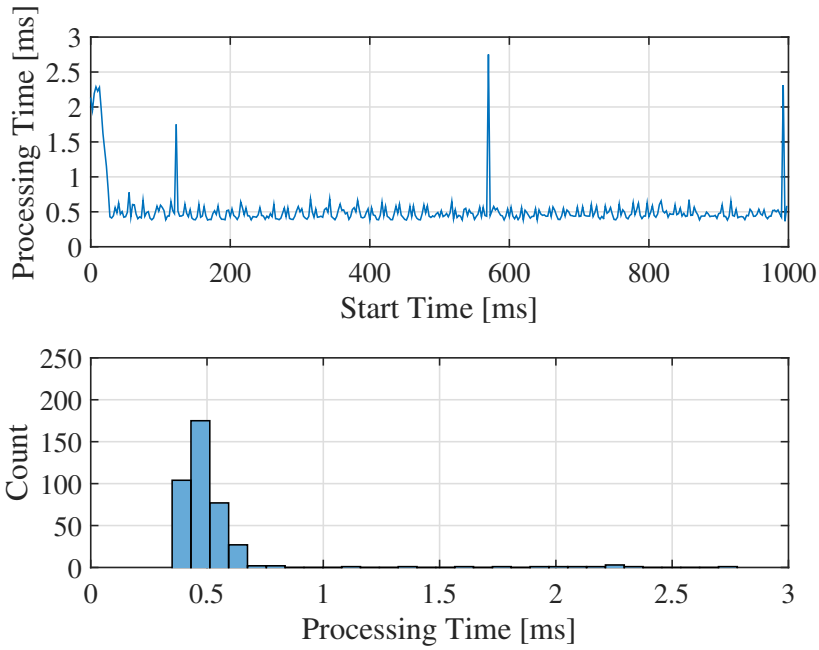

Fig. 5.8 RTC+MPI+Image Capturing: Processing time for a cycle of the trigger generation, MPI data transfer and image capturing at 400 Hz. The mean value was 0.525 ms and the standard deviation was 0.29 ms. [72]

the time difference between the generated and designated trigger was measured. Therefore, from the view of the accuracy in time, using the embedded RTC as a trigger or a system callback function can be considered to be reasonable. Fig. 5.7 shows that the result from the case of RTC+MPI where the time required to complete the data transfer including transmitting and receiving data is measured as 0.19 milliseconds in mean value (with 12.5 milliseconds of standard error). Therefore, time available at each camera node to assign for the image capturing as well as processing can be determined using these statistics. For example, to achieve Six Sigma performance level where 0.00034 of percent defective is a standard, the time margin for the image capturing and processing is calculated as 0.735 millisecond in case of 1 millisecond of processing time form the equation 1-(0.19+6$\times$0.0125), for current system. Practically speaking, it is considered to be enough time for image capturing and processing in a dynamic system, based on the experience from the previous researches using a high-speed camera.

Lastly, Fig. 5.8 shows the result of RTC+MPI+Image capturing where the system using high-speed cameras that capture images at 400 Hz is proved to work with enough synchronization. In this case, the mean value of total processing time was measured as 0.53 milliseconds with 0.29 milliseconds of standard error.

5.4.2 Observation and Tracking at High Speed

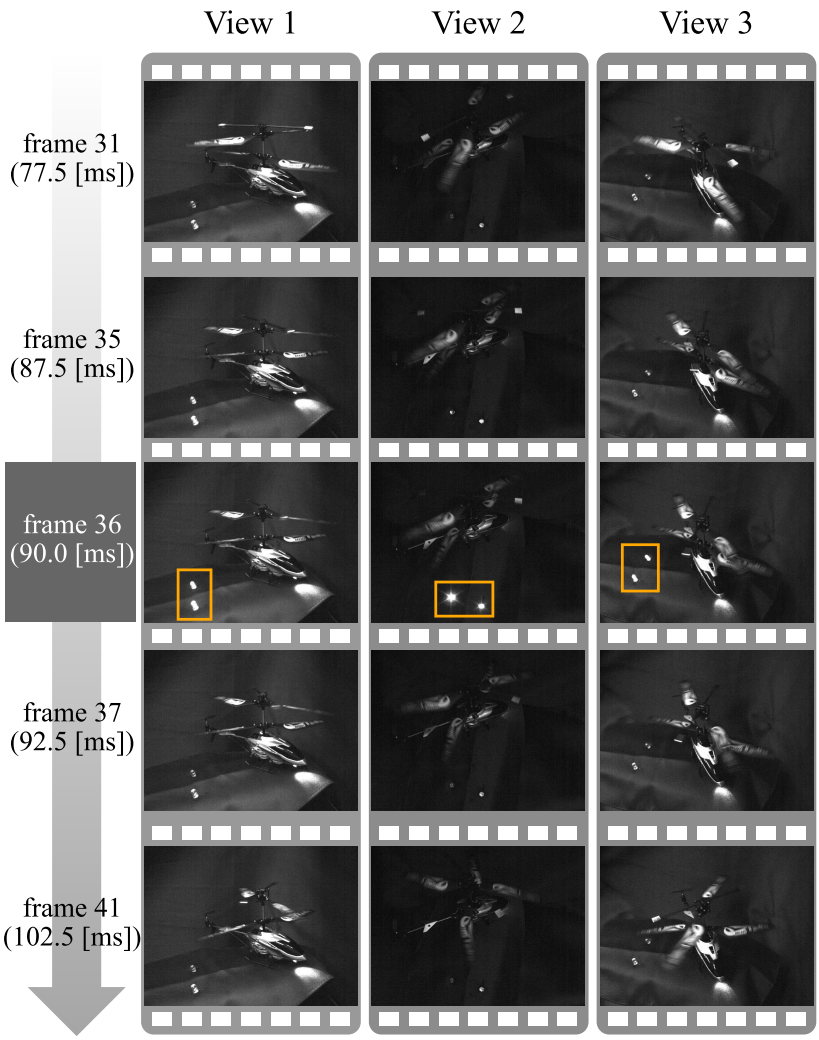

Fig. 5.9 Sequential image set captured at 400 Hz from multiple viewpoints. Three views are synchronized by MPI and RTC at the same frequency. The images of a toy helicopter with blinking LEDs, were captured by three high-speed networked cameras. [72]

High-speed image capturing is conducted in on-line for a thrown object at 400 Hz, and the sequential image sets are recorded with H-DSC system that is equipped with three viewpoint in off-line, after the processing in on-line is completed. Fig.5.9 shows the multi-view images that are captured successfully. Additionally, an object tracking with some image processing at 200 Hz is also performed, and Fig. 5.10 shows that H-DSC system works well in on-line. In this case, the mean value of total processing time was measured as 2.5 milliseconds with 0.84 milliseconds of standard error, as shown in Fig. 5.11.The variety

in the time distribution is slightly large in comparison with the result of RTC+MPI+Image capturing which is shown in the histogram in 5.8, even though it seems to be enough for the high-speed capturing at 400 fps. The reason is probably due to the feature of cameras that are used in the experiment. In fact, the cameras exploited in the experiment show the limitation in that the maximum speed is restricted to 150 fps when the image resolution is 1280×1024. Although it is possible to raise the frame rate up to 480 fps by reducing the image resolution to 640×480, the operation seemed to be unstable, causing a large variety in processing time. If the cameras of higher frame rate such as 1,000 fps are exploited, the system is expected to be stable even at higher speed.

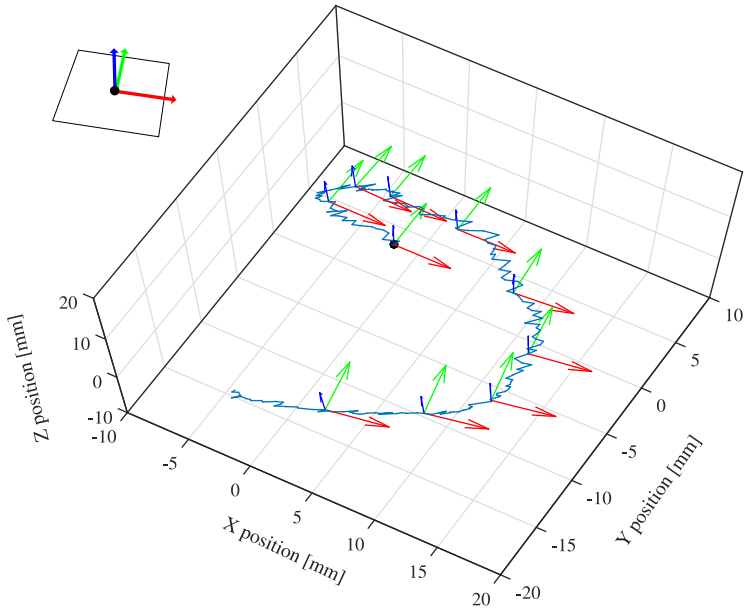

Fig. 5.10 High level information by image processing, such as position and orientation of the object, was extracted and shared across the whole camera network with H-DSC successfully at 200 Hz. Blue line indicates the trajectory of the center position of a square marker, which starts from the black dot. Blue arrows show the normal vectors of the marker and comprise right-handed coordinate system with red and green arrows, which represent x, y and z axis of the marker coordinate, respectively. [72]

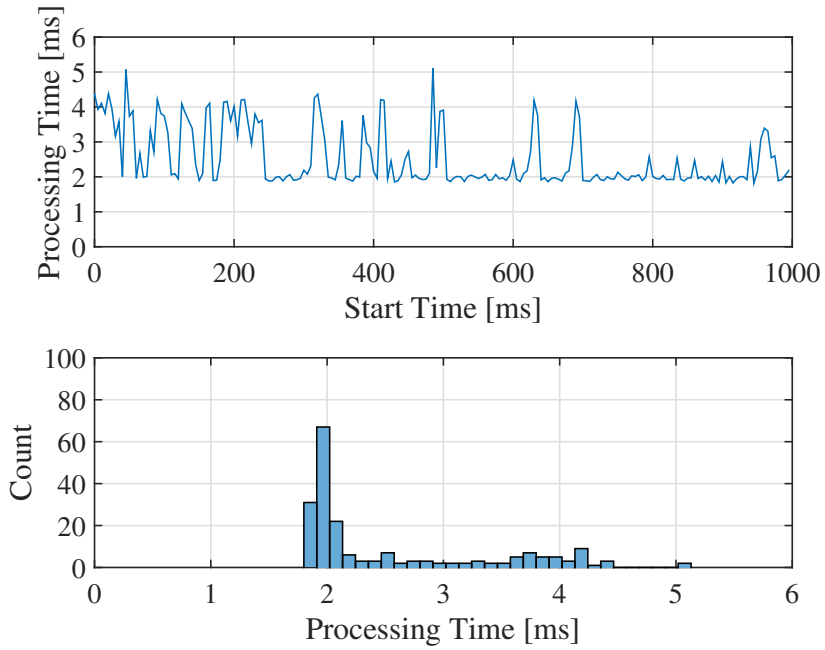

Fig. 5.11 Processing time for a cycle including the whole process in Fig. 5.3. The mean value was 2.5 ms and the standard deviation was 0.84 ms. [72]

5.5 Summary

In this chapter, based on MPI and RTC, a high-speed distributed camera network is constructed and evaluated its performance in regards to the synchronization of camera nodes at high speed. As applications, multiple image capturing as well as an object tracking in real-time is conducted with the network system. Although the operating frequency is set at 400 Hz in the tested network system, the system is proved to have enough timing margin to work with the faster cameras such as 1 kHz of capturing rate. As shown in Fig. 5.2, by adapting MPI in the synchronization of camera network, the suggested system applied in the experiments shows advantageous features such as the simplicity in structure and the easiness in construction. Moreover, owing to its simple feature the suggested system allows easy maintenance such as in coding and in running the program. Therefore, it is anticipated that the H-DSC can help the users who are interested in building distributed smart cameras to construct and exploit the system easily. Developing the applications using H-DSC which produce synergy as a convergence of high-speed and distributed camera remains as a future work. In particular, observing fast moving environment and tracking an object within the region of interest are expected to perform in the future, as verifying the practicality of H-DSC with various tasks.

Chapter 6

Further Applications and Future Works

In the previous chapters, the visual encoder as a measurement method of the rotation angle and the two example applications of robotic manipulation for the rotation control via thread were described. In fact, the robust measurement and control of the rotation via thread that are shown in the respective case of yo-yo and button spinner can be exploited for further applications. Here, the details of the applications are suggested with some experiment results as well as the expectation.

6.1 Part I: Visual Encoder

The visual encoder method is basically a kind of vision-based rotary encoder, but enhances the reliability with its specialized marker. This improved reliability of the visual encoder method is superior than other conventional vision-based methods, and it gives the visual encoder method the chance to be exploited for controlling the mechanical systems where the higher measurement reliability is required. As in the case of all the vision-based method, the visual encoder method also provides with the ability of the remote sensing for the target. The remote sensing ability has the advantage of the multiplication of the sensor as well as the easy maintenance.

Multiple sensing for protection and maintenance

Various rotary systems such as the huge turbines in the factories and the electric motors in the electric vehicles require a high-revel security for the operation. Most of those systems embed the electrical rotary encoder, and the physical trouble of the encoder may bring a disaster during the system operation. As a solution to increase the stability of the high-

speed rotary system, the multiplication of the sensor units can be considered. In this case, the visual encoder method has the advantage in the multiple installation over the traditional rotary encoders due to its remote sensing ability. If it is required, the massive installation is also possible as a high-speed distributed smart camera system. Depending on the situation, the hybrid installation to the existing system can be conducted easily.

Moreover, as well as the enhancement of security, the multiplication of the visual encoder gives a simple way to maintain the rotary system. Even if some defection is detected at a sensor unit, the rotary system can recover the function immediately, by disabling the unit and replacing it with a new unit. This seamless repair reduces the maintenance cost for the huge rotary systems with large moment of inertia. For example, in case of huge turbine adapted in the plants or containerships, the visual encoder makes the repair of such turbines an easy task, otherwise a lot of time and efforts should be consumed for stopping and restarting of the rotary system.

Remote sensing for microsystem and hazardous environment

The remote sensing ability of the visual encoder can be used for the micro actuator. The general types of electric actuator embed many sub components such as magnetic core, coil, and magnet. To embed these components into a small volume of device is not only difficult, but also limits the development of micro actuator. Moreover, in case an encoder is required to be added to the system, the task can be more challenging. In this situation, the visual encoder proves its real worth. Consider a micro actuator consisting of a micro waterwheel and a tube which functions in a microscopic scale, and a fluid flows into a tube that turns the micro waterwheel. Since these components can be easily produced with MEMS technology, by introducing the visual encoder method, the simple structure can work as a micro actuator system where the micro waterwheel plays a role as an end effector like a cutter or a fan. Likewise, the simple structure achieved by adapting the visual encoder method is advantageous in the miniaturized design for the micro actuator.

Furthermore, the remote sensing ability can be applied to the measurement in the hazardous environment where the sensor unit is exposed to the harsh condition, such as extremely low temperature, radioactivity, and toxicity. For example, even in case of space, nuclear reactor, and the workplace with chemical materials, placing the sensor units in the safer location such as a monitoring room apart from the rotor itself is possible when the visual encoder method is applied. This separation contributes not only to the protection of the sensor unit itself but also to the easy maintenance.

Rotation Measurement using Smart Phone

By using visual encoder, various types of less-restricted rotation of a rotor can be measured without introducing a dedicated rotary encoder. Nowadays, high-speed camera, which is the core equipment in the visual encoder method, has been accessible to anyone who wants to use it owing to the reduced price and the performance improvement. For example, recent smart phones such as iPhone already embedded the camera module that is able to capture images at 240 Hz [86, 87]. Also, the RGB marker, the other important part of the visual encoder, can be prepared by printing the color pattern using any available commercial color printers. Therefore, for instance, the high-speed rotation of the bicycle wheels or car wheels can be easily measured, as well as the rotation of any spinning toys, for educational purpose or for entertainment purpose.

Rotation Control of Motor using Visual Encoder

An electric motor without any embedded rotary encoder is difficult to accurately control the rotation. Although it is equipped with a control map between the input and output signal or a mechanical switching structure, the out-of-phase caused by the disturbance is likely to hinder the rotor from achieving the desired rotation. Unlike in the case of the rotary encoder, since the visual encoder is not required to be embedded to the motor, it can be applied to the rotation control of the encoder-less motor by attaching the RGB marker. Since the most of vision-base methods provide with multiple object tracking, only one camera is required to control the rotation of multiple motors simultaneously, as long as the computing power of the image processor allows. As a trial, the rotation control of single motor using the visual encoder was performed successfully, as shown in Fig. 6.1.

Visual Servo-ing for Planar Robot

Visual servo-ing [88, 89] is considered to be one of the promising fields where the visual encoder method can be applied. Whereas the current visual servo-ing basically aims at the control of robotic manipulators based on the visual perception of the robot and the surroundings, the remote sensing of the visual encoder can also be exploited for the joint control of the robot itself. In this case, the visual encoder substitutes for the conventional optical encoder in the electric motor at each joint of the robot. Since the visual encoder is located outside of the robot, the weight of the robot manipulator can be reduced by the weight of the optical encoder when replaced, which can lead the enhancement in the movement speed of the the manipulator. Moreover, applying the visual encoder method instead of the ex-

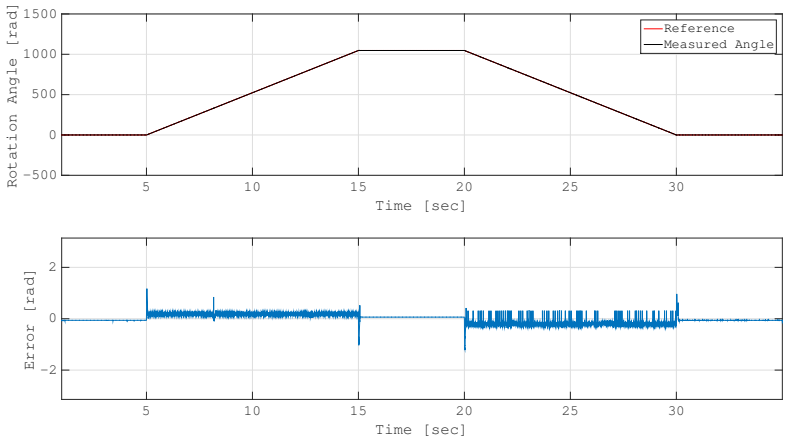

Fig. 6.1 Rotation control of a motor using visual encoder. The forward and backward rotations of the motor was performed at 1,000 rpm.

isting optical encoder helps to decrease the physical constraints in robot motion, by being able to remove the current wirings that are installed for the optical encoder, which increases convenience in the maintenance.

Without introducing of the high-speed distributed camera network to the system, the visual encoder method is still incomplete for the three-dimensional sensing. Therefore, two dimensional motion control of a planar robot is considered as a feasible application for the moment. Since the planar robot has multiple links that move in the same plane [90], visual encoder can be used to measure the joint angle of each link without concerning the occlusion. A 6 DOF planar robot that has two 3 DOF fingers can be a simple example of the practical application, because it can play a role as a gripper. Hence, visual servo-ing of the 6 DOF planar robot is suitable as a preliminary application.

6.2 Part II: Rotation Control via Thread

Shaker and Machine Tools

The ability to easily generate the high-speed rotation is a strong point that a rotary system via thread shows. In this system, the linear hand motion of low frequency can produce a rotation of thousands Hz, simply through the thread. The representative use of this feature is a shaker, which is hung by the a pair of twisted thread. Since this type of shaker has no mechanical parts such as a gear box or a shaft and the thread itself plays a role as a shock absorber, it can be less influenced by the undesirable vibration or heat release. Fig. 6.2

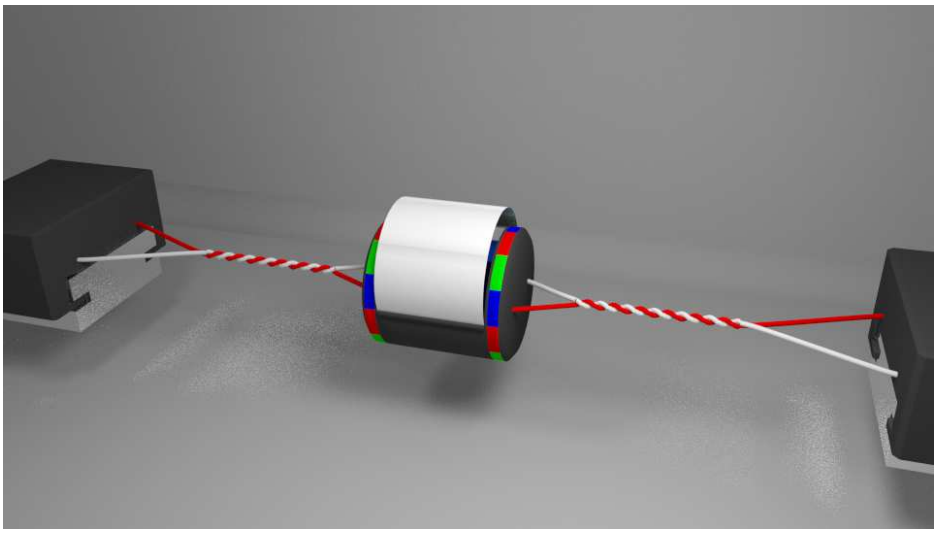

Fig. 6.2 The rotation control via thread using visual encoder can be used for a new type of soft shaker. Retrieved from the youtube movie “Robotic Button Spinner - Manipulation of High-speed Rotating Object via Twisted Thread”

shows the design of the shaker where the twisted thread and the visual encoder are applied. The mechanism of the rotary system via thread can also be utilized for the development of other machine tools such as the grinder and the drill which do not deliver the vibration to the user’s hand.

Recently, a new approach in bioengineering, which is named ‘paperfuge’ [91], has been reported to exploit the mechanism of the button spinner as a hand-powered centrifuge in order to replace the existing costly equipment. However, paperfuge requires hand power to be maintained for about 15 minutes for isolating malaria parasites, which is a tiring work due to the long-time operation. In this case, the robotic manipulation of the paperfuge can reduce the human effort with more accurate rotation control.

Casting Manipulation

The high-speed rotation of a rotor causes high rotatory inertia effect, and this phenomenon can be exploited to the casting manipulation, which is related to the control of the swing motion and the midair motion of an end-effector that includes a flexible arm such as string [92, 93]. In this case, the high rotary inertia can help to maintain the pose of the end-effector constant. Actually, in case of playing yo-yo, the thread suspending yo-yo does not experience the twist along the vertical axis when the rotor spins at high speed, which is otherwise inevitable.

6.3 Summary

In this chapter, the practical applications exploiting the visual encoder method and the mechanism of rotation control via thread are described with several examples. The visual encoder as a robust measurement method for the high-speed rotation of a rotor can be adapted in various applications, not only in the field of portable measurement systems for the rotation but also in the visual servo-ing of planar robot. Also, the rotation control of a rotary system via twisting of thread can be applied to the machine tools as well as a new flexible type of shaker. Lastly, casting manipulation can utilize the rotary system in order to maintain the constant pose of the end-effector.

Chapter 7

Conclusion

In this dissertation, the visual encoder method is developed and suggested as a new robust method to measure the rotation angle of a rotor, and the applications into the field of the robotic manipulation for rotation control were shown by verifying its performance in two example tasks, button spinner and yo-yo.

In chapter 1, the background and the motivation of this research were introduced. The importance of the rotation control was firstly presented with its historical contribution to the industrial field, and the rotation control via thread by the robotic manipulator was explained in the effort to expand the human's skill that robots have not achieved yet. As a systematic solution to reduce the non-linearity caused by the transformation of the flexible object, a high-speed vision-robot system was chosen and the structure design of the system was described. Also, the purpose of this research and the outline of the contents were presented.

In chapter 2, the visual encoder was suggested as a newly developed measurement method in order to alter the conventional method for the measurement of the rotation of a rotor. The principle of the visual encoder, which is a fusion of the conventional optical encoder and the vision-based method, was explained and formulated theoretically. Then, the limitation of the suggested method regarding the resolution and observable speed of rotor was discussed in detail with the experiment results. Consequently, the visual encoder method was able to measure the high-speed rotation of a rotor, even under the condition where the rotor fluctuates and the rotation axis is not fixed. The maximum rotation speed that the visual encoder was capable to measure was about 8,000 rpm, which is 6-7 times faster than the results acquired from the similar previous works with conventional measurement methods. Also, in order to prove the robustness of the visual encoder method, the quantitative measurement experiments were set with various conditions. Furthermore, to enhance the measurement resolution at high-speed, a high resolution method was intro-

duced. With the high resolution method, more than ten times of improvement in resolution was observed in comparison with the measurement result obtained before it is adopted.

In chapter 3, the robotic button spinner was successfully performed using the high-speed vision-robot system and the visual encoder method. With this application, it was proved that the rotation control via thread-twisting can be easily controlled notwithstanding the difficulty in the modeling and the linearizing of a system that includes a flexible part. A geometric model to explain the twisted pairs of thread that appears in the button spinner was also suggested, and the model is applied to the simulation of the thread-twisting in order to show the effectiveness of the visual feedback control. The human hand motion while playing the button spinner was also observed using high-speed camera and analyzed to be exploited as a base of the control reference. In the robotic button spinner, the amplitude of the high-speed rotation of the rotor was successfully regulated as well as the position of rotation axis, using the high-speed visual feedback control. The drift of the controlled position was measured less than 5 pixels, which is only 0.8 mm in actual dimension.

In chapter 4, the robotic yo-yo was played with the rotation-based feedback control instead of the conventional position-based feedback control. First of all, a new winding model of thread around an axle is built for playing yo-yo, since the existing model is less accurate in explaining the actual figure of winding and thus causes control error. Similarly to the case of the robotic button spinner, the strategy for playing the robotic yo-yo is also based on the direct feedback of the rotating angle and takes the reference from the actual human hand motion. As a result, the‘releasing and catching’ and ‘continuous playing’ by the robotic yo-yo were successfully performed. Actually, the direct feedback of the rotation angle and the use of the high-speed vision robot system were effective to run the robotic yo-yo, without exploiting the parameters that are taken from the technical specification of the thread and the yo-yo disc. The conventional simulation using the system identification was also performed to check the characteristics of the robotic yo-yo.

In chapter 5, high-speed distributed smart camera (H-DSC) based on MPI and RTC was introduced to prevent the occlusion problem of the visual encoder. By the combination of the above two basic techniques and high-speed cameras, H-DSC was expected to guarantee the real-time feature, including the enhanced accuracy of event time generation and the synchronized processing of all the camera nodes, in the camera capturing. Therefore, this real-time feature was thoroughly examined with several experiments, such as the precise measurement and estimation of the processing time for the data communication across the camera network, image capturing and processing, and the actual object tracking. As a result, the accurate synchronization of three camera nodes was confirmed at the 400 Hz of system’s

frequency, which is the same of the maximum speed of the used cameras by inspecting the margin of the processing time. Consequently, it is proved that the suggested structure is practical and effective for H-DSC.

In chapter 6, several practical applications that are possible by adapting the visual encoder method were described. For example, the fault detection and the system protection by utilizing the remote sensing, and the application toward the micro actuator system and the substitution in the harsh environment were proposed. Also, rotation measurement using a smartphone, rotation control of a motor, and the visual servo-ing were suggested in detail. Additionally, flexible type of shaker and the machine tools such as a grinder and a drill were introduced as the applications for the rotary system via the thread-twisting. Lastly, the casting manipulation is suggested as an application of the rotary system through the thread-bending.

In conclusion, the contribution of this dissertation is summarized as followings: Firstly, a new robust and accurate method to measure the rotation of a rotor, named as 'visual encoder', was developed and its performance was verified quantitatively by various experiments. Secondly, the robotic manipulation for rotation control via thread was successfully performed with two experimental applications, the button spinner and the yo-yo, where the thread-twisting and thread-bending are examined in the respective case, by introducing the high-speed visual feedback system with the visual encoder method. Thirdly, two transformations of thread, bending and twisting, were explained with new geometric models. Fourthly, a high-speed distributed smart camera was suggested to solve the occlusion problem that the visual encoder method may encounter in actual condition. Finally, with the aforementioned works, it is proved that the high-speed visual feedback system with the visual encoder method is able to handle the nonlinear high-speed rotary system without much effort.

References

[1] http://www.kismeta.com/diGrasse/this_old_wheel.htm.

[2] https://commons.wikimedia.org/wiki/File:340,_341._Rotor_of_Motor_of_A.E.G._Zossen_Motor_Car,_(341_rotor_on_axle).jpg.

[3] https://commons.wikimedia.org/wiki/File:Water_turbine_(en_2).svg.

[4] https://en.wikipedia.org/wiki/Hubcap#.

[5] https://commons.wikimedia.org/wiki/File:Asynch-motor-1.png.

[6] https://ca.wikipedia.org/wiki/Rotor_coaxial#/.

[7] https://robotics.nasa.gov/events/competitions.php.

[8] http://www.darpa.mil/program/darpa-robotics-challenge.

[9] M. Dimmler and C. Dayer. Optical encoders for small drives. *IEEE/ASME Trans. Mechatron.*, 1(4):278–283, 1996.

[10] T. Drummond and R. Cipolla. Real-time visual tracking of complex structures. *IEEE Trans. Pattern Anal. Mach. Intell.*, 24(7):932–946, 2002.

[11] A. I. Comport, É. Marchand, and F. Chaumette. A real-time tracker for markerless augmented reality. In *Proc. IEEE/ACM Int. Symp. on Mixed and Augmented Reality*, pages 36–, Washington, DC, USA, 2003. IEEE Computer Society.

[12] G. Klein and D. Murray. Parallel tracking and mapping for small ar workspaces. In *Proc. IEEE/ACM Int. Symp. on Mixed and Augmented Reality*, pages 225–234, 2007.

[13] R. A. Newcombe, S. J. Lovegrove, and A. J. Davison. Dtam: Dense tracking and mapping in real-time. In *Proc. Int. Conf. Computer Vision*, pages 2320–2327, 2011.

[14] D. G Lowe. Distinctive image features from scale-invariant keypoints. *Int. J. Comput. Vision*, 60(2):91–110, 2004.

[15] H. Bay, A. Ess, T. Tuytelaars, and L. Van Gool. Speeded-up robust features (surf). *Comput. Vision Image Understanding*, 110(3):346–359, 2008.

[16] M. Trajković and M. Hedley. Fast corner detection. *Image Vision Comput.*, 16(2):75–87, 1998.

[17] W. Li, J. Jin, X. Li, and B. Li. Method of rotation angle measurement in machine vision based on calibration pattern with spot array. *Appl. Opt.*, 49(6):1001–1006, 2010.

[18] T. Suzuki, T. Endo, O. Sasaki, and J. E. Greivenkamp. Two-dimensional small-rotation-angle measurement using an imaging method. *Opt. Eng.*, 45(4):043604–043604, 2006.

[19] T. Kadowaki, K. Kobayashi, and K. Watanabe. Rotation angle measurement of high-speed flying object. In *2006 SICE-ICASE International Joint Conference*, pages 5256–5259, 2006.

[20] Y. Watanabe, T. Komuro, S. Kagami, and M. Ishikawa. Multi-target tracking using a vision chip and its applications to real-time visual measurement. *Journal of Advanced Computational Intelligence and Intelligent Informatics*, 17(2), 2005.

[21] Y. Kwon and W. Kim. Development of a new high-resolution angle-sensing mechanism using an rgb sensor. *IEEE/ASME Trans. Mechatron.*, 19(5):1707–1715, 2014.

[22] I. Godler, T. Sonoda, and K. Sakurai. Modeling and evaluation of a twist drive actuator for soft robotics. *Advanced Robotics*, 26(7):765–783, 2012.

[23] I. Gaponov, D. Popov, and J. Ryu. Twisted string actuation systems: A study of the mathematical model and a comparison of twisted strings. *IEEE/ASME Trans. Mechatron.*, 19(4):1331–1342, 2014.

[24] T. Würtz, C. May, B. Holz, C. Natale, G. Palli, and C. Melchiorri. The twisted string actuation system: Modeling and control. In *Proc. IEEE/ASME Int. Conf. Advanced Intelligent Mechatronics*, pages 1215–1220, 2010.

[25] T. Sonoda and I. Godler. Position and force control of a robotic finger with twisted strings actuation. In *Proc. IEEE/ASME Int. Conf. Advanced Intelligent Mechatronics*, pages 611–616. IEEE, 2011.

[26] G. Palli, C. Natale, C. May, C. Melchiorri, and T. Wurtz. Modeling and control of the twisted string actuation system. *IEEE/ASME Trans. Mechatron.*, 18(2):664–673, 2013.

[27] Y. Shin, H. Lee, K. Kim, and S. Kim. A robot finger design using a dual-mode twisting mechanism to achieve high-speed motion and large grasping force. *IEEE Trans. Rob.*, 28(6):1398–1405, 2012.

[28] G. Palli and S. Pirozzi. Optical force sensor for the dexmart hand twisted string actuation system. *Sensors & Transducers*, 148(1):28, 2013.

[29] G. Palli, C. Melchiorri, G. Vassura, U. Scarcia, L. Moriello, G. Berselli, A. Cavallo, G. De Maria, C. Natale, S. Pirozzi, et al. The dexmart hand: Mechatronic design and experimental evaluation of synergy-based control for human-like grasping. *Int. J. Rob. Res.*, 33(5):799–824, 2014.

[30] J. Woroneski. Spinning toy, February 17 1948. US Patent 2,436,158.

[31] P. F. Sola, S. R. Bescós, P. Lamata, J. B. Pagador, F. M. Sánchez-Margallo, and E. J. Gómez. Virtual reality thread simulation for laparoscopic suturing training. *Stud. Health Technol. Inform*, 119:144–149, 2006.

[32] B. Kubiak, N. Pietroni, F. Ganovelli, and M. Fratarcangeli. A robust method for real-time thread simulation. In *Proc. ACM Symp. Virtual Reality Software and Technology*, pages 85–88. ACM, 2007.

[33] M. Servin, C. Lacoursiere, F. Nordfelth, and K. Bodin. Hybrid, multiresolution wires with massless frictional contacts. *IEEE Trans. Vis. Comput. Graph*, 17(7):970–982, 2011.

[34] M. Müller, B. Heidelberger, M. Hennix, and J. Ratcliff. Position based dynamics. *J. Visual Commun. Image Represent.*, 18(2):109–118, 2007.

[35] F. Fend. Rope-pull starter for internal combustion engines, January 2 1968. US Patent 3,361,124.

[36] N. M. Sleeper. Toy airplane, May 24 1932. US Patent 1,859,805.

[37] J. N. Cayo. Spinning or toy top, December 28 1920. US Patent 1,363,718.

[38] H. Wallop. Yo-yos to be 'biggest toy craze of 2010', January16 2010. The Telegraph.

[39] S. G. Miller. *Ancient greek athletics*. Yale University Press, 2006.

[40] S. Kurosu. Dynamics of a human-operated dynamical system (yo-yo control system). *Transactions of the Society of Instrument and Control Engineers*, 14:277–282, 1978.

[41] K. Hashimoto and T. Noritsugu. Modeling and control of robotic yo-yo with visual feedback. In *Proc. IEEE Int. Conf. Robot. Autom.*, volume 3, pages 2650–2655. IEEE, 1996.

[42] H. Jin and M. Zackenhouse. Yoyo dynamics: Sequence of collisions captured by a restitution effect. *J. Dyn. Syst. Meas. Contr.*, 124(3):390–397, 2002.

[43] H. Jin and M. Zacksenhouse. Robotic yoyo playing with visual feedback. *IEEE Trans. Rob.*, 20(4):736–744, 2004.

[44] H. Jin and M. Zacksenhouse. Oscillator-based yoyo control: implementation and comparison with model-based control. In *Proc. Int. Conf. Advanced Robotics*, pages 153–158. IEEE, 2005.

[45] H. Jin, Q. Ye, and M. Zacksenhouse. Return maps, parameterization, and cycle-wise planning of yo-yo playing. *IEEE Trans. Rob.*, 25(2):438–445, 2009.

[46] L. Žlajpah. Robotic yo-yo: modelling and control strategies. *Robotica*, 24(02):211–220, 2006.

[47] T. Yoshioka, T. Sakuma, T. Nemoto, and M. Iwase. Realization of robotic yoyo operation based on analysis of human motion. In *Proc. Int. Workshop on Mechatronics, 2012 9th France-Japan & 7th Europe-Asia Congress on and Research and Education in Mechatronics*, pages 299–306, 2012.

[48] T. Nemoto, T. Sakuma, M. Iwase, and S. Hatakeyama. Realization of yoyo operation called long-sleeper by robot arms. In *Proc. IECON 2011-37th Annual Conference on IEEE Industrial Electronics Society*, pages 265–270, 2011.

[49] A. Namiki, Y. Imai, M.i Ishikawa, and M. Kaneko. Development of a high-speed multifingered hand system and its application to catching. In *Proc. IEEE/RSJ Int. Conf. Intell. Robots Syst.*, volume 3, pages 2666–2671. IEEE, 2003.

[50] T. Senoo, A. Namiki, and M. Ishikawa. Ball control in high-speed batting motion using hybrid trajectory generator. In *Proc. IEEE Int. Conf. Robot. Autom.*, pages 1762–1767. IEEE, 2006.

[51] T. Senoo, A. Namiki, and M. Ishikawa. High-speed throwing motion based on kinetic chain approach. In *Proc. IEEE/RSJ Int. Conf. Intell. Robots Syst.*, pages 3206–3211. Citeseer, 2008.

[52] T. Senoo, Y. Yamakawa, S. Mizusawa, A. Namiki, M. Ishikawa, and M. Shimojo. Skillful manipulation based on high-speed sensory-motor fusion. In *Proc. IEEE Int. Conf. Robot. Autom.*, pages 1611–1612. IEEE, 2009.

[53] T. Senoo, A. Namiki, and M. Ishikawa. High-speed batting using a multi-jointed manipulator. In *Proc. IEEE Int. Conf. Robot. Autom.*, volume 2, pages 1191–1196. IEEE, 2004.

[54] K. Murakami, T. Senoo, and M. Ishikawa. High-speed catching based on inverse motion approach. In *Proc. IEEE Int. Conf. Robot. Biomimetics*, pages 1308–1313. IEEE, 2011.

[55] K. Murakami, Y. Yamakawa, T. Senoo, and M.i Ishikawa. Motion planning for catching a light-weight ball with high-speed visual feedback. In *Proc. IEEE Int. Conf. Robot. Biomimetics*, pages 339–344. IEEE, 2015.

[56] Y. Yamakawa, A. Namiki, M. Ishikawa, and M. Shimojo. One-handed knotting of a flexible rope with a high-speed multifingered hand having tactile sensors. In *Proc. IEEE/RSJ Int. Conf. Intell. Robots Syst.*, pages 703–708. IEEE, 2007.

[57] Y. Yamakawa, A. Namiki, M. Ishikawa, and M. Shimojo. Knotting manipulation of a flexible rope by a multifingered hand system based on skill synthesis. In *Proc. IEEE/RSJ Int. Conf. Intell. Robots Syst.*, pages 2691–2696. IEEE, 2008.

[58] Y. Yamakawa, A. Namiki, and M. Ishikawa. Dynamic high-speed knotting of a rope by a manipulator. *Int. J. Adv. Rob. Syst.*, 10, 2013.

[59] Y. Yamakawa, A. Namiki, and M. Ishikawa. Motion planning for dynamic folding of a cloth with two high-speed robot hands and two high-speed sliders. In *Proc. IEEE Int. Conf. Robot. Autom.*, pages 5486–5491. IEEE, 2011.

[60] http://www.mikrotron.de/.

[61] https://www.ptgrey.com/.

[62] https://www.dspace.com/.

[63] https://www.mathworks.com/.

[64] H. Kim, Y. Yamakawa, T. Senoo, and M. Ishikawa. Visual encoder: robust and precise measurement method of rotation angle via high-speed rgb vision. *Optics Express*, 24(12):13375–13386, 2016.

[65] A. Collet, M. Martinez, and S. S. Srinivasa. The moped framework: Object recognition and pose estimation for manipulation. *Int. J. Rob. Res.*, page 0278364911401765, 2011.

[66] H. Kim, Y. Yamakawa, T. Senoo, and M. Ishikawa. Manipulation model of thread-rotor object by a robotic hand for high-speed visual feedback control. In *Proc. IEEE/ASME Int. Conf. Advanced Intelligent Mechatronics*, pages 924–930, 2014.

[67] H. Kim, Y. Yamakawa, T. Senoo, and M. Ishikawa. Robotic manipulation of rotating object via twisted thread using high-speed visual sensing and feedback. In *Proc. IEEE Int. Conf. Multisensor Fusion and Integration for Intelligent Systems*, pages 265–270, 2015.

[68] J. J. Craig. *Introduction to robotics: mechanics and control*, volume 3. Pearson Prentice Hall Upper Saddle River, 2005.

[69] T. Nemoto, Y. Noguchi, H. Miyakawa, and M. Iwase. Control of robotic yoyo with energy compensation based on an integrated model of a robot and a yoyo. *Journal of Advanced Simulation in Science and Engineering*, 2(2):329–348, 2015.

[70] M. Weber, M. Alexa, and W. Müller. Visualizing time-series on spirals. In *Infovis*, volume 1, pages 7–14, 2001.

[71] F. Miralles, S. Tarongi, and A. Espino. Quantification of the drawing of an archimedes spiral through the analysis of its digitized picture. *Journal of Neuroscience Methods*, 152(1):18–31, 2006.

[72] H. Kim and M. Ishikawa. High-speed distributed camera network based on message passing interface. In *Proc. Int. Conf. Information Fusion*, pages 1768–1773, 2016.

[73] B. Rinner and W. Wolf. An introduction to distributed smart cameras. *Proceedings of the IEEE*, 96(10):1565–1575, 2008.

[74] M. Bramberger, A. Doblander, A. Maier, B. Rinner, and H. Schwabach. Distributed embedded smart cameras for surveillance applications. *Computer*, 39(2):68–75, 2006.

[75] S. Noguchi, Y. Watanabe, and M. Ishikawa. High-resolution surface reconstruction based on multi-level implicit surface from multiple range images. In *Proc. IEEE Int. Conf. Image Proc.*, pages 2140–2144, 2013.

[76] C. Liu and J. W. Layland. Scheduling algorithms for multiprogramming in a hard-real-time environment. *Journal of the ACM (JACM)*, 20(1):46–61, 1973.

[77] D. W. Walker and J. J. Dongarra. Mpi: a standard message passing interface. *Supercomputer*, 12:56–68, 1996.

[78] W. Gropp, E. Lusk, N. Doss, and A. Skjellum. A high-performance, portable implementation of the mpi message passing interface standard. *Parallel computing*, 22(6):789–828, 1996.

[79] V. Springel, N. Yoshida, and S. D. White. Gadget: a code for collisionless and gasdynamical cosmological simulations. *New Astronomy*, 6(2):79–117, 2001.

[80] V. Springel. The cosmological simulation code gadget-2. *Monthly Notices of the Royal Astronomical Society*, 364(4):1105–1134, 2005.

[81] K. Kadau, T. C. Germann, and P. S. Lomdahl. Large-scale molecular-dynamics simulation of 19 billion particles. *International Journal of Modern Physics C*, 15(01):193–201, 2004.

[82] S. Kagami, S. Saito, T.i Komuro, and M. Ishikawa. A networked high-speed vision system for 1,000-fps visual feature communication. In *Proc. ACM/IEEE Int. Conf. Distributed Smart Cameras*, pages 95–100, 2007.

[83] D. L. Mills. Internet time synchronization: the network time protocol. *IEEE Transactions on Communications*, 39(10):1482–1493, 1991.

[84] S. Jun, D. Yu, Y. Kim, and S. Seong. A time synchronization method for ntp. In *Proc. Int. Conf. Real-Time Computing Systems and Applications*, pages 466–473, 1999.

[85] K. Lee, J. C. Eidson, H. Weibel, and D. Mohl. Ieee 1588-standard for a precision clock synchronization protocol for networked measurement and control systems. In *Conference on IEEE*, volume 1588, page 2, 2005.

[86] J. Min, N. J. Gelo, and H. Jo. Real-time image processing for non-contact monitoring of dynamic displacements using smartphone technologies. In *SPIE Smart Structures and Materials+ Nondestructive Evaluation and Health Monitoring*, pages 98031B–98031B. International Society for Optics and Photonics, 2016.

[87] http://www.apple.com/iphone-7/specs/.

[88] P. I. Corke et al. *Visual Control of Robots: high-performance visual servoing*. Research Studies Press Baldock, 1996.

[89] S. Hutchinson, G. D. Hager, and P. I. Corke. A tutorial on visual servo control. *IEEE Transactions on Robotics and Automation*, 12(5):651–670, 1996.

[90] Y. Liu and X. Xin. Controllability and observability of an-link planar robot with a single actuator having different actuator–sensor configurations. *IEEE Transactions on Automatic Control*, 61(4):1129–1134, 2016.

[91] M. S. Bhamla, B. Benson, C. Chai, G. Katsikis, A. Johri, and M. Prakash. Hand-powered ultralow-cost paper centrifuge. *Nature Biomedical Engineering*, 1:0009, 2017.

[92] H. Arisumi, T. Kotoku, and K. Komoriya. A study of casting manipulation (swing motion control and planning of throwing motion). In *Proc. IEEE/RSJ Int. Conf. Intell. Robots Syst.*, volume 1, pages 168–174, 1997.

[93] H. Arisumi, K. Yokoi, and K. Komoriya. Casting manipulation—midair control of a gripper by impulsive force. *IEEE Transactions on Robotics*, 24(2):402–415, 2008.